

TMD factorization and the gluon distribution in high energy QCD

Emil Avsar

^a104 Davey Lab, Penn State University, University Park, 16802 PA, USA

E-mail: eavsar@phys.psu.edu

ABSTRACT: This paper is a part of a series of works where we in detail examine the concept of Transverse Momentum Dependent (TMD), or k_{\perp} , factorization, which is frequently encountered in the literature and is widely used in the phenomenological applications of QCD at very high energies. We address the question of what exactly factorization is, as it is meant in different contexts and formalisms, and we compare the formalisms to each other. We clarify some basic concepts regarding factorization and how it exactly is applied in high energy QCD, and we make important notes on some key and fundamental points that are often overlooked. We offer an extensive analysis of single inclusive particle production, and we analyze the TMD gluon distribution that plays a pivotal role in high energy QCD.

Contents

1. Introduction	2
2. Unintegrated parton distributions	4
2.1 The gluon “number density”	5
2.2 The dipole gluon distribution	7
2.3 On the rapidity variable in the gluon distribution	8
3. Factorization	8
3.1 Hard scattering factorization	9
3.1.1 Basic parton model	10
3.1.2 On the leading momentum regions in field theory	12
3.1.3 Factorization in simple theory	16
3.1.4 Including the gluons, and the Glauber region	21
3.1.5 TMD factorization	23
3.2 Factorization in BFKL	29
3.3 Factorization in the CGC	30
3.3.1 Basics of CGC	31
3.3.2 Power counting and “dilute” and “dense” systems	31
3.3.3 The LLA and basic logic of factorization	33
3.3.4 Comparison to TMD factorization	35
3.3.5 Causality and factorization	37
3.4 Hybrid formalisms	38
4. The fundamentals of single inclusive particle production	42
4.1 The different cases of particle production	42
4.2 The small- x formula for gluon production	46
4.2.1 The kinematics	48
4.3 The use of the light-cone gauge	50
4.4 Non-light-like symmetric axial gauge	55
4.4.1 The coefficient of the formula	58
4.5 Higher order terms in axial gauge, and more complete view	58
4.6 The gluon distribution function	63
5. Summary	72

1. Introduction

Parton distributions, supplemented by factorization theorems, play a crucial role in the understanding and exploration of QCD [1]. In formulating factorization theorems it is desirable to make as little approximations in the kinematics as possible, so as to capture more of the underlying dynamics. Frequently then one encounters the concept of transverse-momentum-dependent (TMD), or k_\perp -dependent, parton distributions which follow from TMD factorization (k_\perp -factorization). The TMD distributions are important because they capture more of the parton kinematics than do the canonical integrated parton distributions, the PDFs, and they therefore play an important role in the study of less inclusive hadronic observables which are sensitive to the details of the parton kinematics [2].

In the high energy, small- x , limit of QCD even inclusive cross sections are sensitive to the TMD distributions, as the so-called Regge kinematics is dominated by the transverse components of the momenta. Large contributions arise from large rapidity separations, and the typical contributing momenta are slightly off-shell, the off-shellness determined by the transverse momentum. Much of the intuition about the TMD distributions is based on concepts directly borrowed from the parton model, and it is for example very frequent to find in the literature the assertion that the TMD parton distributions are field theoretical number densities, and for example that the underlying mechanism of the phenomenon of saturation is related to the saturation of the phase space occupation number of gluons in a hadron, thus implying that there is a upper limit for the number of partons per phase space in the hadron wave function.

While intuitive notions may be helpful in interpreting the dynamics, what is important is the exact formulation of TMD factorization that is a must for any proper definition of the relevant parton distribution, and the resulting distribution may or may not have the number density interpretation. In the small- x literature we find many statements regarding factorization, yet looking closely at these statements, we find that the necessary proofs are not always provided. We have moreover found different meanings attached to the word “factorization”, and we therefore take the task of illuminating what exactly is being meant in different formalisms. We will do this in section 3 where we compare different formalisms with each other.

We should here mention that when we do speak of factorization we shall sometimes use different names to distinguish different formalisms. For example, we frequently use the words “hard scattering factorization” with which we are referring to the basic factorization of QCD processes where a hard scattering is present [1,3–7]. The hard scale sets the relevant momentum scale by which contributions can be classified according to their power as being leading or suppressed. The latter classification is achieved using the power counting arguments of [8,9]. We will go through this factorization approach in section 3.1. We note that usually the hard scattering factorization is referred to as the “collinear factorization” while the small- x Regge type formalisms go under the name of “ k_\perp -factorization”. This is rather misleading, however, since k_\perp -factorization (TMD factorization) is also a central part of the hard scattering factorization approach so that it is important to realize that TMD factorization is not only relevant for small- x physics. Depending on the exact final

state studied, TMD factorization is a necessary tool for QCD studies even when x is not small. We will in section 3 also go through the Color Glass Condensate [10–15] formalism which is based on a physical picture of classical color fields. One of our main objectives will be to compare the picture of factorization that emerges from the CGC with the hard scattering factorization approach. This is important and relevant for understanding much of the phenomenology based on these formalisms that is currently being used.

In section 4 we give a detailed analysis on the validity of factorization in single inclusive particle production at small- x . The main small- x formula, equation (4.8), or some variation of it, has been widely used in the applications of particle production in proton-proton (pp), proton-nucleus (pA) and nucleus-nucleus (AA) collisions (see e.g. [16–32] and references therein). We shall examine the foundations of the formula, the arguments given for its validity, and we shall clarify the exact pre-factor involved in the formula (as there are variations in the literature regarding the pre-factor). Additionally we shall examine what exactly the definition of the corresponding TMD gluon distribution is.

The standard arguments for the validity of the k_\perp -factorization formula are usually based on the use of the light-cone gauge. Here, simplifications occur because the leading gluon contributions are suppressed, and Faddeev-Popov ghosts are absent. However, there appear severe technical difficulties by the introduction of the unphysical singularities in the light-cone gauge propagators. One issue is that these can potentially obstruct the contour deformations that are needed for the complete proof of factorization. Additionally, for the TMD distributions, the singularities of the gauge propagator imply rapidity divergences starting from one loop order, and one must then consistently regularize those divergences.

While in the moderate- x region the important gluon momenta are collinear to the hadron momentum, in the small- x region one enters the Regge kinematics where actually the transverse momentum components are dominating. If k is the gluon momentum then $k^+k^- \ll k_\perp^2$. In this case the gluons are also said to be in the Glauber region. In light-cone gauge then, transversely polarized gluons are no longer power-suppressed. This complicates the general treatment because one can then have arbitrarily many transversely polarized gluons exchanged without power-suppression. To remove the extra gluon contributions and establish factorization, one must then be able to perform contour deformations on the loop momenta out of Glauber region. It is then important that the unphysical singularities in the gauge propagators do not block the necessary contour deformations.

In reference [33] it is shown at least in the deep inelastic scattering of a color-singlet gauge invariant gluon current on a hadron that the contour deformations are possible in low order graphs. However, in [33] specific assumptions are made on the target state that make the application of the Ward identities simpler, at least for the low order graphs. Going to higher order graphs, however, complications can easily arise, and a systematic treatment is therefore needed. We will examine the applications of axial gauge on the particle production process in sections 4.3, 4.4 and 4.5, addressing in particular the ability of making the necessary contour deformations.

Apart from the technical details of the proof of factorization, another issue we address here concerns the exact definition of the TMD gluon distribution that is associated with the factorization formula, equation (4.8). The definitions found in the literature all center

around the so-called “dipole gluon distribution” that is related to a (slightly modified) Fourier transform of the coordinate space dipole scattering amplitude, see equations (2.10) and (4.11). In the arguments leading to the factorization formula, however, one makes use of the axial gauge. In the axial gauge, one necessarily obtains a definition for the gluon distribution that is an expectation value over the transverse gluon fields, $\langle A^i A^i \rangle$. This is canonically identified, not with the dipole distribution, but with the so-called small- x Weizsacker-Williams (WW) distribution which is meant to represent a number density of gluons [34–39]. The WW distribution naturally appears also in the calculation of certain classical quantities, such as the energy density of the so-called Glasma, see for example [40]. There is therefore a potential confusion as to what exactly the gluon distribution is, this is for example apparent in reference [41]. We discuss further the form of the gluon distribution in section 4.6.

We should also mention here that this work is part of a larger project initiated in order to understand the connections and differences between the various TMD factorization formalisms and the TMD gluon distributions which they give rise to. Related points that are not covered here will therefore be discussed and addressed in two separate papers [42, 43].

This paper is somewhat long, the reason being that we cover a variety of topics which are important for the questions regarding factorization and the correct definitions of the TMD gluon distribution, and we do not wish to skip important and subtle points but rather try to explain and illuminate them, as this is the goal of our project. We have also aimed at providing a coherent exposition of the various topics that appear in different formalisms and different set of works but nevertheless all are centered around the concepts of TMD factorization and TMD parton distributions. We have therefore decided to present all the material in a single paper. We believe that it will be of interest for both experimentalists and theoreticians working on related topics.

The paper is organized as follows. In section 2 we analyze and explain some fundamental aspects of unintegrated parton distributions, starting from the elementary parton model definition. We concentrate on the two type of distributions commonly found in the small- x literature. Section 3 contains our main discussion on factorization. In section 3.1 we provide an analysis of the hard scattering factorization approach which leads to both collinear and TMD factorization. Then in sections 3.2 and 3.3 we analyze the formulation of k_\perp -factorization in the small- x region and we compare these to the hard scattering TMD factorization. Section 3.4 gives an account of the formalisms that combine collinear factorization with the small- x formulas. Section 4 gives the detailed analysis of the single inclusive particle production in the small- x region as already explained above. We have divided this section into several subsections according to the different points we cover, as was summarized above. Finally, section 5 contains a brief summary.

2. Unintegrated parton distributions

Our aim in this section is to first recall the basic idea of parton densities. We will outline the basic definition as given by the parton model, and then shortly discuss some of the

modifications induced by the dynamics of QCD. We also examine the validity of the intuitive ideas borrowed from the parton model in the formulation of small- x QCD. We will therefore here go through the commonly used “number density” and “dipole” distributions from the small- x literature.

The concept of parton distributions dates back to the introduction of the parton model itself by Feynman [44, p. 135]. In there, partons of a particular flavor are considered to have a number density in the target hadron. While for the parton model calculation in DIS it is sufficient to consider number densities in the longitudinal momentum component x , the concept also naturally extends to a number density in both x and k_\perp . The intuitive concept of a number density of partons can be formalized using light-front quantization and writing

$$f_{j/h}(x, k_\perp) = \sum_\alpha \frac{1}{2x(2\pi)^3} \frac{\langle P, h | a_{k, \alpha, j}^\dagger a_{k, \alpha, j} | P, h \rangle}{\langle P, h | P, h \rangle}. \quad (2.1)$$

Here j and h label parton and hadron flavor, α is a parton helicity index, $|P, h\rangle$ is the target state of momentum P , and a^\dagger and a are parton creation and annihilation operators respectively.

While intuitively clear, definition (2.1) above is not really correct in full QCD, and it cannot be used in the exact form just given [1]. In the above formula for example, the kinematic variables x and k_\perp are literally the momentum fraction and transverse momentum of the parton probed by the electromagnetic current in DIS. Therefore the unintegrated distribution above is indeed a simultaneous distribution of the partons in both x and k_\perp . In QCD, however, several modifications do occur. The variables x and k_\perp no longer correspond to the literal momentum fractions of any single parton in the hadron state, and additional variables must be introduced which are connected to the divergences that occur in loop calculations (see section 2.3 below and in addition the discussions in section 3.1).

2.1 The gluon “number density”

It is in the small- x literature often implied that the TMD gluon distribution indeed has the meaning of a phase space number density as in the above formula. Thus we often find the statement of a certain “number of gluons per unit phase space”. In the Color Glass Condensate (CGC) model at least, this statement is meant in the sense of the Weizsacker-Williams method of virtual quanta. We recall that in electrodynamics this method replaces the energy density of the classical electromagnetic field created by fast moving charged particles by the equivalent field of pulse radiation. The latter is interpreted semi-classically as consisting of a distribution of energy quanta, that is, photons. From the average energy density of the classical field, $\langle |E|^2 \rangle$, one can then calculate the equivalent number of photons. This is the reason why the gluon distribution appearing in the CGC formalism is referred to as the Weizsacker-Williams (WW) gluon distribution. In the CGC then, one solves the classical Yang-Mills equations for the non-Abelian color field. The energy density of the classical field then relates to the equivalent number density of energy quanta, in this case identified with the gluons. In the light-cone gauge $A^+ = 0$ one defines (for a hadron

with large P^+)

$$\begin{aligned}
f_{WW}(x, k_\perp) &= \sum_{i,a} \frac{1}{2(2\pi)^3} \langle a_a^{\dagger i}(x^+, k) a_a^i(x^+, k) \rangle \\
&= \sum_{i,a} \frac{2(k^+)^2}{(2\pi)^3} \langle A_a^i(x^+, k) A_a^i(x^+, -k) \rangle \\
&= \sum_{i,a} \frac{2}{(2\pi)^3} \langle F_a^{i+}(x^+, k) F_a^{i+}(x^+, -k) \rangle
\end{aligned} \tag{2.2}$$

where $k = (k^+, k_\perp)$, and a and a^\dagger , as in (2.1), denote the parton (in this case gluon) annihilation and creation operators in the sense of light front quantization where x^+ plays the role of time. Notice that $x = k^+/P^+$ should not be confused with the time variable x^+ . The last identity, $\langle F^{+i} F^{+i} \rangle$, can be calculated in a classical approximation, for example using the McLerran-Venugopalan model [34, 35], from which an explicit expression can be obtained for f_{WW} .

The definition of the WW distribution is thus essentially identical to the parton model definition (2.1). One trivial difference is that, by convention, the $1/x$ term in (2.1) is not included in (2.2). As a less trivial difference we also note that while in (2.1) the quantum mechanical averaging is taken over the momentum eigenstates of the target, $|P\rangle$, in the CGC definition (2.2) one rather specifies a classical charge density $\rho(x^-, x_\perp)$ in the transverse and longitudinal planes, and the classical averaging is then performed with respect to the specified profile, using a classical weight functional¹ $W[\rho]$. One is then clearly not averaging over momentum eigenstates. The brackets are defined such that any function, \mathcal{O} , of the classical source ρ has the average

$$\langle \mathcal{O} \rangle = \int D\rho \mathcal{O}[\rho] W[\rho]. \tag{2.3}$$

This averaging is normalized to unity, so that $\langle \mathbb{1} \rangle = 1$, *i.e.* the classical weight functional $W[\rho]$ is such that

$$\int \mathcal{D}\rho W[\rho] = 1. \tag{2.4}$$

A gauge invariant version of (2.2) can be written as (where we now expand the $F^{+i}(x^+, k)$ in terms of $F^{+i}(x^+, x^-, x_\perp)$)

$$\begin{aligned}
f_{WW}(x, k_\perp) &= \frac{2}{(2\pi)^3} \int dx^- dy^- \int d^2 x_\perp d^2 y_\perp e^{ixP^+(x^- - y^-) - ik_\perp(x_\perp - y_\perp)} \\
&\quad \langle F_a^{+i}(x) W_{ab}(x, y) F_b^{+i}(y) \rangle.
\end{aligned} \tag{2.5}$$

Here W denotes a Wilson line in the adjoint representation needed to make the operators within the expectation value gauge invariant. We write down the explicit definitions of the Wilson lines in the following sections.

¹This functional should not be confused with our generic notation for Wilson lines which is also W . We therefore always explicitly indicate the ρ dependence of the classical CGC functional and write $W[\rho]$.

2.2 The dipole gluon distribution

The most commonly encountered “unintegrated gluon distribution” in the small- x formalism is actually different than the above distribution and is related to the so-called dipole scattering amplitude which itself is specified in coordinate space. The dipole scattering amplitude, and the associated “gluon distribution” appears as a result of the use of the dipole formalism [45–49] which canonically is applied to DIS at small- x .

The basic object that enters any definition of the dipole “gluon distribution” is the coordinate space dipole “scattering amplitude”, \mathcal{N} . The standard definition of this object in DIS, or in $\gamma^*\gamma^*$ scattering is given by (see for example [39, 50–52])

$$\mathcal{N}(x_\perp, y_\perp; y) \equiv 1 - \frac{1}{N_c} \left\langle \text{Tr}\{W^\dagger(x_\perp)W(y_\perp)\} \right\rangle_y, \quad (2.6)$$

where we shall freely switch between the coordinates x_\perp and y_\perp , and

$$r_\perp = x_\perp - y_\perp, \quad (2.7)$$

$$b_\perp = (x_\perp + y_\perp)/2, \quad (2.8)$$

which are respectively the dipole “size” and “impact parameter” in transverse coordinate space. In (2.6), W denotes the eikonal Wilson line given by

$$W(x_\perp) = P \exp \left(-ig_s \int_{-\infty}^{\infty} d\lambda n \cdot A^a(x_\perp + \lambda n) t_F^a \right). \quad (2.9)$$

Here P denotes path ordering with respect to λ , and t_F^a is the SU(3) color matrix in the fundamental representation. The vector n is taken along the light-like direction, and the trace in (2.6) is meant with respect to the color matrices t_F . The assertion of the dipole model is that this quantity is relevant for DIS [49, 53, 54], $\gamma^*\gamma^*$ scattering [50, 51], and also for quark, or prompt photon production in hadron-hadron collisions (see for example [55–57]).

As for the momentum distribution referred to as the “dipole gluon distribution” [16, 20, 28, 58], or also very commonly as simply the “unintegrated gluon density” [18, 19, 21–24, 26, 27], it is given by a modified Fourier transform of the dipole scattering amplitude. Most commonly we do in the literature find the definition

$$f_{dip}(k_\perp; y) = \mathcal{C} \int d^2r_\perp d^2b_\perp e^{-ik_\perp \cdot r_\perp} \nabla_r^2 \mathcal{N}(r_\perp, b_\perp; y), \quad (2.10)$$

where now we have used the variables r_\perp and b_\perp instead of x_\perp and y_\perp . We write the pre-factor simply as \mathcal{C} since there does not seem to be any universally accepted value for it, and different papers use different pre-factors. Note also that a fully gauge invariant definition of (2.6), and therefore also of (2.10), requires that one also insert transverse gauge links at $\pm\infty$.

Formula (2.10) is not exactly linked to the parton model definition of the unintegrated gluon distribution in (2.1). It is therefore also distinct from the Weizsacker-Williams distribution, and also from the gluon distributions obtained in the TMD factorization approach that we go through in section 3.1.5. We examine the derivation of the Wilson lines in the definition (2.10) in [42].

A version of the dipole gluon distribution in the adjoint representation appears also in single inclusive gluon production, equation (4.11), which we shall examine in detail in section 4.

2.3 On the rapidity variable in the gluon distribution

It is also common to denote the rapidity dependence of the dipole distribution (2.10) by x , using $y = \ln 1/x$. We emphasize, however, that the rapidity variable in (2.10) is conceptually different than the variable x which appears in (2.1) and (2.2). In the dipole distribution, $y = \ln 1/x$ enters as a rapidity cut-off, either as the scale in the CGC formalism where the functional $W_y[\rho]$ is evaluated, or as the non-zero slope of the Wilson lines in the formalism by Balitsky [50, 51]. On the other hand, in (2.1), $x = k^+/P^+$, where k^+ is the momentum of the parton entering the hard scattering. Similarly in the light-cone gauge definition of the WW distribution (2.2) it again has the meaning of the momentum fraction of the gluon entering the hard scattering. Of course, to avoid rapidity divergences in (2.2) a cut-off must be inserted just as in (2.10). There must therefore be present an additional variable, ζ , which plays the same role as $y = \ln 1/x$ in (2.10). Thus we have

$$f_{WW} = f_{WW}(x, k_\perp; \zeta), \quad (2.11)$$

and we must generally distinguish x and ζ . It is customary to choose $\zeta = x$ where for example in DIS x is taken to be the Bjorken variable.

One may then naturally ask why only y and k_\perp appear in the definition of the dipole distribution. The answer is that k^+ is actually set to 0 (this is why the Wilson line (2.9) is integrated in x^- from $-\infty$ to $+\infty$). Thus the variable x which appears in f_{WW} is instead set to 0 in f_{dip} . If therefore for example the brackets in f_{dip} are evaluated fully in the classical approximation without any effects of quantum corrections, say in the MV model, then there is no x dependence, unlike f_{WW} which has a x dependence even in the classical computation.

3. Factorization

As the word “factorization” is often used in the literature, and as there are many formalisms which go under the name of “ k_\perp -factorization”, we want to examine these formalisms, to explain the similarities and the differences among them. We believe this to be a relevant task since it is important especially for the experimental community to have clear understanding on what exactly is meant in the different formalisms. This is also of interest for theorists, however, and especially in the case of small- x physics where many statements are put forward, particularly regarding k_\perp -factorization and unintegrated parton distributions. We must then once for all analyze these statements and the assertions made.

The original concept of factorization is to be found in the hard scattering factorization approach [3–7] where for a given process the contributing Feynman graphs are shown to be factorizable into different components each of which is associated with a particular type of momentum region. The leading momentum regions are determined by a power counting analysis that we go through in section 3.1.2. There is a hard part specified by

the large momentum scale Q , and dominated by short distance, $d \sim 1/Q$, contributions. The hard scattering factorization does not directly deal with the small- x region where \sqrt{s} is asymptotically large, and where there may or may not be present in addition the hard scale Q . For an up-to-date and comprehensive overview of factorization in QCD, see [1]. We go through the hard scattering factorization in section 3.1.

After going through the hard scattering factorization, we shall in section 3.2 examine the basic aspects of the BFKL formalism [59–61]. Here the emphasis is put on the so-called Multi-Regge-Kinematics (MRK), and ideas borrowed from the pre-QCD Regge theory [62–64] play an important role. Even though the methods are rather different than the hard scattering factorization, one can actually identify a structure where different factors are associated with different momentum regions as in the hard scattering factorization (see [42] for further discussions).

There is also the CCH approach [65–67] which is based on BFKL but is meant to build on a structure that is closely related to the hard scattering factorization since again emphasis is put on a hard scattering coefficient. We will here not go through CCH since we give a detailed analysis in [42]. In [42] we also go through in more detail the CCFM formalism [68–70] that is also based on the CCH approach and is meant to interpolate between the small- x BFKL formalism and the collinear limit at high Q encoded in the DGLAP evolution.

There is then the CGC approach [10–15, 18, 22–25, 39] which uses a very different language in terms of classical fields, A_{cl} , and their corresponding sources, ρ . In this case emphasis is put on a power counting in $g_s \rho$ where the strong coupling g_s is taken as a fixed variable which can be made as small as possible. A difference between “dilute” and “dense” systems is emphasized, where for dilute systems $g_s \rho \ll 1$ while for dense systems $g_s \rho \sim 1$. The structure of the factorization formula is therefore rather different than the hard scattering factorization. We analyze factorization within the CGC formalism in section 3.3. We shall then in section 3.4 analyze some formalisms where the ideas of collinear factorization and the CGC are mixed.

We may also mention the dipole approach encountered above where the scattering process of parton impinging upon a target hadron is modeled via the insertion of Wilson lines as in (2.9), where for a quark the Wilson line is taken in the fundamental representation while for a gluon the color matrices in (2.9) are instead taken in the adjoint representation. The dipole formalism is easily embedded into the CGC picture because the CGC formalism, or the MV formalism, gives an explicit way of calculating the averages of the Wilson lines that are present in the dipole formalism. Actually factorization is more or less asserted in the dipole formalism. In [42, 43] we analyze the underlying structure in more detail.

3.1 Hard scattering factorization

We now review and explain the factorization which is applied to processes where a hard scale is present. As we shall see, however, there is a structure which does not depend on the existence of the hard factor. It will then be important to understand the overall structure here, since it can also be applied to the Regge region. We will start with the most simple

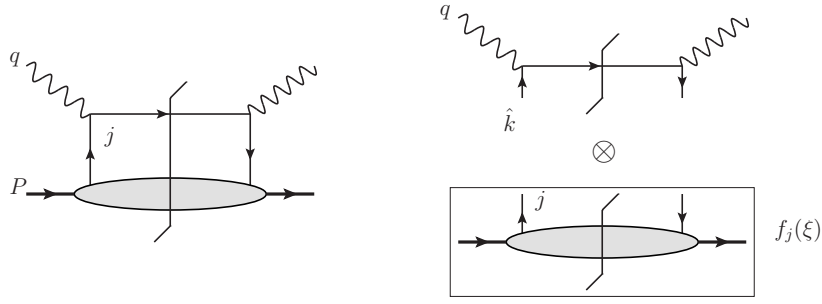


Figure 1: DIS in the simple parton model. Right: Factorized structure in the parton model.

case of the parton model, and then move on to the more complicated cases in QCD, and eventually to TMD factorization which is the main interest of this paper.

3.1.1 Basic parton model

In order to understand the basic idea of the hard scattering factorization, it is useful to first look at the interpretation of DIS within the parton model. The advantage of the simple parton model is that the intuitive ideas about the scattering and the structure of hadrons can be quantified in a mathematical manner which then paves the way for an understanding of the more complicated case of full QCD. The quantitative analysis of the model is simplified by the understanding of the kinematics involved, and in DIS it is convenient to consider the frame where the target hadron has momentum $P = (P^+, m^2/2P^+, 0_\perp)$, while the virtual photon has momentum $q = (q^+, q^-, 0_\perp)$ where of course $-2q^+q^- = Q^2$. The scattering in the parton model approximation proceeds as shown in figure 1 (left graph). The parton which is struck by the virtual photon has momentum k . In the rest frame of the target all the components of k are of the order of the typical hadronic scale m . A large boost in the plus direction then brings the momentum of P into the above form, and implies that k^+ is the largest component, being of order Q , while k^- and k_\perp are of order m^2/Q and m respectively. This corresponds to the region where the longitudinal momentum fraction $\xi = k^+/P^+$ is not much smaller than 1.

According to the parton model one can neglect the effects of the strong interaction during the time of the interaction with the photon, and all the effects of the long distance strong interactions is put into the parton distribution functions. This structure is shown in figure 1 (right graph). In the upper part which contains the hard scattering, one can set $k = \xi P$. In particular since the minus component of P is power suppressed with respect to the plus component, one can make the collinear approximation whereby only k^+ is kept in the calculation of the hard scattering coefficient. We denote by $\hat{k} = (k^+, 0^-, 0_\perp)$ the approximated momentum.

We define the DIS hadronic tensor $W^{\mu\nu}$ as

$$\begin{aligned} W^{\mu\nu}(q, P) &= \frac{1}{4\pi} \int d^4z e^{iq \cdot z} \langle P | J^\mu(z) J^\nu(0) | P \rangle \\ &= 4\pi^3 \sum_X \delta(p_X - P - q) \langle P | J^\mu(0) J^\nu(0) | P \rangle. \end{aligned} \quad (3.1)$$

A factorization formula using the basic assumptions of the parton model can then be easily obtained for $W^{\mu\nu}$. Using the general structure of the contributing graphs shown in figure 1, we can write the hadronic tensor as

$$W^{\mu\nu} = \sum_j \frac{e_j^2}{4\pi} \int \frac{d^4k}{(2\pi)^4} \text{Tr} \gamma^\mu U_j(k+q) \gamma^\nu L_j(k, P) \quad (3.2)$$

where U refers to the upper part of the diagram while L refers to the lower blob. The trace refers to the Dirac trace. In the upper part only k^+ is important so we replace k by \hat{k} . Then in the lower part one can replace $k^+ \rightarrow xP^+$ since $\xi = x(1 + \mathcal{O}(m^2/Q^2))$. Thus we get

$$W^{\mu\nu} = \sum_j \frac{e_j^2}{4\pi} \text{Tr} \gamma^\mu \left[\int dk^+ U_j(k^+, q^-, 0_\perp) \right] \gamma^\nu \left[\int \frac{dk^- d^2k_\perp}{(2\pi)^4} L_j(xP^+, k^-, k_\perp, P) \right] + \text{p.s.c.} \quad (3.3)$$

where “p.s.c.” stands for “power suppressed corrections”. To finally obtain a fully factorized structure we notice that the leading contribution from the lower part comes from the component which is enhanced by the factor Q in the boost along the plus direction from the hadron rest frame. Using Lorentz invariance, this leading component can be written as $L_{\text{leading}} = \gamma^- \tilde{L}^+ = (1/4) \text{Tr} \gamma^+ L$. Thus the factorized structure is given by

$$\begin{aligned} W^{\mu\nu} &= \sum_j \frac{e_j^2}{4\pi} \text{Tr} \left[\gamma^\mu \int \frac{d\xi}{\xi} U_j(\xi P^+, q^-, 0_\perp) \gamma^\nu \frac{\hat{k}}{2} \right] \\ &\quad \times \text{Tr} \left[\int \frac{dk^- d^2k_\perp}{(2\pi)^4} \frac{1}{2} \gamma^+ L_j(xP^+, k^-, k_\perp, P) \right] + \text{p.s.c.} \end{aligned} \quad (3.4)$$

The factor in the second row defines the unpolarized integrated quark distribution in the parton model and it can be shown to be equivalent to (2.1). The unintegrated density is obtained simply by undoing the k_\perp integral. Thus

$$f_j(\xi) = \int d^2k_\perp f_j(\xi, k_\perp) \quad (3.5)$$

in the parton model. Note that the integral is over *all* k_\perp . Actually as we review in detail in [42], much of the literature on the TMD gluon distribution in small- x physics uses very much the same ideas as above. We shall also see in section 4 that very similar arguments are used in the treatment of single inclusive gluon production in small- x QCD.

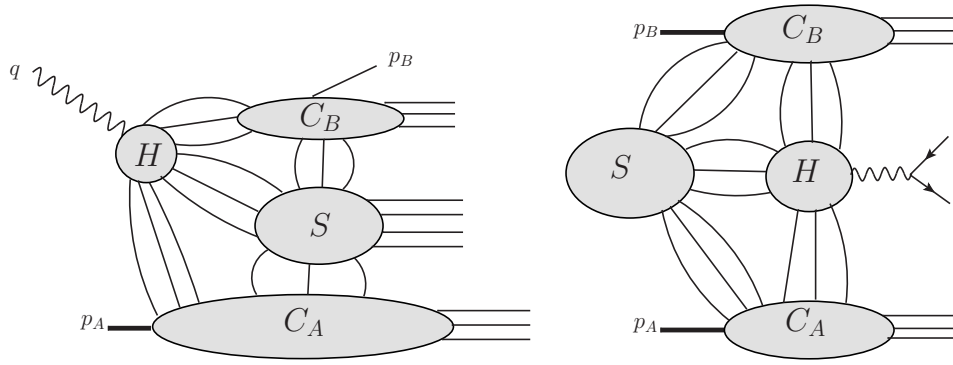


Figure 2: Left: Reduced graphs for SIDIS where a hadron with momentum p_B is detected. Right: Reduced graphs for the Drell-Yan process of lepton pair production in hadron-hadron scattering.

3.1.2 On the leading momentum regions in field theory

In trying to simplify generic graphs in a field theory, so as to extract a factorized form, it is important to systematically classify the structure of the leading contributions. In each graph at any given order in perturbation theory there may be many loop momenta that give rise to a rather complicated manifold of momentum regions. It turns out, however, that there is a correspondence between divergences in massless theories and the leading configurations in high-energy processes [8, 9].

These leading regions are non-UV regions that are important when the hard scale Q gets large. The UV region for momenta above Q of course gives divergent contributions but these contributions are handled by renormalization which effectively cuts off the integrals above the renormalization scale μ that conveniently may be taken as Q .

If one considers the complex momentum plane, then as $Q \rightarrow \infty$, many of the momentum integrations can be deformed away from the propagator singularities, and those give therefore vanishing contributions at asymptotic Q . There may, however, be contributions which cannot be deformed away from the propagator poles. These contributions arise from surfaces in loop momentum space which are called “pinch-singular surfaces” (PSSs). The PSSs therefore give important contributions which must be taken into account. To determine the strengths of the different PSSs a power counting analysis is employed. Via the power counting one also can see the appropriate approximations to be made in the different momentum regions, and this is highly relevant for factorization.

The interesting regions where there might be large contributions to the graphs for any given process are thus regions where a given loop momentum k has small virtuality, $|k^2| \ll Q^2$. Consider semi-inclusive DIS where a hadron of momentum p_B is produced away from the target, *i.e* the large component of p_B is its minus component. The target hadron has momentum p_A which is large in the plus direction.

We show in figure (left graph) 2 a so-called “reduced graph” for the important PSSs. In obtaining a reduced graph from the full Feynman graph one contracts to points all the lines whose denominators are not pinched. This follows from the observation that those lines

in the limit $Q^2 \rightarrow \infty$ carry much larger momentum than the pinched lines and therefore in a space-time picture they would reduce to points. The regions H, C_A, C_B, S denote the different momentum regions where the momenta are large and of order Q (for H), collinear to p_A (for C_A), collinear to p_B (for C_B), and small of order m (for S). In the asymptotic limit, p_A and p_B become exactly light-like, and the exact PSSs correspond to these limits where the virtuality vanishes. Of course in the realistic (non-asymptotic) case the momenta are not exactly light-like so the exact PSSs form a sort of skeleton of the corresponding region (for example the PSS for C_A is the skeleton where the given momentum k is exactly parallel to the light-like limit of p_A , while the whole region of C_A also contains momenta which are approximately collinear to p_A). The soft PSS corresponds to the exact limit of S where all momentum components of k are 0. Thus in general, momenta belonging to S have all their component small (no component is enhanced by any factor of Q , and they stay fixed as $Q \rightarrow \infty$). The soft lines can therefore connect to any other region. If k_S is a soft line and is added to say k_A which is in C_A , then $k_S + k_A$ still belongs to C_A . We notice, however, that lines in C_B and C_A cannot be directly added to each other because adding two light-like momenta in opposite directions gives a non-light-like momentum far off shell, and such a line does not belong to any of the two regions (it actually belongs to the hard region H). The collinear lines can, however, be added to the hard part since the result is again a hard momentum. Thus one finds the connections between the regions as in figure 2. We also show in figure 2 (right graph) the Drell-Yan lepton pair production where again there are two collinear regions associated with the incoming momenta p_A and p_B , and in addition there is the hard part where all momenta are of order Q , and there is again the soft graph connecting possibly to any of the other regions.

In a collinear pinch, say collinear to the $+$ direction, the typical scales for the momenta are $k^+ \sim Q$, $k^- \sim m^2/Q$ and $k_\perp \sim m$. In the soft pinch on the other hand all components satisfy $k^\mu \sim m$, while in the hard region the virtuality is large $|k^2| \sim Q^2$. There can also be several collinear regions C_i in a given process. For example in DIS we can have several jets emerging from the hard scattering, each defining its own collinear region. Notice also that a *single* Feynman graph can have multiple leading PSSs. This is so because for any given momentum line k in the original graph, we have the possibility that k is in any of the allowed regions for that graph.

Consider now in QCD gluons exchanged between the different regions. Let us assume we have a collinear-to- A gluon k exchanged between the hard part H and C_A . We then have a contribution of the type

$$H^\mu N_{\mu\nu}(k) C_A^\nu. \quad (3.6)$$

Since C_A contains momenta which are large in the $+$ direction, the contribution proportional to C_A^+ is boosted by a factor Q , and we see that the leading contribution satisfies

$$H^\mu N_{\mu\nu}(k) C_A^\nu \approx H^- N^{+-}(k) C_A^+. \quad (3.7)$$

Similar relations hold for gluons exchanged between H and C_B . If, however, a gluon is exchanged between H and the soft region S , there is no large boost factor associated

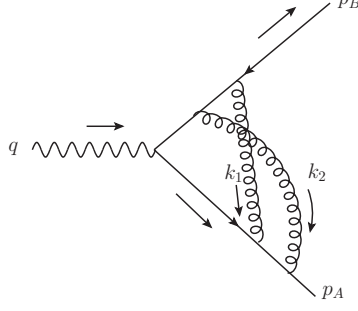


Figure 3: A two loop contribution to the Sudakov form factor.

with S . In fact the H -to- S couplings give power suppressed corrections and therefore the leading power contribution does not contain any lines attaching H to S (see below). As a simple example consider figure 3 where a time-like photon q produces an exclusive pair of an anti-quark with large minus momentum p_B , and a quark with large plus momentum p_A (this is a two-loop contribution to the Sudakov form factor). In the Feynman graph shown in figure 3, one possibility is that the gluon k_1 is collinear to p_A , while k_2 is soft. It is then easily seen that $p_A - k_1 - k_2$ and $p_A - k_2$ are collinear to p_A , while $p_B + k_1$ and $p_B + k_1 + k_2$ are hard lines (since their virtualities are of order Q^2). The reduced graph for this Feynman graph is shown in figure 4 (left graph). The contribution is proportional to

$$g_s^4 \bar{u}(p_A) \gamma^{\mu_2} \frac{\not{p}_A - \not{k}_2}{(p_A - k_2)^2 + i\epsilon} \gamma^{\mu_1} \frac{\not{p}_A - \not{k}_1 - \not{k}_2}{(p_A - k_1 - k_2)^2 + i\epsilon} \frac{N_{\mu_1 \nu_1}(k_1)}{k_1^2 + i\epsilon} \gamma^\mu \frac{\not{p}_B + \not{k}_1 + \not{k}_2}{(p_B + k_1 + k_2)^2 + i\epsilon} \gamma^{\nu_2} \frac{\not{p}_B + \not{k}_1}{(p_B + k_1)^2 + i\epsilon} \gamma^{\nu_1} v(p_B) \frac{N_{\mu_2 \nu_2}(k_2)}{k_2^2 + i\epsilon}. \quad (3.8)$$

To pick up the leading contributions we project out the $+$ component inside the C_A part (which consists of the factors to the left of γ^μ). This part can then be written as

$$\gamma^+ \frac{2p_A^+}{-2p_A^+ k_2^- + i\epsilon} \frac{\not{p}_A - \not{k}_1}{-2(p_A^+ - k_1^+) k_2^- + i\epsilon} \frac{N^{-+}(k_1)}{k_1^2 + i\epsilon} \sim \frac{Q}{Q \lambda_s} \frac{Q}{Q \lambda_s} \frac{1}{\lambda_A^2}. \quad (3.9)$$

Here we have introduced typical momentum scales for the collinear and soft regions, λ_A and λ_s respectively, such that for any collinear-to- A (C_A) momentum, k_A , we have $k_A^2 \sim \lambda_A^2$, while for the soft momentum, k_s , we have $k_s^2 \sim \lambda_s^2$. Notice that since $k_A^+ \sim Q$, this means that $k_A^- \sim \lambda_A^2/Q$. The soft region in (3.8) simply consists of the soft propagator $1/k_2^2 \sim 1/\lambda_s^2$, and the momentum integral $\int d^4 k_s \sim \int d\lambda_s \lambda_s^3$. The collinear-to- B region, C_B , is elementary while the hard region power counts as

$$\frac{\not{p}_B}{2p_B^- k_1^+ + i\epsilon} \gamma^- \frac{\not{p}_B}{2p_B^- k_1^+ + i\epsilon} \gamma^- \sim \frac{Q}{Q^2} \frac{Q}{Q^2}. \quad (3.10)$$

The PSSs then give

$$\int^{\sim Q} d\lambda_A \lambda_A^3 \int^{\sim Q} d\lambda_s \lambda_s^3 \frac{1}{Q^2} \frac{1}{\lambda_A^2} \frac{1}{\lambda_s^2} \frac{Q}{Q \lambda_s} \frac{Q}{Q \lambda_s} = \int^{\sim Q} \frac{d\lambda_A}{\lambda_A} \left(\frac{\lambda_A}{Q} \right)^2 \int^{\sim Q} \frac{d\lambda_s}{\lambda_s}. \quad (3.11)$$

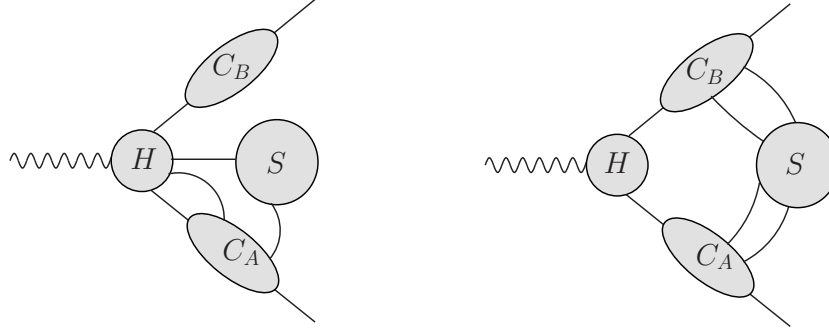


Figure 4: Examples of reduced graphs for the two loop Sudakov form factor.

The complete result is given by multiplying (3.11) with the LO graph.

In figure 4 (right graph) we show the case where both k_1 and k_2 are soft gluons. Here, the hard part is elementary while the soft part now contains both gluon propagators. It is easy to see that we get in this case

$$\int^{\sim Q} d\lambda_{s,1} \lambda_{s,1}^3 \int^{\sim Q} d\lambda_{s,2} \lambda_{s,2}^3 \frac{Q^2}{(Q\lambda_{s,1})^2} \frac{Q^2}{(Q\lambda_{s,2})^2} \frac{1}{\lambda_{s,1}^2} \frac{1}{\lambda_{s,2}^2} = \int^{\sim Q} \frac{d\lambda_{s,1}}{\lambda_{s,1}} \int^{\sim Q} \frac{d\lambda_{s,2}}{\lambda_{s,2}}. \quad (3.12)$$

The contribution from the PSS (3.12) as we see has no suppression compared to the LO graph, while (3.11) has a power suppression. The power suppression comes from the coupling of the soft part to the hard part.²

For a given amplitude, cross section or structure function to be analyzed we denote the leading power obtained by dimensional analysis as Q^p , where $p = 4 - E_L$ with E_L counting the number of external lines. For the Sudakov form factor in figure 3, $E_L = 3$, so the lowest order contribution grows as Q . For DIS, $E_L = 4$ and the leading power is Q^0 . For a given PSS, we then generally have integrals of the form

$$Q^{p_1} \int^{\sim Q} \frac{d\lambda}{\lambda} \lambda^{p_2}, \quad (3.13)$$

where p_1 and p_2 are different powers.

Making use of dimensional analysis and Lorentz invariance, one then finds in QCD the following results [1]: For a collinear region C , every line joining C to H gives a power λ/Q *except* for longitudinally polarized gluons, carrying polarization N^{+-} , for which there is no suppression. For the soft region, every gluon coupling S to H gives a factor λ/Q (as in the example of (3.11)) while every fermion gives $(\lambda/Q)^{3/2}$. Every fermion coupling S to C gives a factor $(\lambda/Q)^{1/2}$. Thus all couplings between S and other regions are suppressed, *except* for longitudinally polarized gluons between S and C for which there is no suppression.

²It may seem in (3.11) that performing the λ_A integral gives a contribution of order unity since we integrate all the way up to Q . However, the integral is completely dominated by the upper limit where the momentum is no longer collinear-to- A but is instead is hard. In the definition of the hard region there will be a subtraction of the smaller PSSs, for example C_A . That subtraction will cancel the dominant contribution of the integral and ensure that (3.11) is truly power-suppressed.

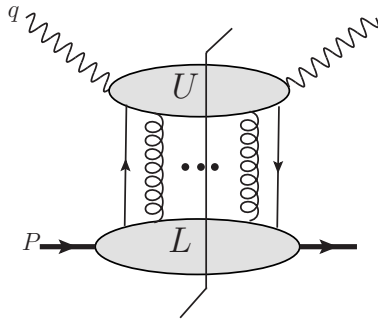


Figure 5: Generic contribution to inclusive DIS in simplified case.

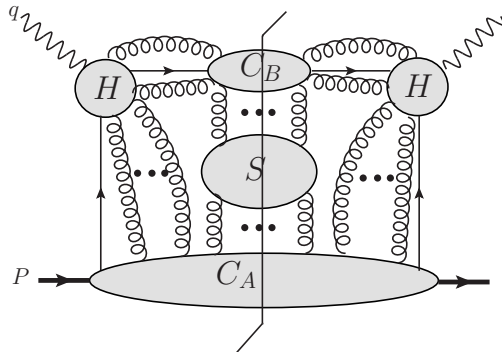


Figure 6: Generic contribution to inclusive DIS.

There is thus no penalty for coupling C and H , and S and C via longitudinally polarized gluons. For more details, see [1, 8, 9]. In the cases where there is no suppression, the integrals (3.13) usually produce logarithms $\ln Q^2/m^2$ that accompany the leading power (this is due to the renormalizable nature of QCD in which the coupling is dimensionless), as for example in (3.12).

3.1.3 Factorization in simple theory

The results above show that in QCD one has to take into account arbitrarily many gluon exchanges, of longitudinal polarizations, between the different regions (except for S -to- H couplings which are always power suppressed regardless of polarization). The proof for factorization is then more complicated compared to the simple parton model in figure 1 where gauge bosons are not present. Let us first, however, study a simplified situation by using the results from the power counting. This example will be illustrative for understanding the small- x calculations in section 4.

In figure 5 we show an example of inclusive DIS where arbitrarily many gluons are exchanged between the lower part L , which is collinear to the target hadron P , and the upper part U , which contains the hard scattering. Of course where the final state cut goes

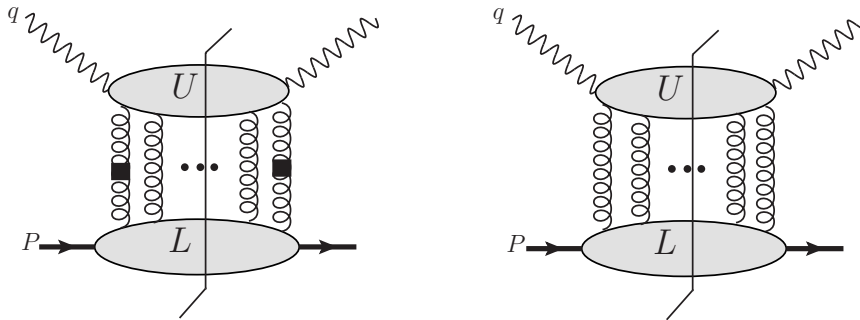


Figure 7: Pure gluonic contributions to DIS. Left: The black squares indicate transversely polarized gluons while all other gluons are longitudinally polarized. Right: Longitudinally polarized gluons only give a super-leading contribution in the hard scattering region.

through U , the cut lines are necessarily on-shell, but the bubble will still contain internal lines that are far off-shell. In a more complete picture one must consider instead the class of graphs shown figure 6. It can, however, be shown in the inclusive case by a sum-over-cuts argument that the momenta in the collinear region can be deformed out to the region where it is far off-shell, effectively reducing the leading graphs to that shown in figure 5. We thus treat the upper part of the diagram as the hard region. According to the analysis in the previous section, we then see that soft gluon couplings do not arise in the leading contributions.

We notice that one may also consider pure gluon exchanges between the upper and lower parts. If all gluons are longitudinally polarized, *i.e* contributing via N^{-+} , then a super-leading contribution arises which has power Q^2/m^2 relative to the leading case. However, Ward identities apply for these contributions, and a careful treatment shows that the super-leading piece actually cancels, leaving behind a remainder term that is leading only [71]. A leading contribution is also obtained when one of the gluons at each side of the cut is transversely polarized, we show this in figure 7 (left graph) where we denote the transversely polarized gluons using the black squares. Pure gluon exchange terms are important for the analysis in the small- x region which we come back to later.

The parton model result reviewed above can be exactly reproduced in a model field theory which is non-gauge (this removes all gauge boson attachments between L and U) and super-renormalizable (this implies that the hard part U is trivial as in figure 1). As a simplified case we instead imagine a theory which is still non-gauge but is renormalizable. This means that the higher order corrections to the hard part are not power suppressed anymore. Moreover it means that one has to also take into account the UV renormalization. At the same time it implies that the gauge boson exchanges shown in figure 5 are absent, and one obtains instead figure 8. Now, another way to think of this case is to actually consider full QCD in light-cone gauge $A^+ = 0$. In this case the leading gluon coupling vanishes since

$$N^{-+}(k) = g^{-+} - \frac{n^-k^+ + n^+k^-}{k^+n^-} = 1 - 1 = 0. \quad (3.14)$$

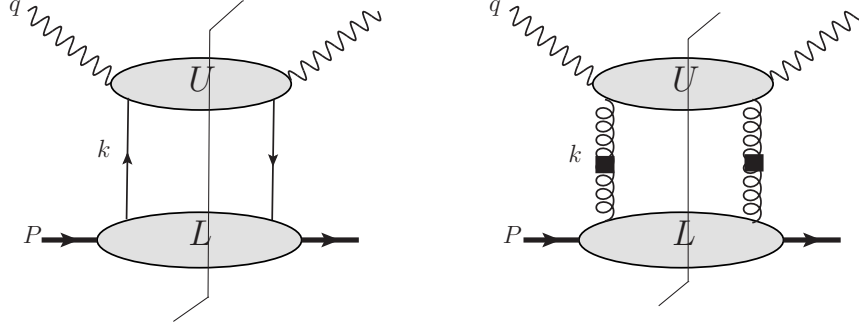


Figure 8: Leading contribution in the simplified case in non-gauge theory (only left graph) or in light-cone gauge QCD (both graphs).

Therefore in figure 5, all gluon couplings again vanish to leading power. In figure 7 it means on the other hand that only the two transversely polarized gluons remain, as shown in figure 8.

A factorization formula for figure 8 can now be obtained rather easily by assuming that there is a clear separation in momenta for the exchanged line k , namely that it can either be hard or collinear to P . We can then write the hadronic tensor as (neglecting photon indices)

$$W = \int \frac{d^{4-2\epsilon}k}{(2\pi)^{4-2\epsilon}} U^{\{\alpha\}}(k, q) L_{\{\alpha\}}(k, P), \quad (3.15)$$

where the index $\{\alpha\}$ collectively denotes all relevant labels such as flavor, color, polarization³. We again make the approximation of replacing k in U by $\hat{k} = (k^+, 0, 0_\perp)$. Thus one gets

$$W \sim \int \frac{dk^+}{k^+} U^{\{\alpha\}}(\hat{k}, q) k^+ \int \frac{dk^- d^{2-2\epsilon}k_\perp}{(2\pi)^{4-2\epsilon}} L_{\{\alpha\}}(k, P). \quad (3.16)$$

This formula is not yet in a fully factorized form, however, since there is still the sum over the labels $\{\alpha\}$. We note that U must be diagonal in the color indices since the photon is color singlet. Consider first the quark contribution shown in figure 8 (left graph). To fully factorize F we can then apply exactly the same argument as in the parton model case in going from equation (3.3) to (3.4). We then get just as in (3.4)

$$W \sim \int \frac{d\xi}{\xi} \left[\text{Tr} U_j(\xi P^+, q^-, 0_\perp) \frac{\hat{k}}{2} \right] \left[\text{Tr} \int \frac{dk^- d^{2-2\epsilon}k_\perp}{(2\pi)^{4-2\epsilon}} \frac{1}{2} \gamma^+ L_j(k, P) \right]. \quad (3.17)$$

Summation over the color indices in L is kept implicit. Corrections to the factorization formula are power suppressed by the analysis in section 3.1.2.

³Of course in a non-gauge theory we need not consider the color indices but as the analysis is also relevant for light-cone QCD we include all quantum labels.

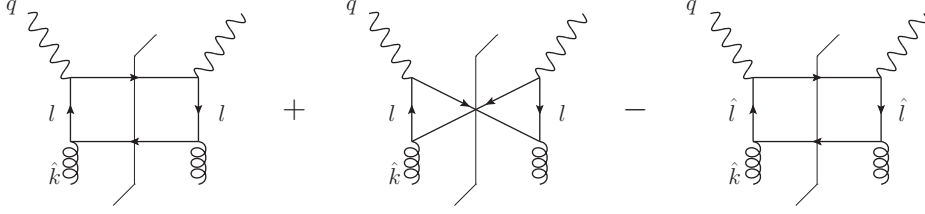


Figure 9: Example of subtraction in the NLO gluon coefficient. The subtraction removes the contribution where the loop momentum l is target-collinear, indicated by \hat{l} in the last graph.

For the gluon contribution shown in the right graph of figure 8 we instead find

$$W \sim \int \frac{dk^+}{k^+} U^{ij}(\hat{k}, q) k^+ \int \frac{dk^- d^{2-2\epsilon} k_\perp}{(2\pi)^{4-2\epsilon}} L_{aa}^{ij}(k, P). \quad (3.18)$$

We then notice that the upper part U is diagonal in the transverse and color indices which gives the factorized form

$$W \sim \int \frac{d\xi}{\xi} \left[\frac{1}{2} U^{jj}(\hat{k}, q) \right] \left[\xi P^+ \int \frac{dk^- d^{2-2\epsilon} k_\perp}{(2\pi)^{4-2\epsilon}} L_{aa}^{ii}((\xi P^+, k^-, k_\perp), P) \right]. \quad (3.19)$$

The second factor here defines, preliminarily, the integrated gluon distribution. We shall see in section 4 that the elementary definition of the TMD gluon distribution in axial gauge in the small- x limit is given by the very same set of approximations.

This simple derivation of factorization cannot be strictly true, however. Namely, the main assumption that a clear separation of scales is possible is not generally true in a renormalizable theory like QCD. For example in the above calculation we assume that $k_\perp \sim m$, while the case $k_\perp \sim Q$ would have instead contributed to the next-to-leading order correction to the hard part H . There is, however, also an intermediate region, where $m \lesssim k_\perp \lesssim Q$, and k is neither exactly target collinear nor exactly hard, and as a consequence it is not clear in the above formalism how to exactly handle k in this case. For the assumptions above to thus hold, it must be true that this intermediate region can be safely omitted. This is, however, not the case. In fact, the renormalizability of QCD implies that there are in general logarithmic contributions,

$$\int_{\sim m^2}^{\sim Q^2} \frac{dk_\perp^2}{k_\perp^2} \sim \ln Q^2/m^2. \quad (3.20)$$

There is therefore no power suppression of the intermediate region, and in fact it is even enhanced by a logarithm. A full treatment must therefore treat such regions correctly, and this can in general be done by a subtractive formalism [1]. This means that each PSS is defined with subtractions of the smaller PSSs that it contains, to prevent double counting and ensure that it indeed is dominated by the momenta associated with it. For the hard part U in figure 8, one should therefore include a subtraction of the target-collinear PSS. We show examples of these subtractions in DIS for the gluon and quark contributions in

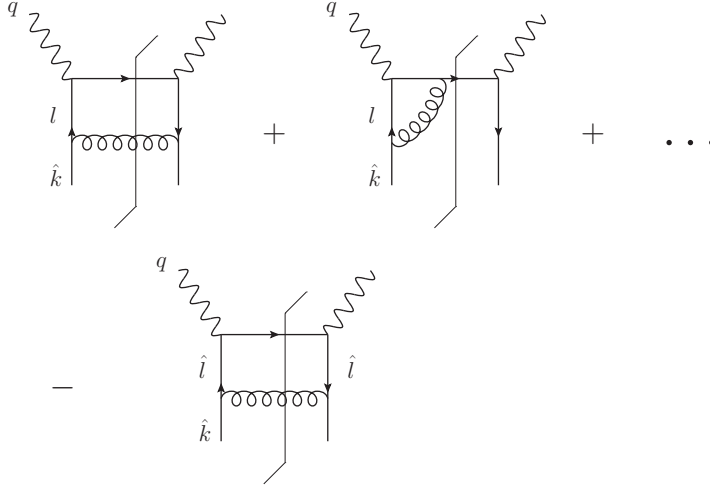


Figure 10: Example of subtraction in the NLO quark coefficient. The subtraction removes the contribution where the loop momentum l is target-collinear, indicated by \hat{l} in the last graph.

figures 9 and 10 respectively. If we denote by $d\Pi$ the phase space measure for the momenta contained in U then a more correct version of (3.19) reads

$$W \sim \int \frac{d\xi}{\xi} \left[\frac{1}{2} \int d\Pi \left[U^{jj}(\hat{k}, q) - \text{subtractions} \right] \right] \times \left[\xi P^+ \int \frac{dk^- d^{2-2\epsilon} k_\perp}{(2\pi)^{4-2\epsilon}} L_{aa}^{ii}((\xi P^+, k^-, k_\perp), P) \right]. \quad (3.21)$$

The integrated (bare) gluon distribution is thus given by

$$\begin{aligned} f_g^{(0)}(\xi) &= \xi P^+ \int \frac{dk^- d^{2-2\epsilon} k_\perp}{(2\pi)^{4-2\epsilon}} L_{aa}^{ii}((\xi P^+, k^-, k_\perp), P) \\ &= \int \frac{dx^-}{2\pi \xi P^+} e^{i\xi P^+ x^-} \langle P | F_{(0)a}^{+i}(0^+, x^-, 0_\perp) F_{(0)a}^{+i}(0) | P \rangle \end{aligned} \quad (3.22)$$

where the last result holds in $A^+ = 0$ gauge in QCD, apart from some technical problems associated with this gauge that we are neglecting.

As indicated in (3.22), the basic operator definitions of the parton distributions are for the bare fields of the Lagrangian. Note that it is these fields which have the canonical gauge transformation properties, and thus in discussing the gauge transformation properties of the parton distributions one necessarily refers to the operator definitions constructed out of the bare fields. The renormalization of the bare parton distributions is then an issue of the renormalization of non-local operators. While in the case of local field operators, the renormalization factor can be taken as a multiplicative constant which is independent of momenta and masses, for the non-local operators appearing in the definitions of the bare parton distributions one instead finds that there is a convolution with a renormalization factor. Basically if we denote the bare parton distribution for a parton of flavor j as

obtained from either (3.18) or (3.19) by $f_j^{(0)}(\xi)$, and the renormalized distribution by $f_j(\xi)$, we find

$$f_j(x; \mu) = \lim_{\epsilon \rightarrow 0} Z_{jj'}(\xi, \mu, \epsilon) \otimes_{\xi} f_{j'}^{(0)}(x/\xi; \mu, \epsilon), \quad (3.23)$$

where the convolution is an integral in ξ as in (3.18) and (3.19). The evolution of $f_j(x; \mu)$ with respect to μ is given by the DGLAP equations.

3.1.4 Including the gluons, and the Glauber region

For a fully satisfactory treatment of factorization in full QCD one needs, however, to deal with the gluon emissions. As we recall from section 3.1.2, in QCD we can without any power suppression exchange arbitrarily many longitudinally polarized gluons between the hard and collinear, and the soft and collinear regions respectively. We indicated this possibility already in figures 6 and 7. In the previous section we argued that in the collinear factorization of inclusive DIS at least, the structure of the leading graphs can be simplified by choosing the light-cone gauge $A^+ = 0$ which eliminates the leading longitudinally polarized gluons.

There is, however, a good reason to try to avoid the light-cone gauge in the generic treatment (see also sections 4.3, 4.4 and 4.5 below). Note from the arguments in the previous sections that the treatment of factorization is based on first analyzing the analytic structure of the Feynman graphs, identifying the PSSs, and then using power counting to extract the leading PSSs. To guarantee that the power counting arguments work properly, contour deformations must be performed when necessary. In particular, if k is a momentum in the soft region, then there is the possibility that the components of k do not all scale with the same power λ_s , but that the longitudinal components k^+ and k^- might be parametrically much smaller than k_{\perp} . This happens if k^+ or k^- is pinched by the collinear lines it attaches to. For example, if k couples to a collinear line p_A then a propagator,

$$(p_A + k)^2 + i\epsilon, \quad (3.24)$$

arises. The pole for k^- is then

$$k^- \sim \frac{m^2}{Q} - i\epsilon. \quad (3.25)$$

Thus k^- is parametrically much smaller than $\lambda_s \sim m$. When this happens, we say the momentum is in the Glauber region, $k^+ k^- \ll k_{\perp}^2$. Now, if no other such pole is present, or if all such poles lie in the same part of the imaginary plane (all below or above the real axis), then we can deform the contour away from this pole to keep $k^- \sim \lambda_s$. If, however, another pole exists simultaneously, such that

$$k^- \sim \frac{m^2}{Q} + i\epsilon \quad (3.26)$$

then the k^- contour is pinched, and cannot be deformed. It might still be possible to deform on k^+ but if not, then the standard power counting fails. The longitudinal polarizations

then no longer dominate and one cannot use the eikonal approximations needed to obtain factorization.

The use of the light-cone gauge implies that the analytic structure of the individual Feynman graphs is altered, since now an additional pole $1/k^+$ is introduced with each propagator. This has obvious implications for the factorization proofs. These poles might for example introduce pinch points that are not present in a covariant gauge. Moreover, the gauge poles $1/k^+$ commonly give rise to integrals of the form

$$\int_0^\infty dk^+ \frac{1}{k^+} I(k^+, k_\perp), \quad (3.27)$$

and these diverge as $k^+ \rightarrow 0$. Notice that the divergences arise from end point singularities and can therefore not be treated by any $i\epsilon$ prescription or principal value. In fact there exists no generalized function which is a “canonical regularization”, in the sense described in [72], of this integral.

These divergences are in fact the rapidity divergences we mentioned in sections 2.2 and 2.3. They also arise when the eikonal approximation is used in a covariant gauge. In the integrated distribution, there is actually a cancellation between real and virtual terms, which means that in (3.27)

$$\int d^2 k_\perp I(k^+ = 0, k_\perp) = 0. \quad (3.28)$$

This leads to the well-known “plus prescription”, $\left(\frac{1}{1-z}\right)_+$. In TMD distributions, however, no cancellation occurs, since $I(0, k_\perp) \neq 0$, and the light-cone gauge therefore introduces problems. The light-cone gauge is moreover not useful when several different collinear directions are relevant.

The general method for factorizing the arbitrary order gluon couplings between the different regions is based on exploiting the gauge symmetries of the leading terms, and to use Ward identities (Slavnov-Taylor-Ward identities). The basic technique can be understood as follows. In Feynman gauge, let k be a soft gluon coupling the regions S and A . We then have a contribution of the type

$$A^\mu(k, p_A) g_{\mu\nu} S^\nu(k). \quad (3.29)$$

Generally of course there will be many other couplings, and A and S will depend on additional momenta but that does not matter for the approximation we are explaining. The leading contribution is then

$$\begin{aligned} A^\mu(k, p_A) g_{\mu\nu} S^\nu(k) &\sim A^+(\hat{k}_B, p_A) S^-(k) \\ &= A^\mu(\hat{k}_B, p_A) \frac{\hat{k}_{B,\mu} n_{A,\nu}}{k \cdot n_A} S^\nu(k), \end{aligned} \quad (3.30)$$

where

$$\hat{k}_B = (k \cdot n_A) n_B = (0^+, k^-, 0_\perp). \quad (3.31)$$

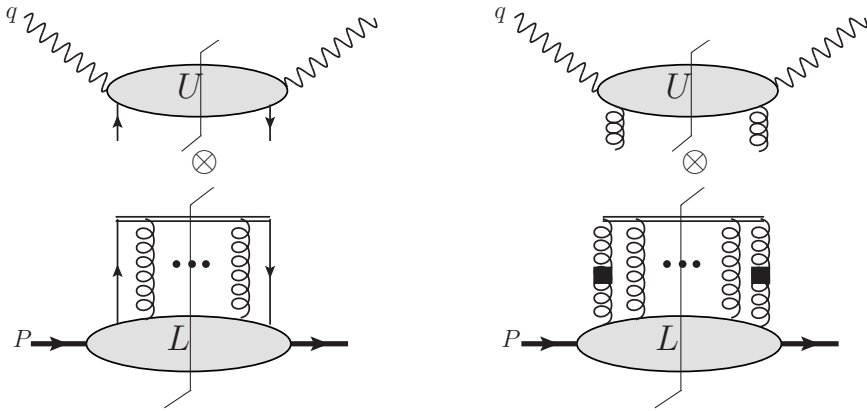


Figure 11: Factorized structure in inclusive DIS in covariant gauge. The longitudinal gluon emissions are factorized into eikonal Wilson lines (double lines) to provide gauge invariant definitions of the parton distributions. Left: Quark distribution. Right: Gluon distribution where the gluons with black squares are transversely polarized gluons.

Here n_A is a light-like vector in the direction of p_A , with $n_A \cdot V = V^-$ for any V . Thus $\hat{k}_B \cdot n_A = k \cdot n_A$. Since now the polarization of the gluon k is multiplied by its momentum in the coupling to A , Ward identities can be applied. The eikonal denominator in (3.30) gives a contribution in S from a Wilson line. The all-order gluon couplings between A and S can then be successively factorized into a Wilson line contribution in S .

One can similarly make approximations for the H -to- A couplings. The eikonal terms that arise are then absorbed into A to provide gauge invariant definitions of the basic parton distributions (or fragmentation functions). An example in the case of inclusive DIS is shown in figure 11 where the Wilson lines are indicated by double lines. The procedure of using the Ward identities for extracting the gluon exchanges between the different regions proceeds very much the same whether one is formulating collinear factorization or TMD factorization.

As we have seen, Wilson lines appear in the small- x formalisms as well, both in the Weizsacker-Williams distribution (2.5) and the dipole distribution (2.10). It is then rather important to understand the exact structure and derivation of these lines, in particular since differences appear between the dipole definition and the TMD distributions. We analyze these points in detail in [42].

3.1.5 TMD factorization

In the hard scattering formalism, the need for TMD factorization becomes obvious when one considers observables which are more sensitive to the exact kinematics of the final state. A typical example concerns the almost back-to-back production of hadrons [4] in e^+e^- annihilation shown in figure 12. Other relevant processes where one needs to consider TMD factorization are single-inclusive hadron production at low p_\perp in DIS (SIDIS) also shown in figure 12, and Drell-Yan lepton pair production shown in figure 13 where the total

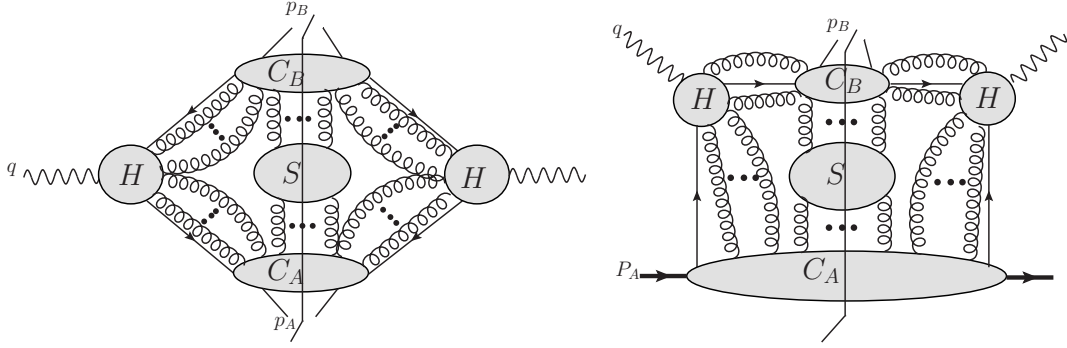


Figure 12: Processes where TMD factorization is relevant. Left: Di-hadron production in e^+e^- . Right: Hadron production in SIDIS.

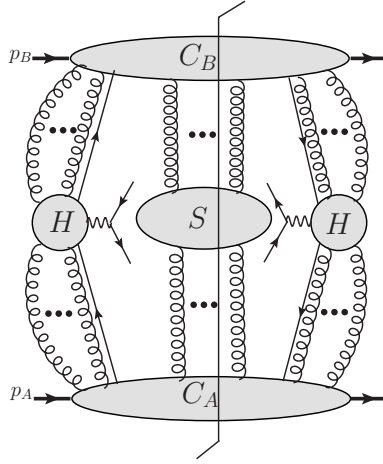


Figure 13: Leading regions for TMD factorization in Drell-Yan lepton pair production.

transverse momentum of the lepton pair is much smaller than the hard scale. In all these cases the kinematics is sensitive to low values of the observable transverse momentum q_\perp , and one cannot therefore neglect any of the transverse momenta flowing through the regions C_A , C_B and S , as doing so would significantly change the kinematics of the observable final state products. If on the other hand the relevant transverse momentum observables are large, of the order of the hard scale Q , then the effects of the transverse momentum flowing out from the collinear regions via the soft region is power suppressed and can be neglected. In that case one obtains the standard integrated (collinear) factorization.

Note, however, that the transverse momentum flowing directly into the hard part H from the collinear regions C_A and C_B can still be neglected, since the error involved in this approximation is of order q_\perp/Q which is small in the validity region of TMD factorization. As $q_\perp \rightarrow Q$ the TMD formula loses its accuracy but then one enters the region where ordinary integrated factorization is valid. When $q_\perp \sim Q$, the transverse momentum must

be a part of the hard region, physically it corresponds to the case where several high q_\perp partons emerge from H . Thus what determines the need for TMD parton distributions and fragmentation functions is the kinematics of the final state. The momenta entering H from the collinear region C_A or C_B can still be approximated to be on-shell, even in the case of TMD factorization. This is somewhat different than the small- x formulation where the gluon momentum entering the hard scattering (if there is any) is off-shell, its virtuality being determined by the transverse momentum.

The factorization formula in case of hadron pair production in e^+e^- annihilation involves the transverse momentum convolution of two fragmentation functions (since there is no hadronic initial state in this process). The factorized formula for the relevant hadronic tensor is obtained by applying the appropriate Ward identities for the longitudinally polarized gluons exchanged between leading regions shown in figure 12 (left graph). If the momentum entering regions C_A , C_B and S is denoted respectively by k_A , k_B and k_S , then the factorized formula is given by (we denote C_A by A , and C_B by B for clarity)

$$W^{\mu\nu} = \int d^4k_A d^4k_B d^4k_S A(k_A) B(k_B) S(k_S) H^{\mu\nu}(q) \delta^{(4)}(q - k_A - k_B - k_S). \quad (3.32)$$

The delta function can be used to fix $k_{S,\perp}$, k_A^+ and k_B^- . One furthermore makes the approximation of ignoring k_A^- (k_B^+) everywhere but in A (B), and ignoring k_S^\pm everywhere but in S . These approximations are allowed since the corrections are power-suppressed at least as m^2/Q^2 . The integrals over these variables can then all be short circuited and one gets

$$\begin{aligned} W^{\mu\nu} &= \int d^2k_{A,\perp} d^2k_{B,\perp} \left(\int dk_A^- A(k_A) \right) \left(\int dk_B^- B(k_B) \right) \left(\int dk_S^+ dk_S^- S(k_S) \right) H^{\mu\nu}(q) \\ &= \int d^2k_{A,\perp} d^2k_{B,\perp} A(z_A, k_{A,\perp}) B(z_B, k_{B,\perp}) S(q_\perp - k_{A,\perp} - k_{B,\perp}) H^{\mu\nu}(q). \end{aligned} \quad (3.33)$$

Each respective factor in the parentheses gives the basic operator definition of the fragmentation functions and the soft factor. We mentioned in sections 3.1.2 and 3.1.3 that each given PSS contains subtractions of the smaller PSSs. Thus the collinear factors A and B in (3.33) contain subtractions of the soft region. Now, the unsubtracted collinear parts contain Wilson lines which arise from the factorized gluon couplings to the hard part H . This is done by using the approximation in (3.7), rewriting this as in (3.30) and applying the Ward identities. For the A -to- H couplings, the approximated momenta from (3.7) are $\hat{k}_A = (k^+, 0^-, 0_\perp) = (k \cdot n_B) n_A$ and therefore we get a Wilson line in the direction n_B :

$$W(x; n_B) = P \exp \left(-ig_s \int_0^\infty d\lambda A(x + n_B \lambda) \cdot n_B \right). \quad (3.34)$$

For the B part we instead get a Wilson line in the direction n_A . In figure 14 we graphically represent the unsubtracted collinear part, including the Wilson line (3.34) shown by double lines, for both a parton distribution (top two graphs) and a fragmentation function (bottom two graphs). The color representation of the Wilson line (3.34) is determined by the particle at the end of the double lines in figure 14: Fundamental for a quark (top and bottom left), adjoint for a gluon (top and bottom right).

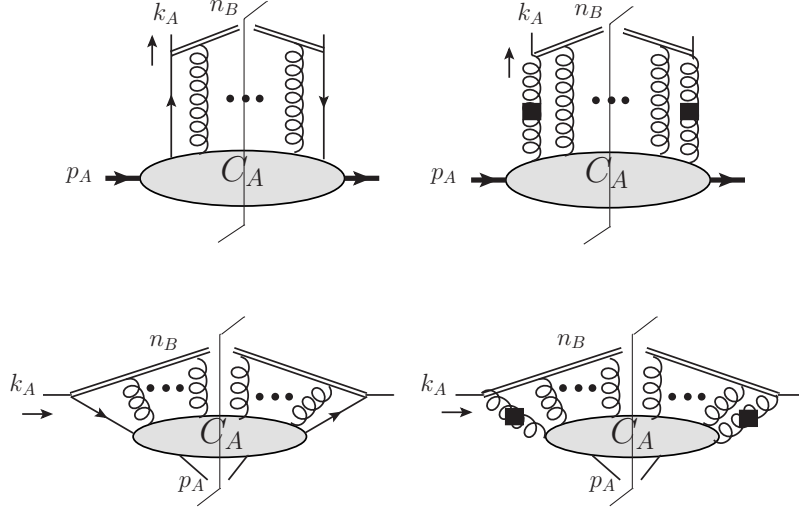


Figure 14: Graphical representation of the unsubtracted collinear part after the gluon couplings to the hard part have been factorized into Wilson lines in the direction n_B . Left: Quark distribution. The black squares indicate transversely polarized gluons. Top: Collinear part in a parton distribution. Bottom: Collinear part in a fragmentation function.

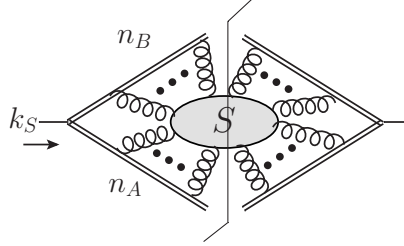


Figure 15: The factorized soft part. On each side of the cut, the gluons that couple to regions A and B are factorized into Wilson lines in the directions n_A and n_B respectively.

The soft gluons are similarly summed into Wilson lines using (3.30). From the A side we see we get a line in the direction of n_A while from the B side we instead get a line in the direction of n_B . The definition of the collinear part involves always the hadron state $|P\rangle$, either as incoming (for a parton distribution) or as outgoing (for a fragmentation function). The soft factor on the other hand does not contain such a hadron so it is defined as a vacuum expectation value which we represent in figure 15.

As seen from (3.33), it is convenient to make a Fourier transform into transverse coordinate b_\perp to obtain

$$W^{\mu\nu} = \int d^2b_\perp e^{-iq_\perp \cdot b_\perp} A(z_A, b_\perp) B(z_B, b_\perp) S(b_\perp) H^{\mu\nu}(q) \quad (3.35)$$

which is simpler than the momentum convolution written above.

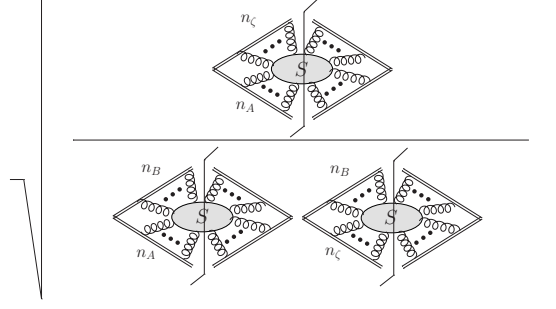


Figure 16: The soft factor absorbed into the unsubtracted parton distributions and fragmentation functions. In the final result, n_A and n_B can be taken exactly light-like since the rapidity divergences cancel those in the unsubtracted collinear factor. The vector n_ζ cannot be taken light-like, however.

In the final definition, the soft factor is absorbed completely into the collinear factors to define the final subtracted fragmentation functions given by [1]

$$D_{H_A/f}(z_A, b_\perp; \zeta, \mu) = D_{H_A/f}^{\text{unsub}}(z_A, b_\perp; n_B) \times \sqrt{\frac{S(b_\perp; n_A, n_\zeta)}{S(b_\perp; n_A, n_B)S(b_\perp; n_\zeta, n_B)}} \times Z \quad (3.36)$$

Here n_A and n_B are taken light-like, and Z is the UV renormalization factor. The somewhat strange looking factor in the square root is shown in figure 16. The precise motivation for it is described in detail in [1, Ch. 13]. The final definition is free from divergences associated with Wilson line self-energy corrections. The vector n_ζ defining the directions of the Wilson line in the soft factors serves as the rapidity cut-off which we indicate by the ζ dependence of the fragmentation function. The unsubtracted factor D^{unsub} is given exactly by the factors in figure 14 (bottom left graph in current example), defined in addition with integral over k^- as in (3.33), and the Fourier transform from k_\perp to b_\perp . A similar definition applies for the second fragmentation function associated with the region B . The final factorization formula then reads

$$W^{\mu\nu} \propto \frac{z_A z_B}{Q^2} H_f^{\mu\nu}(Q; \mu) \int d^2 b_\perp e^{-iq_\perp \cdot b_\perp} D_{H_A/f}(z_A, b_\perp; \zeta, \mu) D_{H_B/\bar{f}}(z_B, b_\perp; \zeta, \mu), \quad (3.37)$$

where $z_{A,B} = p_{A,B}/k_{A,B}$, and

$$H_f^{\mu\nu} = \text{Tr} \not{k}_A H_f^\nu \not{k}_B H_f^{\mu\dagger}. \quad (3.38)$$

H^ν and $H_f^{\mu\dagger}$ stand for the hard blobs shown in figure 12, defined to be irreducible in the collinear lines, and containing subtractions of the collinear and soft regions, just like in (3.21).

The tensor $W^{\mu\nu}$ of course cannot depend on the rapidity cut-off ζ , and this requirement is embedded in the Collins-Soper evolution equation of the fragmentation functions with respect to ζ . In SIDIS we instead have a convolution of one parton distribution (for the incoming target hadron) and one fragmentation function (for the final state hadron),

$$W^{\mu\nu} \propto \frac{z}{Q^2} H_f^{\mu\nu}(Q; \mu) \int d^2 b_\perp e^{-iq_\perp \cdot b_\perp} f_{f/H_A}(x, b_\perp; \zeta, \mu) D_{H_B/\bar{f}}(z, b_\perp; \zeta, \mu) \quad (3.39)$$

where $H_f^{\mu\nu}$ is given by the same expression as in (3.38) (but of course the hard factors $H^{\mu\dagger}$ and H^ν are different in e^+e^- and DIS), and $x = k_A^+/p_A^+$ and $z = p_B^-/k_B^-$. Thus the change is that one fragmentation function is simply exchanged for the parton distribution function of the target hadron. The parton distribution f is defined exactly as in (3.36) to include the soft factors, one simply needs to change D^{unsub} to f^{unsub} which means (for quarks) replacing the bottom left graph in figure 14 with the top left one.

Finally in the Drell-Yan process we instead have two parton distributions and there is no fragmentation function since the observed final state is leptonic. Thus

$$W^{\mu\nu} \propto \frac{s}{Q^2} H_f^{\mu\nu}(Q; \mu) \int d^2 b_\perp e^{-iq_\perp \cdot b_\perp} f_{f/H_A}(x_A, b_\perp; \zeta, \mu) f_{\bar{f}/H_B}(x_B, b_\perp; \zeta, \mu) \quad (3.40)$$

where now the hard coefficient $H^{\mu\nu}$ is the tensor for the on-shell partonic reaction $f\bar{f} \rightarrow \gamma^*$. The extra factor s in front of the integral arises from the definition of the hadronic tensor for the Drell-Yan process which reads

$$W^{\mu\nu} = s \int d^4 x e^{iq \cdot x} \langle p_A, p_B | J^\mu(x) J^\nu(0) | p_A, p_B \rangle. \quad (3.41)$$

In order to obtain a reliable estimate of $H^{\mu\nu}$ it is optimal to let $\mu \sim Q$ so as to avoid large logarithms. The higher order corrections are then subleading in factors of $\alpha_s(\mu \sim Q) \ll 1$ without any logarithmic enhancements, and thus fixed order perturbative calculations are reliable. Notice again that in all formulas above, the hard tensor $H^{\mu\nu}$ is always outside the transverse momentum (or coordinate) integral and the lines entering it are on-shell.

Thus we see that the TMD parton distributions or fragmentation functions, compared to the basic parton model definitions, depend additionally on the variables ζ and μ . They consequently satisfy evolution equations with respect to both these variables. The evolution in μ is given by the standard DGLAP equations while the evolution with respect to the rapidity variable ζ is given by the (Collins-Soper) CS evolution equation [1]. The CS kernel controlling the rapidity evolution is the same for all the above reactions because it is determined by the soft factor which is the same in all the above examples.

We have above outlined the fundamentals of factorization in QCD, in processes where a hard scale Q is present, and where the collinear directions scale with Q . In the small- x region there may or may not be present a hard scale. The traditional process to study is small angle two-particle elastic scattering where the momentum transfer t is much smaller than the cms energy s , and where the collinear momenta scale with \sqrt{s} . In this case the hard region, if present, has a scale Q which is fixed, and is therefore not proportional to the asymptotic variable \sqrt{s} . The leading regions are therefore somewhat different than in the hard scattering factorization. We will outline the relevant regions for the small- x case in section 4.1 where we examine single inclusive particle production. We now go through the main formulations of k_\perp -factorization in the BFKL and CGC formalisms, and compare these to the hard scattering case just discussed.

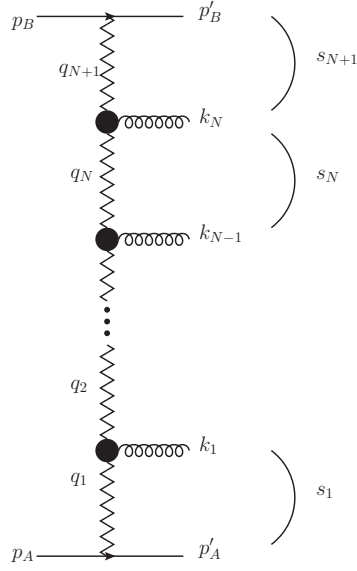


Figure 17: The multi-Regge-factorized form of the scattering amplitude in BFKL.

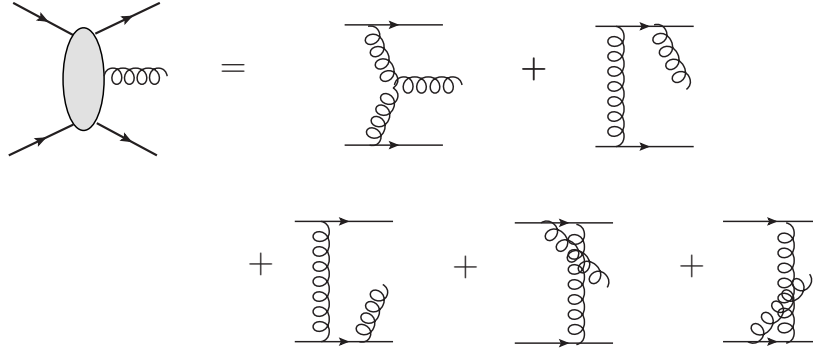


Figure 18: Graphs contributing to Lipatov vertex.

3.2 Factorization in BFKL

“Factorization” in the BFKL formalism refers to the Regge factorization in which a given $2 \rightarrow n$ scattering amplitude is, in the asymptotic limit $s \rightarrow \infty$, written as a factorized product of effective vertices and couplings of “reggeized gluons”. This is known as the “multi-Regge form”. The arguments for the factorized form of the $2 \rightarrow n$ amplitudes go back to the pre-QCD days of Regge theory, and the so-called “multi-peripheral” models [62–64, 73].

We illustrate the multi-Regge form in figure 17. Here the zig-zag lines denote the Reggeons, and each black circle denotes the Reggeon-Reggeon-gluon vertex. Figure 17 is in the Regge theory valid when $s_i \rightarrow \infty$ for all i [63, 64].

In BFKL, the vertical zig-zag lines in figure 17 are given by gluons whose propagators

(in Feynman gauge) are obtained by

$$P_{\mu\nu}(q_i) = \frac{-ig_{\mu\nu}}{q_i^2 + i\epsilon} \rightarrow P_{\mu\nu}(q_i, s_i) = \frac{-ig_{\mu\nu}}{q_i^2 + i\epsilon} \left(\frac{s_i}{q_{\perp,i}^2} \right)^{\omega(q_{\perp,i}^2)-1} \quad (3.42)$$

where

$$\omega(q_{\perp,i}^2) - 1 = \alpha_s N_c \int \frac{d^{2+2\epsilon} \kappa_{\perp}}{(2\pi)^{2+2\epsilon}} \frac{-q_{\perp,i}^2}{\kappa_{\perp}^2 (\kappa_{\perp} - q_{\perp,i})^2}, \quad (3.43)$$

The function ω is called the “gluon Regge trajectory”. The vertices in figure 17 are given by the Lipatov vertex which is an effective three-gluon vertex. The Lipatov vertex is derived from the tree-level graphs of the $2 \rightarrow 3$ partonic amplitude shown in figure 18. The external partons may be quarks or gluons, the use of the eikonal approximations implies that the vertex is independent of the flavor of these particles (at least when the external particles are individual quarks or gluons).

The fundamental assertion of the BFKL formalism is that the multi-Regge form shown in figure 17 is valid for all $2 \rightarrow n$ amplitudes. It has been argued in reference [74] that the multi-Regge result can be shown to be correct to all orders, once it has been shown to be correct to one-loop order for *all* $2 \rightarrow n$ amplitudes, by essentially using the same techniques (s -channel unitarity relations) developed in Regge theory in [63, 64]. We are, however, not aware of any explicit higher order calculations in QCD of the $2 \rightarrow n$ amplitudes for $n > 3$. For the $2 \rightarrow 3$ amplitude, the multi-Regge form has been derived in reference [75] up to one-loop corrections to the graphs in figure 18.

As we saw in the previous section, factorization has to be shown to hold for all orders. In section 4.6 we shall show some examples of higher order corrections where TMD factorization is known to be violated. Since the multi-Regge formula leads to a k_{\perp} -factorized form (see further [42]) it is of relevance to consider such higher order graphs. As we will see, the breakdown of factorization might be hidden until higher order corrections. For example, figures 34, 36 and 37 show that factorization breakdown is not visible until 4 and 5 gluon exchange in the $2 \rightarrow 2$ amplitudes. If we consider only one side of the cut $2 \rightarrow 2$ amplitude, then factorization breaking graphs appear in 2 or 3 loop corrections to the $2 \rightarrow 4$ amplitude. Similar factorization breaking terms might be present in the $2 \rightarrow 3$ gluon amplitudes at 2 loop corrections as well. It may therefore very well be that one-loop corrections do not exhibit any TMD factorization breaking.

3.3 Factorization in the CGC

The Color Glass Condensate (CGC) [10–15] is a semi-classical approach developed to deal with the QCD physics of “large” objects such as heavy ions.

The set-up of the CGC formalism is rather different than the hard scattering factorization. The main assertion here is that the color degrees of freedom of a given hadron, such as a large nucleus, can be described by classical fields generated by a distribution of random color sources, ρ_a (a being the color index), which arise due to the “fast” moving partons, i.e., those partons which are in the collinear region. These then act as sources for the softer gluons whose dynamics depend on the classical sources.

3.3.1 Basics of CGC

The classical fields generated by these sources are determined by the solutions to the classical equations of motion

$$D_\nu F_a^{\mu\nu}(x) = J_a^\mu, \quad (3.44)$$

with D_ν the usual covariant derivative. The generic solutions to (3.44) give classical fields A_{cl}^a that are highly non-linear in the sources ρ_a . In the classical McLerran-Venugopalan (MV) model [34, 35], the sources are assumed to originate from the valence quarks of the nucleons which are randomly distributed according to some weight functional, $W[\rho]$. This is the distribution we encountered earlier in equations (2.3) and (2.4).

In the case of a single particle traveling in the plus direction, the classical current is taken as

$$J_a^\mu(x) = \delta^{\mu+} g_s \rho_a(x^-, x_\perp) \quad (3.45)$$

where the classical source $\rho(x^-, x_\perp)$ has a very narrow support in x^- . In the case of two particle scattering, with the incoming hadrons traveling along the opposite light-cones, one takes instead

$$J_a^\mu(x) = \delta^{\mu+} g_s \rho_{1,a}(x^-, x_\perp) + \delta^{\mu-} g_s \rho_{2,a}(x^+, x_\perp). \quad (3.46)$$

The model is defined at some scale $\Lambda^{\hat{\mu}}$ which sets the applicability of the classical description. Here $\hat{\mu} = +$ or $\hat{\mu} = -$. For a hadron with large momentum P^μ along the direction $\hat{\mu}$, this means that all fields with $k^{\hat{\mu}} > \Lambda^{\hat{\mu}}$ are taken to be described by the classical sources ρ . The distribution $W[\rho]$ is therefore specified at the scale $\Lambda^{\hat{\mu}}$. Physical quantities of interest in the model are calculated by functional averages using the classical distribution $W[\rho]$ as in (2.3) for a single hadron, and

$$\langle \mathcal{O} \rangle = \int D\rho_1 D\rho_2 W_{\Lambda_1^+}[\rho_1] W_{\Lambda_2^-}[\rho_2] \mathcal{O}[\rho_1, \rho_2], \quad (3.47)$$

in two hadron scattering. Of course, (3.47) is already in a factorized form.

3.3.2 Power counting and “dilute” and “dense” systems

The treatment of two particle processes is then based on a power counting argument of the classical sources $g_s \rho$. A “dilute” particle in this power counting is defined to be one described by a source such that $|g_s \rho| \ll 1$. For such a particle then, in the calculations only the first order dependence $(g_s \rho)^1$ is kept. Given a functional $\mathcal{O}[\rho_1, \rho_2]$ which depends on both ρ_1 and ρ_2 , expand it as a polynomial

$$\mathcal{O}[\rho_1, \rho_2] = \sum_{n=1}^{\infty} \sum_{m=1}^{\infty} \mathcal{O}_{nm} (g_s \rho_1)^n (g_s \rho_2)^m. \quad (3.48)$$

The definition of particle 1 being dilute then means that

$$\mathcal{O}[\rho_1, \rho_2] \rightarrow \mathcal{O}[\rho_1, \rho_2] \Big|_{1, \text{dilute}} = \sum_{m=1}^{\infty} \mathcal{O}_{1m} (g_s \rho_1) (g_s \rho_2)^m. \quad (3.49)$$

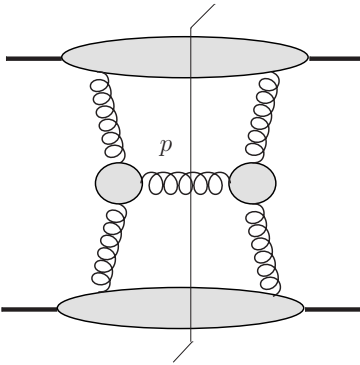


Figure 19: Diagrammatic representation of particle production in “dilute-dilute” scattering in the language of CGC.

Conversely a particle is defined to be “dense” if it is described by a source satisfying $|g_s \rho| \sim 1$. In that case, the dependence on $g_s \rho$ is retained to all orders. As for real particles, a proton or a deuteron is defined as being “dilute”, while heavy ions such as gold or lead nuclei are defined to be “dense”. Thus “dilute-dilute” scattering refers essentially to pp or $p\bar{p}$ scattering, while “dilute-dense” scattering refers to pA or deuteron-Nucleus (dA) collisions, and finally “dense-dense” scattering refers to AA collisions (lead-lead or gold-gold). Of course a proton in the CGC becomes “dense” at sufficiently high energies since the classical sources grow as a function of energy.

In this setting, the quantum evolution is based on the logic of the leading logarithmic approximation (LLA) where the coupling g_s is fixed and small, $g_s \ll 1$. Therefore for a “dilute” object we have $\rho \lesssim 1$, while for a “dense” object we have $\rho \sim 1/g_s \gg 1$. These assumptions lead to the formulation of factorization in the CGC approach [17, 18, 22–25].

We immediately notice that this power counting is rather different in logic than the power counting described in section 3.1.2. Here the emphasis is put on the classical source $\rho(x)$ specified in space-time coordinates. Any correction beyond the classical approximation is calculated to order g_s^2 which amounts to a one-loop calculation. For processes involving protons then, calculations are kept at linear order in $g_s \rho$ for each proton which in a diagrammatic analogy means that at most two gluon couplings are considered. In figure 19 we show an example of single inclusive gluon production in “dilute-dilute” scattering. Thus in the dilute limit factorization is essentially identical to that in the parton model we considered in section 3.1.1.

In general, however, the extra gluon emissions between the different PSSs considered in section 3.1.2 all have small virtualities and they therefore couple strongly. In particular the soft gluons have all their momentum components small, and the QCD coupling of these gluons is therefore strong. That is, we do not have a situation where $g_s \ll 1$. Even in the case of a weak coupling at all relevant scales, however, such as in QED, is the formalism outlined in 3.1.2 and the factorization theorems rather useful for controlling the higher order corrections which still might be enhanced by kinematical factors.

In the CGC higher order corrections are needed because the classical sources ρ can

have large values, $|\rho| \gg 1$, but g_s itself is always small. Pure perturbative calculations are thus performed when $|\rho| \lesssim 1$, which happens in the case of “dilute” particles. In the general treatment of factorization in QCD, or in generic field theories, however, large contributions arise from surfaces in the multi-dimensional space of momentum integrals where the integration contours are forced to go close to the singularities of the propagators, the pinch singular surfaces. In QCD the momentum lines in the PSSs have large couplings. This is the reason why factorization must be proven to all orders, and it is then convenient to employ the power counting analysis of the PSSs. Corrections are then guaranteed to be power suppressed in the large scale Q . In the case of small- x therefore, ideally we would want to formulate factorization (“ k_\perp -factorization”) up to power suppressed corrections in \sqrt{s} .

Of course the treatment of factorization cannot be purely perturbative for the reasons just explained. It is important to emphasize that the power counting methods of section 3.1.2 rely generically on dimensional analysis and Lorentz invariance, and thus not exclusively on perturbation theory. The explicit calculations are of course performed using Feynman graphs, but the structures obtained have a meaning beyond strict perturbation theory. One can therefore apply the same methods to the small- x region where any hard scale might be absent.

3.3.3 The LLA and basic logic of factorization

As the LLA is important for the formulation of factorization in the CGC, we shortly outline the logic behind it. An all order result can be obtained by calculating the one-loop graphs using the eikonal approximation, and then exponentiating the result. If the one loop result for a certain process is Γ_1 , and the tree level result is Γ_0 , then usually one finds

$$\Gamma_1 = g_s^2 \int_0^Y dy K_s(y) \cdot \Gamma_0, \quad (3.50)$$

where $dy = \frac{dk^+}{k^+}$ and the limits on y are determined by the kinematics of the given process. The kernel K_s is found by applying the approximations appropriate for a soft term. We can then write the complete result up to one loop as

$$\Gamma_0 + \Gamma_1 = \left(1 + g_s^2 \int_0^Y dy K_s(y) \right) \Gamma_0. \quad (3.51)$$

For infinitesimal change in the scale we can write this as

$$\Gamma_{dY} = (1 + g_s^2 dY K_s(dY)) \Gamma_0, \quad (3.52)$$

so that

$$\frac{\Gamma_{dY} - \Gamma_0}{dY} = g_s^2 K_s \Gamma_0. \quad (3.53)$$

This gives the all order LLA result

$$\Gamma_Y^{LLA} = \exp \left(g_s^2 \int_0^Y dy K_s(y) \right) \Gamma_0. \quad (3.54)$$

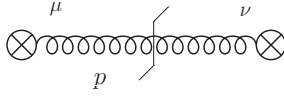


Figure 20: Particle production by classical sources in the CGC. The crosses denote the classical field insertions.

A similar construction is used in the CGC [17, 18, 22–25]. The idea is to start with a formula at the classical level, where the correlator of the classical fields is calculated using (3.47), and then to perform a one loop calculation as in (3.50) and show that at this level the classical structure (3.47) still holds. The resulting one loop formula can then be resummed as in (3.52) and (3.54) to obtain a final formula in the LLA.

Take for example the single inclusive particle production in the scattering of two hadrons, described by sources ρ_1 and ρ_2 , which is studied in [17, 18, 22–25]. The basic classical formula which is equivalent to a tree level calculation is given by

$$\left\langle E_p \frac{dN}{d^3p} \right\rangle = \frac{1}{2(2\pi)^3} \sum_{\lambda} \langle |\mathcal{M}_{\lambda}(p)|^2 \rangle \quad (3.55)$$

where

$$\mathcal{M}_{\lambda}(p) = p^2 A_{\mu}^{cl}(p) \epsilon_{(\lambda)}^{*\mu}(p). \quad (3.56)$$

We illustrate this in figure 20 where the crosses denote the insertions of the classical fields $A^{cl}(p)$. Note that $A^{cl}(p)$ is a function of both ρ_1 and ρ_2 so it contains the effects of both hadrons. At the pure classical level, one evaluates (3.55) using (3.47). This gives

$$\langle A_{\nu} A_{\mu} \rangle_0 = \int D\rho_1 D\rho_2 W_{\Lambda^+}[\rho_1] W_{\Lambda^-}[\rho_2] (A_{\nu}^{cl} A_{\mu}^{cl})[\rho_1, \rho_2] \quad (3.57)$$

where the subscript on the left hand side is to denote that this corresponds to the tree level calculation. The weight functionals can at this level be fully parametrized using the MV model from which an explicit result can be obtained for (3.55).

The one-loop correction to the tree level result is then found to be [24, 25]

$$\langle A_{\nu} A_{\mu} \rangle_1 = \int D\rho_1 D\rho_2 W_{\Lambda^+}[\rho_1] W_{\Lambda^-}[\rho_2] \left[\ln \frac{\Lambda^+}{p^+} H_1 + \ln \frac{\Lambda^-}{p^-} H_2 \right] (A_{\nu}^{cl} A_{\mu}^{cl})[\rho_1, \rho_2] \quad (3.58)$$

where each H_i corresponds to the “JIMWLK Hamiltonian”. Each H_i is a Hermitian differential kernel [39] (in the sense of functional differentiation) that acts on the classical fields $A_{\nu}^{cl} A_{\mu}^{cl}$ in (3.58). We see that this result is analogous to (3.50). To understand the logarithmic factors in (3.58), note that if $K_s(y)$ is independent of y (which it nearly always is), then the integral in (3.50) simply gives $Y \cdot K_s$. The rapidity Y exactly corresponds to the logarithmic factors in (3.58) and we see that K_s corresponds⁴ to H_i . Using that the

⁴The JIMWLK Hamiltonian is of order g_s^2 in the quantum fluctuations, but it contains the classical sources $g_s \rho$ to all orders.

H_i are Hermitian one can then rewrite the complete one-loop result (3.58) as [24, 25]

$$\begin{aligned} \langle A_\nu A_\mu \rangle_1 + \langle A_\nu A_\mu \rangle_0 &= \int D\rho_1 D\rho_2 \left(1 + \ln \frac{\Lambda^+}{p^+} H_1 \right) W_{\Lambda^+}[\rho_1] \left(1 + \ln \frac{\Lambda^-}{p^-} H_2 \right) W_{\Lambda^-}[\rho_2] A_\nu^{cl} A_\mu^{cl} \\ &\equiv \int D\rho_1 D\rho_2 W_{p^+}[\rho_1] W_{p^-}[\rho_2] (A_\nu^{cl} A_\mu^{cl})[\rho_1, \rho_2] \end{aligned} \quad (3.59)$$

In this rewriting one uses that formally the term containing the product $H_1 H_2$ in (3.59) is of higher order (it is not of LLA) and thus neglected. One then gets exactly as in (3.54) the LLA result

$$W_{dY} = (1 + dY H) W_0 \rightarrow W_Y^{LLA} = \exp \left(\int_0^Y dy H(y) \right) W_0. \quad (3.60)$$

Equation (3.59) is referred to as the “high energy factorization”, or “JIMWLK factorization”, formula [17, 18, 22–25].

3.3.4 Comparison to TMD factorization

In its derivation, (3.59) is rather different than the TMD factorization described in section 3.1.5. For example, in (3.59) there is a factorized product of the classical weight functionals $W[\rho_i]$ rather than a product of parton distributions and/or fragmentation functions.

Equation (3.59) is in the literature implied to be a generalization of ordinary TMD factorization. In section 5 of reference [24] we can for example read that

“JIMWLK factorization proven here is far more general and robust in comparison to the k_\perp -factorization often discussed in the literature.”

The statement on the wider generality of the CGC formula is motivated by the observation that one can for “dilute” systems obtain from (3.59) a formula which looks like a k_\perp -factorized formula. Since this “dilute” limit involves a simplified approximation within the CGC formalism, it is therefore said that (3.59) is more general. For example, for the single inclusive gluon production using (3.55) and (3.59) one gets in the “dilute” limit a formula that looks like equation (4.8) below which is the k_\perp -factorization formula canonically used in the small- x region. Moreover, within the CGC, the TMD gluon distribution can be calculated explicitly if $W[\rho]$ is given. For example, the WW gluon distribution can be calculated from (2.5) once $W[\rho]$ is specified. The converse statement on the other hand is not true: It is not enough to have an explicit formula for (2.5) in order to extract $W[\rho]$ uniquely.

In this sense, it can indeed be said that (3.59) is more general than the TMD factorization. However, from a different perspective we find that this statement is misleading and not correct. Moreover, as we shall explain now, the factorization explained in section 3.1 is actually more robust.

Equation (3.59) is namely only derived at one loop order using the logic of the LLA while the TMD factorization is much more general and accurate than that. The LLA result for example gives no hint at all as to what the higher order corrections might look like. There are even instances where it gives the wrong result, even qualitatively, an example being the Drell-Yan cross section at zero transverse momentum where the LLA gives a

vanishing result while the true result that can be obtained from the factorization approach is non-zero [76]. Contrary to the LLA, in the factorization approach the higher order corrections are well controlled, and even if the explicit calculations of the higher order corrections can be difficult in practice, one can nevertheless make reliable estimates of their importance [1]. It is therefore not correct to say that the “JIMWLK factorization” is more robust than the TMD factorization. In fact the opposite is clearly true with regards to the accuracy of the derivation.

Moreover, when in the CGC the dilute limit is taken, the TMD gluon distribution that appears in the factorization formula is given by [18, 24, 39]

$$\begin{aligned} f(x, k_\perp; \zeta) \big|_{\text{dilute}} &= \frac{1}{k_\perp^2} \langle \rho(k) \rho(-k) \rangle_{W_{\zeta P^+}} = \langle F^{+i}(k) F^{+i}(-k) \rangle_{W_{\zeta P^+}} \\ &= \int d^3x d^3y e^{ixP^+(x^- - y^-) - ik_\perp(x_\perp - y_\perp)} \langle F_a^{+i}(x) F_a^{+i}(y) \rangle_{W_{\zeta P^+}}. \end{aligned} \quad (3.61)$$

The subscripts on the correlators imply that the averages using $W[\rho]$ are performed at the scale ζP^+ . Acting with the dilute limit of the JIMWLK Hamiltonian on the classical sources in (3.61) one then recovers the BFKL equation for the object $f(x, k_\perp; \zeta)$ (for a simple demonstration of this, see [39]). Thus the BFKL formalism can be identified with the dilute limit of the JIMWLK formalism. Since for example the CCH formalism [65, 66] is based upon BFKL it is indeed correct that (3.59) presents a generalization of the work in [65, 66]. Moreover, as the work in [65, 66] is frequently referred to as the “ k_\perp -factorization” formula, in this sense (*i.e.* if “ k_\perp -factorization” is understood to refer to [65, 66]) (3.59) is more general than “ k_\perp -factorization”. The CCH formalism is, however, also based on the LLA, and neglected terms are therefore not power-suppressed.

The argument for factorization in [65, 66] is based on the use of the light-cone gauge (in DIS) or axial gauge (in hadron-hadron collisions). The final expression in (3.61) actually equals the earlier light-cone gauge expression in (2.2). A similar definition also appears in the factorization approach as we discussed in reference to figure 8. It is, however, important to realize that (3.61) is supposed to hold in the dilute limit for *any* gauge, even a covariant gauge. This is in fact in line with the power counting we discussed in section 3.3.2 above, where the definition of the dilute limit is that $g_s \rho \ll 1$. This is of course why equation (3.61) is second order only in ρ (the first order term $\langle \rho \rangle$ vanishes when, as usual, the distribution $W[\rho]$ is taken to be a Gaussian).

It is then important, however, to realize that the distribution thus obtained in (3.61) is *not* the TMD gluon distribution in the TMD factorization approach. One cannot in the TMD factorization in covariant gauge simply drop the Wilson lines because as mentioned above, the soft gluons exchanged between different regions have strong coupling. The TMD factorization therefore does not correspond to the dilute limit of the CGC. The factorization (3.59) does indeed represent a different structure than the TMD factorization, but it cannot be said to be more general since it contains only a one-loop calculation while the TMD factorization is valid to leading power, rather than to leading logarithm.

We want to emphasize that this point is important and not merely a technical detail. The reason is that if we wish to establish factorization for a given process, then a possible

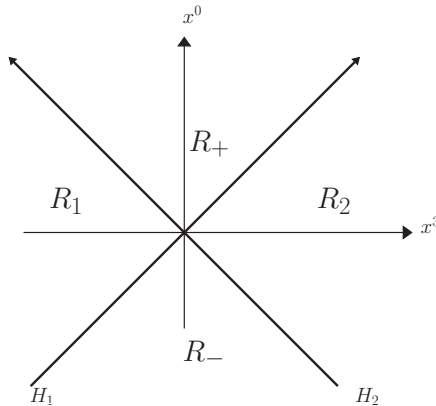


Figure 21: Space-time illustration of the scattering of two hadrons H_1 and H_2 . In the classical solutions of CGC, one has independent solutions in the non-casually-connected regions R_1 and R_2 . The solutions in the forward light-cone region R_+ are however non trivial and give rise to the so-called Glasma [79].

breakdown of factorization may not show up until higher order corrections are considered, beyond the dilute limit. In section 4.6 below we shall discuss this point in the context of the small- x single inclusive gluon production formula. As we explain there for example, the factorization breaking graphs studied in [77, 78] do not show up until one considers two gluon corrections to the parton model graphs, see figures 34 and 36. In terms of Feynman diagrams, the parton model graphs themselves are already at two loop order, so the factorization breaking does not appear until 4 loop graphs. In the dilute limit considered above, or in the logic of the LLA, however, this would have been completely missed.

It is therefore difficult to discuss the validity of factorization at one loop order, or in a “dilute” approximation in the sense described in section 3.3.2. In that case for example proton-proton collisions become rather trivial but the real situation is far more complicated than that, as should be obvious from our discussion in section 3.1.

3.3.5 Causality and factorization

An argument given for the validity of (3.47) is based partly on causality (see for example [24]), namely that two fast moving hadrons as shown in figure 21 cannot interact with each other prior to the collision. This by itself, however, does not imply that there must be a factorized structure for the observable under study. In covariant gauge, it is true that the hadrons cannot interact prior to the collision, and they are therefore causally disconnected before the collision. To write a factorization formula, however, one must be able to factorize the soft emissions which can occur at late times after the collision. Even though the hadrons are casually disconnected prior to the scattering, the scattering might produce color entangled states which break factorization (see section 4.6 below).

Moreover, the causality argument does not hold in “physical gauges”, such as the Coulomb gauge or the axial gauge, where manifest Lorentz invariance is broken and faster-

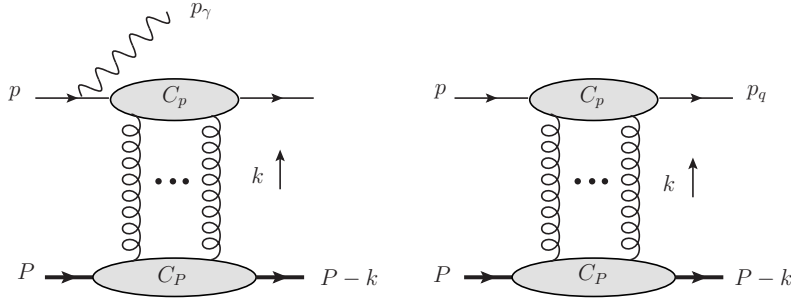


Figure 22: Examples of processes considered in the hybrid formalisms. Left: Photon production in quark-Nucleus scattering. Right: Quark production in quark-Nucleus scattering.

than-light propagation is possible in individual graphs. The causality violating contributions should cancel in the final, physical results, but the proofs can be very non-trivial. It was in fact early reported that [80, 81] the faster-than-light interactions in the physical gauges would correlate the hadrons prior to the collision and break factorization in hadron-hadron collisions such as in the Drell-Yan process.

Factorization, both collinear and TMD, in fact holds in Drell-Yan [1]. The problematic gluons are precisely the Glauber (Coulomb) gluons which complicate the proofs. However, in covariant gauge one can consistently deform the integration contours away from the Glauber region and restore factorization. Whether this can be done for more complicated interactions is of course the real question. We discuss this more in section 4 below. What is clear, however, is that the proof of factorization is much more intricate than what general causality arguments would suggest.

3.4 Hybrid formalisms

Some of the applications of the CGC model falls into a category that we shall call the “hybrid formalisms”, since they combine the CGC treatment above with that of collinear hard scattering factorization (see e.g. [55–57, 82–84]). These formalisms are used especially in proton-nucleus (pA) collisions. Typical examples include photon production, Drell-Yan, and soft particle production in the forward region (all in pA collisions). As we shall show here, however, these formalisms do not address the question whether there is factorization for the given process, and the validity of the proposal to mix collinear factorization with the CGC treatment is not at all clear to us.

We illustrate in figure 22 two examples of the processes considered in this framework. The upper incoming line refers to a quark of momentum p while the lower thick line with momentum P refers to the nucleus. The proton is therefore not treated explicitly. Only interactions between the active quark and the nucleus are considered as indicated in the figure. The gluon attachments between the lower and the upper blobs is described by a Wilson line exactly as in (2.9).

Consider the quark production case. The incoming quark is here on-shell and has zero transverse momentum [56, 83]. Thus the transverse momentum of the “observed” final state

quark is determined by the momentum transferred from the nucleus. This dependence is then given directly by the Fourier transform of the Wilson line (2.9),

$$\hat{W}(k_\perp) = \int d^2x_\perp e^{-ik_\perp \cdot x_\perp} W(x_\perp). \quad (3.62)$$

There are two possibilities, that the observed particle has low transverse momentum, of order of the typical intrinsic transverse momentum, *i.e.* $k_\perp \sim m$, or that it has large transverse momentum, of the order of a hard scale Q . The cases in figure 22 suggest that the particle is produced at low transverse momentum, since the k_\perp dependence is directly determined by (3.62). In that case, however, there is no reason to neglect the transverse momentum from the proton side, as this could completely change the kinematics of the observed final state particle. One must therefore formulate a TMD factorization formula, with the TMD parton distribution and fragmentation function of the proton taken into account. If on the other hand the produced particle has large transverse momentum, then a hard region must properly be included in the process. This, however, is not the case in figure 22.

The central idea of the hybrid formalisms is based on what is called the “factorization of mass singularities”. Here an emphasis is put on the mass divergences that appear in massless on-shell partonic reactions [85]. This procedure is in fact widely found in the literature when dealing with collinear factorization. Despite its wide use, however, it is a physically misleading procedure. It is in fact a rather different approach than the factorization explained in section 3.1 above. In this approach it is first *asserted* that a hadronic cross section σ_h , or a structure function W_h , is a convolution of the corresponding partonic cross section σ_p , or structure function W_p , and a so-called “bare parton density”, f^{bare} :

$$W_h(q, P) = W_p(q, \xi P) \otimes f^{\text{bare}}(\xi). \quad (3.63)$$

The convolution in the variable ξ is here the same as in equations (3.18) and (3.19). In the appendix of [83] (see also [86]) it is for example asserted for single inclusive hadron production that the differential cross section is given by

$$d\sigma_h(p, p_h; P) = f^{\text{bare}}(\xi) \otimes D^{\text{bare}}(z) \otimes d\sigma_p(z, \xi; P) \quad (3.64)$$

where p , p_h and P are the momenta of the incoming proton, the produced hadron and the incoming nucleus respectively. For the forward particle production shown in figure 22 (right graph), the incoming quark has momentum ξp while the outgoing quark has momentum p_h/z and it subsequently fragments to produce the observed hadron p_h .

In both cases, the calculations are then performed with massless partons and with the parton entering the scattering taken to be on-shell with zero transverse momentum. With these assumptions, collinear divergences appear in the partonic cross sections. It has been shown in the case of (3.63) that the result for W_p can be written as a convolution of a divergent factor, D (not to be confused with the fragmentation function), and a finite cross section $\hat{\sigma}$ [87, 88]. Using the associativity of the convolution operation \otimes , one can then

write

$$W_h = (\hat{\sigma} \otimes D) \otimes f^{\text{bare}} = \hat{\sigma} \otimes (D \otimes f^{\text{bare}}) = \hat{\sigma} \otimes f^{\text{ren}} \quad (3.65)$$

where the “renormalized” parton distribution is given by $f^{\text{ren}} = D \otimes f^{\text{bare}}$. This final result is actually just like that in (3.23). The just outlined procedure is, however, problematic for several reasons.

To begin with, there is no proof for the assertion (3.63) or (3.64), which actually *is* the statement of factorization. In the hybrid formalisms, it is simply stated that the proton side can be treated by integrated distributions. It is also in this case not exactly clear what the “bare parton density” is. According to the set up of the formalism, it is supposed to represent a distribution of on-shell and massless partons in the proton. This, however, is physically an ill-defined concept since quarks and gluons never exist as on-shell particles inside real hadrons. Moreover, if quark masses are retained in the calculations, there are no collinear divergences. It is therefore dangerous to emphasize the importance of the mass divergences since they appear only due to the approximation of using massless on-shell partons, and are therefore of a spurious nature. The “regularization” procedure just above is therefore conceptually different than (3.23), and crucially, it is not in any way related to factorization even if this might seem to be implied.

In the analysis of section 3.1 what factorization means is that a given cross section or structure function can be written in a factorized form where each factor is associated with a given momentum region. For example, in the case of DIS it means that we can factorize the hadronic tensor as

$$W \sim \int_x^1 \frac{dz}{z} C_j^{(0)}(Q/\mu, z/x, \epsilon) f_j^{(0)}(z; \mu, \epsilon) \quad (3.66)$$

up to power-suppressed corrections. We can also write this simply as

$$W \sim C_j^{(0)} \otimes f_j^{(0)}. \quad (3.67)$$

The meaning of the bare parton distribution is then that it is the gauge invariant integrated or TMD parton distribution constructed out of the bare fields of the Lagrangian. An example is the light-cone gauge definition of the bare integrated gluon distribution in (3.22). In fact any gauge invariant definition of a parton distribution involving suitable Wilson lines, as for example in the WW distribution (2.5) or the dipole distribution (2.10), must refer to the bare distribution, because the gauge transformation properties are obeyed by the gauge links constructed out of the bare fields. So strictly speaking we should have denoted all those distributions as in (3.22) and (3.66), *i.e* by a superscript $f^{(0)}$. It is important, however, to realize that this bare distribution, constructed out of the bare fields, cannot be the same as the undefined quantities in (3.63) and (3.64). For it is clear that it does not represent any distribution of on-shell, massless partons as is implied by (3.63) and (3.64). Once factorization has been proved as in (3.66) (or in (3.37), (3.39) and (3.40)), which itself is a very non-trivial statement, then renormalization is a matter of removing UV divergences by a suitable redefinition of the parameters of the Lagrangian.

Order by order in perturbation theory this means adding the necessary counter terms from the Lagrangian, for example in the $\overline{\text{MS}}$ scheme. One then finds the renormalized parton distribution via a formula as in (3.23). For (3.66) we find that

$$\begin{aligned}
W &\sim C_j^{(0)} \otimes f_j^{(0)} = C_{j'}^{(0)} \otimes \delta_{j'j} \otimes f_j^{(0)} \\
&= C_{j'}^{(0)} \otimes (Z^{-1} \otimes Z)_{j'j} \otimes f_j^{(0)} \\
&= (C_{j'}^{(0)} \otimes Z_{j'j''}^{-1}) \otimes (Z_{j''j} \otimes f_j^{(0)}) \\
&= C_j \otimes f_j
\end{aligned} \tag{3.68}$$

where f_j is the renormalized distribution given by (3.23), and the Kronecker delta in the first line also includes delta functions with respect to the momentum convolutions. This procedure still applies if the quark masses are retained in which case there are no collinear divergences at all.

Now, in the factorization approach, one can indeed approximate the momentum entering the hard scattering factor as massless and on-shell. It is crucial, however, that the hard scattering factor, C in (3.68), is defined with suitable subtractions (as we indicated in (3.21) and showed in figures 9 and 10) so that it genuinely describes a wide angle scattering with scale Q (we also note that the UV divergences of the subtraction terms are regulated by Z^{-1} in (3.68)). In the TMD factorization in section 3.1.5 for example, the errors in neglecting the transverse momenta, q_\perp , in the hard factor goes as q_\perp/Q which indeed is small in the validity region of the formalism. In (3.63) and (3.64), however, this is no longer the case (in particular in (3.64) the partonic part still contains the scattering off the nucleus). Moreover for particle production at low transverse momentum, the neglected transverse momentum, from the proton side, is of the same order as the transverse momentum of the final state particle which means that the error is substantial.

What is also non-trivial is that TMD factorization is mixed into the formalism of the factorization of mass singularities. If in fact we want to treat the given problem using TMD distributions, then in the small- x case where the produced particle is typically soft, one must consider off-shell matrix elements, precisely because of the reason just explained above. The off-shell matrix elements must then carefully be specified, to ensure gauge invariance (or rather gauge-independence), and one cannot use on-shell incoming partons. For the lowest order contributions, gauge independent off-shell scattering coefficients have been calculated in the CCH approach [65, 66], and an explicit all order definition in the case of BFKL is given in [89]. See also [90–93] for more recent considerations.

To summarize this section, the hybrid formalisms do not really address the question of factorization. Factorization is in a sense assumed from the start, via equation (3.63) or (3.64). In fact the real problem is to show a factorization like in (3.66) to start with. Moreover, the procedure which is referred to as the renormalization of the parton densities is conceptually very different from what is the case in the hard scattering factorization. It is moreover physically a misleading procedure since the basic structures are not well-defined. Additionally we have seen that for particles produced at low transverse momentum, TMD distributions must be used also from the proton side, but then of course one must first

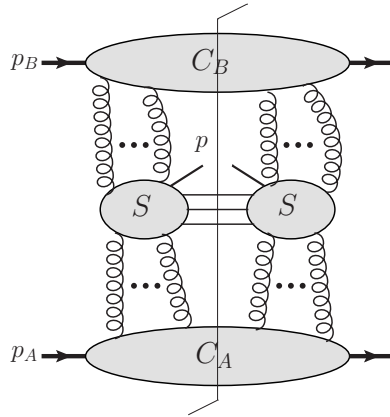


Figure 23: Production of soft hadrons in the small- x limit. The observed hadron p is associated with the soft region.

formulate a valid TMD factorization formula first, which might not be possible. We will in the coming sections analyze single particle production in the small- x region.

4. The fundamentals of single inclusive particle production

We will now give a comprehensive analysis of single inclusive particle production in high energy QCD, explaining many details which are usually overlooked. We will start by going through the basics of particle production, giving an overview of the leading regions in different kinematical situations. We then go on to analyze single inclusive gluon production in hadron-hadron scattering which is a process that has been widely studied (see e.g. [16–20, 22–31, 94–96] and references therein) in the small- x region. We will first go through the process using the axial gauge which is essentially the gauge on which the arguments for factorization are based, for example in [33, 94–96]. We will in detail explain the technical difficulties of the axial gauge, and why after all it is not convenient for proving factorization. We will then discuss hadron production from a more complete point of view, by building upon the analysis of the leading regions for the different kinematical cases. Finally we shall address the exact form of the TMD gluon distribution associated with this process, finishing with a discussion of the validity of factorization.

4.1 The different cases of particle production

In figures 23, 24 and 25 we list the possible scenarios for single inclusive particle production at small- x . In this section we explain the physics of the different cases.

Figure 23 represents a typical scenario of particle production in the Regge region, namely that of a soft particle produced at a typical small angle scattering event. In this case there is no hard region. All virtualities are of the typical soft scale m^2 . The momentum p of the produced particle therefore typically scales as $|p^\mu| \sim m$. This case is relevant for soft particle production at mid-rapidity. The inclusive charged particle spectrum at mid-

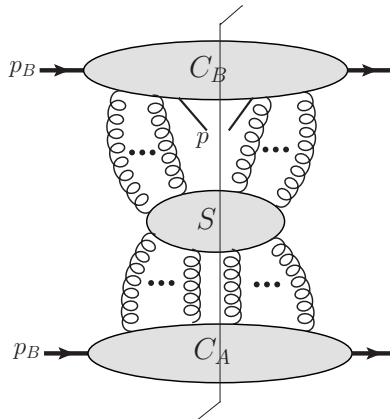


Figure 24: Production of hadrons in the fragmentation region of particle B in the small- x limit. The observed hadron p has rapidity close to that of B . A similar graph exists for production in the opposite direction close to A . These cases require the use of fracture functions rather than ordinary parton distributions and fragmentation functions.

rapidity,

$$\left. \frac{dN_{ch}}{d\eta} \right|_{\eta=0}, \quad (4.1)$$

has been measured by the different experimental groups at the LHC; ATLAS [97], CMS [98] and ALICE [99, 100]. This also happens to be the mostly studied case in the applications of small- x physics [16, 20, 26–31, 101].

Next, in figure 24 we show particle production in the case where the produced particle is close in rapidity to one of the hadron beams. This case therefore covers the forward production of particles. At the LHC, the CMS detector can detect particles in the pseudorapidity range $|\eta| < 5$ thanks to the hadronic forward calorimeters. Since the particles traveling in the forward region have enormous longitudinal momentum, they must of course have high p_\perp as well, since otherwise they would have too large rapidity and escape detection via the beam pipes. In CMS for example [102] forward *jets* (not hadrons) in the rapidity range $3.2 < |\eta| < 4.7$ have $p_\perp \geq 35$ GeV. One can also arrange for events where a hard di-jet is produced at central rapidity, to accompany the forward jet. The correlations between the forward jet and the central jets then offer important insight into the parton kinematics, see e.g. [92, 103, 104]. Actually if the momentum of the produced hadron belongs to either C_A or C_B , then one has to use so-called fracture functions rather than ordinary fragmentation functions or parton distributions.

Finally in figure 25 we show the case where the hadron is produced with large rapidity separation to both beams (for example in the central region) and where a hard region is present. This could for example be the case where the components p^μ are typically of order $Q \gg m$ or where we are looking at an event where a hard collision is present, that is jets with large p_\perp are produced in addition to the particle we tag (we do not show these additional jets in figure 25). The region decomposition here needs some explanation.

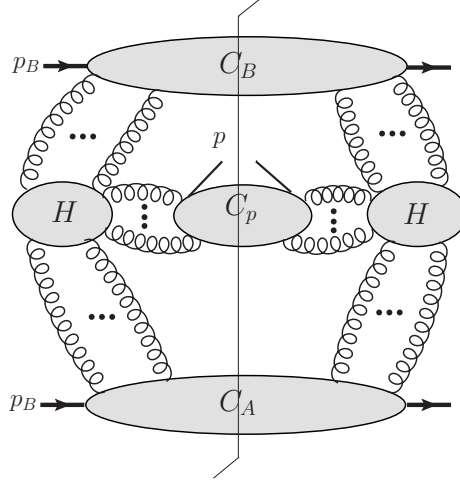


Figure 25: Production of hadron in the presence of a hard factor. The soft region coupling the collinear regions is also present, and additional collinear factors emerging from the hard scattering may be present as well, but for simplicity we do not show these here.

In section 3.1.2 we classified momenta according to different possible scalings. The external scales in that case were set by Q which also happens to be the hard momentum scale in the process. Therefore such a classification is appropriate when the components of the hard momenta scale with the longitudinal momenta of the external particles. The decomposition is thus appropriate when x is not too small. In that case we noticed that the only real possibilities for a pinch of a given momentum k^μ were as follows:

- None of k^μ scales with Q . Then we can characterize k^μ by the typical soft scale m , *i.e.* $k^\mu \sim m$. Then $k \in S$.
- A longitudinal component, say k^+ or k^- scales with Q . Then we have $k^+ \sim Q$, $k^- \sim m^2/Q$, $k_\perp \sim m$ and vice versa. In this case $k \in C_A$ (or $k \in C_B$ in opposite case).
- $k_\perp \sim Q$ in which case also $k^+k^- \sim Q^2$. Thus $k^\mu \sim Q$ and in that case $k \in H$.

Using this classification we then saw that a power counting analysis gives that at leading power, C_A and C_B can be connected to S via arbitrarily many soft longitudinally polarized gluons, while again arbitrarily many collinear gluons can be exchanged between H and the respective collinear region.

In the small- x case we have a different situation. In this case the large components of the external particles scale with \sqrt{s} but the momentum transfer remains fixed as $\sqrt{s} \rightarrow \infty$. Thus in this case there is no region in which all momentum components scale with the asymptotic parameter \sqrt{s} . In the soft production case one has the possibilities that

- None of k^μ scales with \sqrt{s} . Then generally $k \in S$.
- k^+ or k^- scales with \sqrt{s} . In this case $k \in C_A$ or $k \in C_B$ respectively.

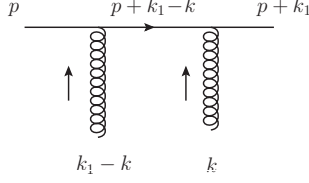


Figure 26: Coupling of two gluons from C_A to H .

There may, however, also be present hard collisions which give rise to jets or hadrons of several tens of GeV. Thus we may very well have regions where $k^\mu \sim Q$. We then propose the following classification

- If k^+ or k^- scales with \sqrt{s} , then just as above we let $k \in C_A$ or $k \in C_B$ respectively.
- Let $|k^\mu|/\sqrt{s} \rightarrow 0$ as $\sqrt{s} \rightarrow \infty$, but such that for example $|k^+|/|k^-| \gg 1$ and $|k^+|/|k^i| \gg 1$. Then even though $k^+ \ll \sqrt{s}$, we shall let $k \in C_A$. In the opposite case we of course let $k \in C_B$. To characterize such cases we shall let $k^+ \sim Q \ll \sqrt{s}$ (or $k^- \sim Q \ll \sqrt{s}$) where $Q \gg m$.
- We define the region where $k^+k^- \sim Q^2$ to be the hard region. Thus in figure 25 there is momentum $k^- \sim Q$ flowing into H from C_B , and momentum $k^+ \sim Q$ flowing in from C_A . The momenta going out from H to the final state is then characterized by the scale Q .
- Momenta such that $|k^\mu| \sim m \ll Q$ are as before classified as soft. In figure 25 we do not explicitly draw the soft subgraph to keep the notation simple.

With this classification we can then understand figure 25. Notice that the momentum lines whose large components scale with \sqrt{s} , and therefore belong to one of the collinear regions, cannot join the collinear region to the hard region H , since in that case a large momentum \sqrt{s} would be transferred to H , and we would no longer be in the small- x region. Thus in figure 25 the lines joining $C_{A,B}$ to H belong to the second class above. This is a different situation then in section 3.1.2 where any line in $C_{A,B}$ can join that region to H .

We shall now argue that the power counting is essentially the same as in section 3.1.2, despite the somewhat different kinematics. In figure 26 we show an example where two gluons from C_A couple to H as defined above. These two gluons have $k^+ \sim Q$, and in the lower end (not shown in the figure) they couple to collinear-to- A gluons which may have momenta scaling as \sqrt{s} in the plus direction. The leading contribution is then given by

$$\int d^4k_1 \int d^4k \frac{\not{p} + \not{k}_1}{(p + k_1)^2} \gamma^- \frac{\not{p} + \not{k}_1 - \not{k}}{(p + k_1 - k)^2} \gamma^- \frac{\not{p}}{p^2} \frac{1}{k_1^2} \frac{1}{k^2} A^{++}(k_1, k, p_A) \quad (4.2)$$

where $p \in H$. We then write this expression as

$$\int d^4k_1 \int d^4k \frac{\not{p}}{2p^-k_1^+} \gamma^- \frac{\not{p}}{2p^-(k_1^+ - k^+)} \gamma^- \frac{\not{p}}{p^2} \frac{1}{k_1^2} \frac{1}{k^2} A^{++}(k_1, k, p_A). \quad (4.3)$$

Now, as in section 3.1.2 we characterize the momentum coupling C_A to H by a scale λ_A , such that $k^- \sim \lambda_A^2/Q$ and $k_\perp \sim \lambda_A$. When the momentum k in figure 26 couples to $A^{++}(k_1, k, p_A)$, there will be a typical contribution of

$$\frac{\sqrt{s}}{(p_A + k)^2} \sim \frac{\sqrt{s}}{p_A^+ k^-} \sim \frac{\sqrt{s}}{\sqrt{s} \lambda_A^2 / Q} = \frac{Q}{\lambda_A^2}. \quad (4.4)$$

The factor \sqrt{s} in the numerator comes from the large boost of A in the $+$ direction. Remember that in the case covered in section 3.1.2 we have

$$\frac{Q}{(p_A + k)^2} \sim \frac{Q}{Q \lambda_A^2 / Q} = \frac{Q}{\lambda_A^2}. \quad (4.5)$$

As we see (4.4) agrees with (4.5). We therefore essentially have the same situation as before, that is arbitrarily many longitudinally polarized gluons of the second type in the classification above can connect the collinear regions to H in figure 25. Indeed the contribution from figure 26 gives

$$\left[\int d^4 k_1 \frac{\not{p} + \not{k}_1}{(p + k_1)^2} \gamma^- \frac{\not{p}}{p^2} \frac{1}{k_1^2} A^+ \right] \int d\lambda_A \lambda_A^3 \frac{1}{Q} \frac{1}{\lambda_A^2} \frac{Q}{\lambda_A^2}. \quad (4.6)$$

The term in the brackets corresponds to the contribution from gluon k_1 only. The factor outside therefore gives the contribution from attaching the additional gluon k and we see that it gives a logarithmic contribution

$$\int \frac{d\lambda_A}{\lambda_A} \quad (4.7)$$

so that there is no power suppression for coupling the extra gluon k to H .

To ensure the validity of all these arguments it is again important that one can perform contour deformations out of the Glauber region. We will in the next sections give a careful analysis of the factorization arguments that are based on the use of axial gauge, and we will show the difficulties associated with such arguments. We will continue the general discussion of single particle production in section 4.5 below. Before that, however, we want in the coming sections to concentrate on the small- x single inclusive gluon production cross section that has been widely used for phenomenological applications.

4.2 The small- x formula for gluon production

The most basic process for gluon production is depicted in figure 27 where the idea is that two gluons, k_A and k_B , each belonging to one of the incoming hadrons, fuse to produce a gluon of momentum l which then emerges in the final state. The argument for the validity of figure 27 is based on the use of axial gauge. The situation is similar to that in figure 8 where the use of the light-cone gauge eliminates all higher order gluon exchanges to leading power.

The factorization formula being used is given by [16, 20, 26, 33, 96]

$$\frac{d\sigma}{d^2 l_\perp dy} = \frac{2\alpha_s}{C_F l_\perp^2} \int d^2 k_\perp f_A(y, k_{A,\perp}) f_B(Y-y, k_{B,\perp}) \quad (4.8)$$

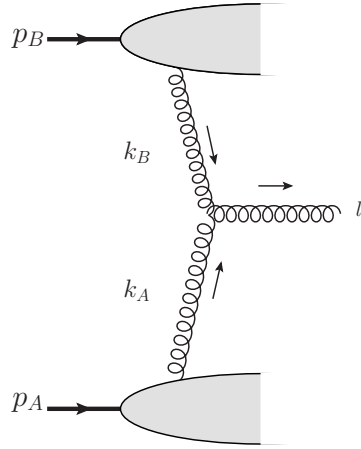


Figure 27: Single inclusive gluon production in hadron-hadron scattering according to equation (4.8).

where

$$k_A \equiv k, \quad k_B \equiv l - k, \quad (4.9)$$

y is the rapidity of the produced gluon with respect to the right moving hadron p_A . The functions f_A and f_B represent the respective TMD gluon distributions, and we shortly write down the definitions used. The origin of equation (4.8) goes back to the GLR papers [94–96] where the function f is “defined” as the derivative of the integrated gluon distribution (which is called the “gluon structure function” in [94–96])

$$f(y, k_\perp) = \frac{\partial x G(x, k_\perp)}{\partial k_\perp^2}, \quad y = \ln 1/x. \quad (4.10)$$

We note that this relation (or rather the inverted integral version of it) is a direct application of the parton model result (3.5), although in the parton model the integral over the unintegrated distribution is over all k_\perp . There are several good reasons for why one should be very cautious with the naive application of the parton model result. We will discuss this more in [42], and see also the comments just after equation (4.94) below.

As for the validity the factorization formula (4.8), it is in the literature common to cite the works [33, 41]. Reference [41] makes use of the dipole formalism in studying the deep inelastic scattering on a large nucleus, where the nucleus is taken to be described by the classical MV model. In this case the “unintegrated gluon distribution” is taken to be

$$f(k_\perp; y) = \frac{N_c}{(2\pi)^4 \alpha_s} \int d^2 r_\perp \int d^2 b_\perp e^{-ir_\perp \cdot k_\perp} \nabla_r^2 \mathcal{N}_G(r_\perp, b_\perp; y), \quad (4.11)$$

where \mathcal{N}_G has the same meaning as \mathcal{N} in (2.6) but is instead written in the adjoint representation as

$$\mathcal{N}_G(r_\perp, b_\perp; y) \equiv 1 - \frac{1}{N_c^2 - 1} \left\langle \text{Tr} \{ \tilde{W}(b_\perp + r_\perp/2) \tilde{W}^\dagger(b_\perp - r_\perp/2) \} \right\rangle_y. \quad (4.12)$$

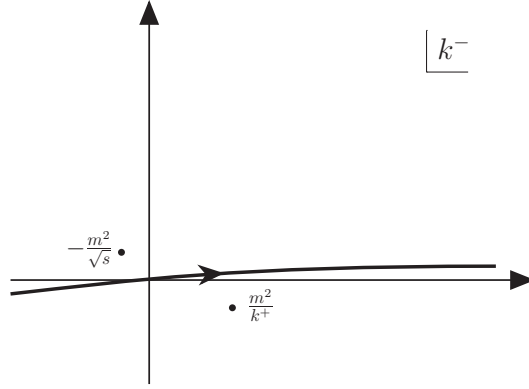


Figure 28: Poles in the plane of k^- and possible integration contour.

The Wilson line \tilde{W} has the same form as in (2.9), but with the replacement $t_F^a \rightarrow T^a$ where T^a is the adjoint color matrix. As can be seen we have indicated the dependence on the rapidity variable y a bit differently in (4.11) than in (4.8). We have in fact done this in purpose and it should later on be clear why we have done so. Notice for now that (4.11) is essentially the dipole distribution (2.10), with the difference that it is here written using Wilson lines in the adjoint representation. It is important to note, however, that (4.11) is not directly derived from the formalism in [41]. Its form is rather asserted by the *assumption* that the dipole formalism used in [41] is equivalent to the factorization formula (4.8).

The results of [41] are in turn partly based on [33] where the light-cone gauge is employed and it is argued that the leading regions have the structure shown in the figure 27. We also note that a similar factorized formula is found in the classical DDT paper [105] from the early days of QCD.

We will therefore now go through the light-cone gauge calculation. First, however, we need to specify the kinematics more carefully.

4.2.1 The kinematics

We denote as usual the incoming momenta by p_A and p_B . In the cms frame in the limit of very high energy and neglecting the masses one has

$$p_A = (\sqrt{s/2}, 0, 0_\perp) \quad (4.13)$$

$$p_B = (0, \sqrt{s/2}, 0_\perp) \quad (4.14)$$

so that $s = 2p_A \cdot p_B = 2p_A^+ p_B^-$.

We now ask which of the cases in section 4.1 above that is relevant here for figure 27. From figure 27 we see that there will be a typical contribution of the type

$$\frac{\text{Numerator}}{(k_A^2 + i\epsilon)(k_B^2 + i\epsilon)((p_A - k_A)^2 + i\epsilon)((p_B - k_B)^2 + i\epsilon)} \times (\text{Rest of graph}). \quad (4.15)$$

Let us now consider the k_A part, and the integral over k_A^- . We note that if $k_A^+ < 0$ or $k_A^+ > p_A^+$ then the poles in the k_A^- plane are either both in the upper or in the lower half plane respectively. In those cases we can deform away from the poles simultaneously and we get a power suppressed contribution. Thus we have $0 < k_A^+ < p_A^+$. In this case the pole from the k_A propagator is in the lower half plane, while the pole from the lower blob is in the upper half plane and the integration contour is therefore trapped. We show the pole structure in figure 28. We here simply denote the order of the magnitude of the poles, setting $k_\perp \sim m$. If we denote the two poles in k_A^- by k_1^- and k_2^- we see that the distance between them satisfies

$$\begin{aligned} |k_1^- - k_2^-| &= \frac{k_{A,\perp}^2}{2} \left(\frac{1}{k_A^+} + \frac{1}{p_A^+ - k_A^+} \right) \\ &\sim \frac{k_\perp^2}{2k_A^+}. \end{aligned} \quad (4.16)$$

Thus when $k_\perp \rightarrow 0$ (and all masses in the theory are neglected) we get an exact pinch. As $k_A^+ \rightarrow \sqrt{s}$ we also see that the poles are increasingly pinched and there is potentially a large contribution (from the collinear PSS). This, however, corresponds to the non-Regge region and is therefore not relevant for us. Now, we can let the integration contour pass near the $p_A - k_A$ pole in which case $|k_A^-| \sim m^2/\sqrt{s}$ (if actually the lower blob consists of a single spectator line then this pole becomes exact because there will be a delta function setting the spectator line on-shell).

We might, however, also ask what happens if there is a hard region as in figure 25. Assume for example that $l_\perp \sim Q$. As described in section 4.1, we must then have $k^+ \sim Q$ and $(l - k)^- \sim Q$ (we now use that $k_A = k$ and $k_B = l - k$). Then

$$k^+ \sim Q, \quad k^- \sim Q^2/\sqrt{s}, \quad (4.17)$$

and thus

$$k^+ k^- \sim \frac{Q}{\sqrt{s}} Q^2 \ll Q^2 \sim k_\perp^2. \quad (4.18)$$

The last estimate comes from $k_\perp \sim |l_\perp - k_\perp| \sim l_\perp \sim Q$. This, however implies $k^2 \sim Q^2$, which means that k is actually not in the collinear-to- A PSS. It instead belongs to H and one can see that this case is suppressed. To get a leading contribution we want $k^2 \sim m^2$, and similarly $(l - k)^2 \sim m^2$, but then it is easy to see that we cannot have $l_\perp^2 \sim Q^2$. Thus for the graph shown in figure 27 we do not have the situation in figure 25. To have a situation with a hard region like in figure 25 we must instead consider an additional collinear, unobserved, jet that emerges from H . This, however, makes the situation rather complicated and changes the physics involved quite a bit. We shall briefly come back to this case in the discussions in sections 4.5 and 4.6 below.

For analyzing the small- x formula (4.8) we consider the situation where $k^+ \sim m$. That is we essentially have the soft (or perhaps semi-hard) case in figure 23. A similar analysis as in above for the $l - k$ line implies that in this case

$$|k^-| \sim m^2/\sqrt{s}, \quad |l^+ - k^+| \sim m^2/\sqrt{s}. \quad (4.19)$$

Therefore

$$|k| \sim (m, m^2/\sqrt{s}, m), \quad (4.20)$$

so that

$$k^+ = l^+ + \mathcal{O}(m^2/\sqrt{s}), \quad l^- \gg |k^-|. \quad (4.21)$$

Thus

$$k^+ \sim k^i, \quad (l^- - k^-) \sim l^i - k^i, \quad (4.22)$$

and

$$|k^+ k^-| \sim m^3/\sqrt{s} \ll m^2 \sim k_\perp^2 \quad (4.23)$$

$$|(l^+ - k^+)(l^- - k^-)| \sim m^3/\sqrt{s} \ll m^2 \sim (l_\perp - k_\perp)^2. \quad (4.24)$$

Both gluons k and $l - k$ are therefore in the Glauber region where the transverse momentum components dominate. In light of what we have said earlier it would seem that we better avoid the Glauber region. Note, however, that there is no Glauber pinch here so we can deform out of the Glauber region if necessary.

4.3 The use of the light-cone gauge

The main argument for the validity of (4.8) given in [33] is based on the use of the light-cone gauge. Since an axial gauge is also used in [96] to argue for the validity of (4.8), we now go in through the derivation in these gauges. We shall start with the light-cone gauge in this section and then in the next section give an account based on the non-light-like axial gauge. We notice that axial or light-cone gauge is also used in establishing the factorization formulas in the CCH [66] and CCFM [70] formalisms.

There is in fact problem with the kinematical arguments given above in the light-cone gauge. If we choose the gauge $A^+ = 0$ then the treatment of the A part is as we just described. However, we do get a problem of the treatment of the B side. Similarly we do get a problem of the treatment of the A side if we work in $A^- = 0$ gauge. In fact the latter is the gauge on which the arguments in [33] are based. What we want to demonstrate in this section is that the light-cone gauge is clearly improper for the treatment of hadron-hadron collisions (be it proton-proton, proton-nucleus or nucleus-nucleus collisions). We will offer several reasons for this, and we return to the just mentioned issue at the end of this section. We will now simply push forward with the light-cone gauge and then see that it leads to severe problems.

Let us now denote the gluon propagators by

$$P^{\mu\nu}(k) = \frac{-iN^{\mu\nu}(k)}{k^2 + i\epsilon}. \quad (4.25)$$

Then in the light-cone gauge $n \cdot A = 0$ we have

$$N^{\mu\nu}(k) = g^{\mu\nu} - \frac{n^\mu k^\nu}{k \cdot n} - \frac{n^\nu k^\mu}{k \cdot n}. \quad (4.26)$$

We shall write $N^{\mu\nu}(k)$ as

$$N^{\mu\nu}(k) = \overrightarrow{G}^{\mu\nu}(k) - \overleftarrow{K}^{\mu\nu}(k), \quad (4.27)$$

where

$$\overrightarrow{G}^{\mu\nu}(k) \equiv g^{\mu\nu} - \frac{n^\mu k^\nu}{k \cdot n} \quad (4.28)$$

$$\overleftarrow{K}^{\mu\nu}(k) \equiv \frac{k^\mu n^\nu}{k \cdot n}. \quad (4.29)$$

Our notation here is inspired by the so-called K - G decomposition introduced by Grammer and Yennie [106]. The directions of the harpoons indicate whether it is the left or the right Lorentz index that is carried by the momentum k ; $\overrightarrow{G}^{\mu\nu}(k)$ (and $\overrightarrow{K}^{\mu\nu}$) contains k^ν , while $\overleftarrow{K}^{\mu\nu}(k)$ (and $\overleftarrow{G}^{\mu\nu}$) contains k^μ . Notice that the standard Grammer-Yennie decomposition which is applied to the Feynman gauge propagators is in this notation given by

$$N_{Feyn}^{\mu\nu} = g^{\mu\nu} = \overleftarrow{G}^{\mu\nu}(k) + \overleftarrow{K}^{\mu\nu}(k) = \left(g^{\mu\nu} - \frac{k^\mu n^\nu}{k \cdot n} \right) + \frac{k^\mu n^\nu}{k \cdot n}. \quad (4.30)$$

The K - G decomposition is important in proving factorization in the hard scattering domain since Ward identities can be applied to the K terms which are the dominant contributions. Remember from the analysis in section 3.1 that there can be arbitrarily many longitudinally polarized gluons exchanged between the hard and collinear regions, H and C , and between the collinear and the soft regions, C and S . These gluons precisely correspond to the K terms. If we choose n such that $n \cdot A = A^+$, then for the G terms we have

$$\overrightarrow{G}^{-+}(k) = g^{-+} - \frac{k^+}{k^+} = 0, \quad \overleftarrow{G}^{+-}(k) = g^{+-} - \frac{k^+}{k^+} = 0, \quad (4.31)$$

while for the K terms

$$\overleftarrow{K}^{-+}(k) = \frac{k^+}{k^+} = 1, \quad \overleftarrow{K}^{+-}(k) = \frac{k^+}{k^+} = 1. \quad (4.32)$$

For the dominant polarization N^{-+} we therefore see that only the K terms contribute. The key step to proving factorization is then to repeatedly apply the Ward identities on the K terms.

If, however, k is dominated by its transverse component, then one can no longer neglect the transverse G contributions to which the Ward identities do not apply. If for example we have momentum which scales as $l - k$ in the above example, then

$$|\overrightarrow{G}^{-i}(l - k)| = \left| \frac{(l - k)^i}{(l - k)^+} \right| \gg 1, \quad |\overleftarrow{K}^{i-}(l - k)| = \left| \frac{(l - k)^i}{(l - k)^+} \right| \gg 1. \quad (4.33)$$

This means that the transverse components cannot be neglected in favor of the $+-$ components. Moreover, even for the K terms, the application of the Ward identities leave non-factorizing remainder terms which are complicated. These can be neglected in the collinear limit but not in the Glauber region. Therefore in all the higher order corrections to figure 27 we must be able make all necessary contour deformations so as to power suppress these contributions.

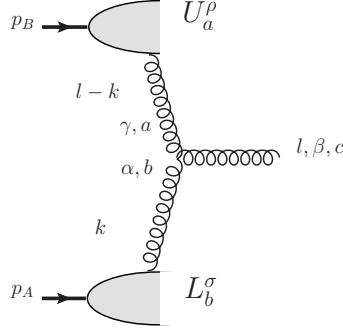


Figure 29: The graphical representation of formula (4.8).

In the axial gauge, the singular propagators must be regularized. A canonical regularization is obtained by treating the singularities as principal values. Now, in [33] the regularization is instead performed by choosing

$$N^{\mu\nu}(k) = g^{\mu\nu} - \frac{n^\mu k^\nu}{k \cdot n - i\epsilon} - \frac{n^\nu k^\mu}{k \cdot n + i\epsilon}. \quad (4.34)$$

Here the momentum flows from μ towards ν . The vector n is now chosen so that $n \cdot A = A^-$. There is, however, a fundamental problem with this gauge, and it shows up already for the lowest order contribution in figure 29. It is related to the fact that the light-cone gauge does not treat the hadrons symmetrically. We now demonstrate this problem by calculating the contribution in figure 29.

The polarization vector of the produced gluon l is chosen in [33] to satisfy $\epsilon^+(l) = 0$. Since $l \cdot \epsilon(l) = 0$ one has $\epsilon^-(l) = l^i \epsilon^i / l^+$. The contribution from the process depicted in figure 29 is given by

$$-g_s \epsilon_\beta^*(l) U_a^\rho(p_B, l-k) (\vec{G}_{\rho\gamma}(l-k) - \overleftarrow{K}_{\rho\gamma}(l-k)) V_{abc}^{\gamma\alpha\beta} (\vec{G}_{\sigma\alpha}(k) - \overleftarrow{K}_{\sigma\alpha}(k)) L_b^\sigma(p_A, k) \quad (4.35)$$

where V is the three-gluon vertex. The dominant component of the lower part is $L^+ \propto \sqrt{s}$, while the dominant component of the upper part is $U^- \propto \sqrt{s}$. We notice that in the above expression,

$$U_a^\rho(p_B, l-k) \overleftarrow{K}_{\rho\gamma}(l-k) = L_b^\sigma(p_A, k) \overleftarrow{K}_{\sigma\alpha}(k) = 0 \quad (4.36)$$

by the use of the Ward identity. One is then left with

$$-g_s \epsilon_\beta^*(l) U_a^\rho(p_B, l-k) \vec{G}_{\rho\gamma}(l-k) V_{abc}^{\gamma\alpha\beta} \vec{G}_{\sigma\alpha}(k) L_b^\sigma(p_A, k). \quad (4.37)$$

It is easily seen that the leading contributions are

$$\vec{G}^{\sigma\alpha}(k) L_{b,\sigma}(p_A, k) \approx \vec{G}^{-\alpha}(k) L_b^+(p_A, k) = g^{-\alpha} L_b^+(p_A, k) \quad (4.38)$$

and

$$U_{a,\rho}(p_B, l-k) \vec{G}^{\rho\gamma}(l-k) \approx U_a^-(p_B, l-k) \vec{G}^{+\gamma}(l-k). \quad (4.39)$$

For the γ index, the $\gamma = -$ component gives zero because of the gauge $A^- = 0$, while

$$|\vec{G}^{++}(l-k)| = \frac{|l^+ - k^+|}{|l^- - k^-|} \ll \frac{|l^i - k^i|}{|l^- - k^-|} = |\vec{G}^{+i}(l-k)| \quad (4.40)$$

so the leading term comes from $\gamma = i$. From (4.38), taking also into account the contribution from the complex conjugate amplitude, we see that we have for the lower part (we neglect the color indices for the moment)

$$\begin{aligned} L^{+\dagger}(p_A, k) L^+(p_A, k) &= \sum_X \int d^4x e^{ik \cdot x} \langle p_A | A^+(x) | X, \text{out} \rangle \langle X, \text{out} | A^+(0) | p_A \rangle \\ &= \sum_X \frac{1}{(k^-)^2} \int d^4x e^{ik \cdot x} \langle p_A | (k \cdot A(x) + k^i A^i(x)) | X, \text{out} \rangle \\ &\quad \langle X, \text{out} | (k \cdot A(0) + k^i A^i(0)) | p_A \rangle \\ &= \sum_X \frac{1}{(k^-)^2} \int d^4x e^{ik \cdot x} \langle p_A | k^i A^i(x) | X, \text{out} \rangle \langle X, \text{out} | k^i A^i(0) | p_A \rangle \end{aligned} \quad (4.41)$$

where in the second equality we used the fact that $A^- = 0$, while in the last equality we used the Ward identity. For the upper part we instead have for the leading term

$$\left(U^- \vec{G}^{+i} \right)^\dagger \left(U^- \vec{G}^{+i} \right) = \int d^4x e^{i(l-k) \cdot x} \langle p_B | A^i(x) A^i(0) | p_B \rangle. \quad (4.42)$$

In the gauge $A^- = 0$, the canonical definition of the TMD gluon distribution is (which directly corresponds to the parton model definition (2.1))

$$\begin{aligned} &k^- \int \frac{dk^+}{(2\pi)^4} \int d^4x e^{ik \cdot x} \langle p_B | A^i(x) A^i(0) | p_B \rangle \\ &= \int \frac{dk^+}{(2\pi)^4} \frac{1}{k^-} \int d^4x e^{ik \cdot x} \langle p_B | F^{-i}(x) F^{-i}(0) | p_B \rangle. \end{aligned} \quad (4.43)$$

This is for example also the case for the Weizsacker-Williams distribution in the CGC, with the only trivial difference being that in that case the pre-factor in the first line above is taken to be $(k^-)^2/p_B^- = \bar{x}k^-$ instead of k^- (with $\bar{x} = k^-/p_B^-$). We notice, however, that the so-called dipole gluon distribution cannot be really fully consistent with (4.43). The reason is that for the dipole gluon distribution, in the corresponding derivation one must actually set k^- to 0 (this is why the Wilson lines (2.9) are integrated from $-\infty$ to $+\infty$ in the longitudinal direction). One can therefore not multiply the definition with k^- as above, in order to obtain the canonical form (4.43). In that case one may instead multiply the integral by p_B^- .

While it is straightforward to put (4.42) into the proper form, this is not so with the lower component (4.41). Going now back to the evaluation of the graph in figure 29 we

thus have

$$\begin{aligned}
& g_s \epsilon^{*\beta}(l) U_a^-(l-k) L_b^+(k) \frac{(l-k)_\perp^\gamma}{l^- k^-} g^{-\alpha} V_{\gamma\alpha\beta}^{abc} \\
&= -g_s U_a^-(l-k) L_b^+(k) f^{abc} \frac{1}{l^- k^-} [-\epsilon^{*-}(l_\perp^2 - k_\perp^2) - \epsilon^{*i}(l^i - k^i)(k^- - 2l^-)] \\
&\approx -g_s U_a^-(l-k) L_b^+(k) f^{abc} \left[-\frac{\epsilon^{*i} l^i}{l^- l^+} (l_\perp^2 - k_\perp^2) + 2\epsilon^{*i}(l^i - k^i) \right]
\end{aligned} \tag{4.44}$$

where k^- has been neglected with respect to l^- . Using $2l^+l^- = l_\perp^2$ one then gets

$$g_s \frac{2U_a^-(l-k) L_b^+(k) f^{abc}}{l_\perp^2} (\epsilon^{*i} l^i (l_\perp^2 - k_\perp^2) - \epsilon^{*i} (l^i - k^i) l_\perp^2). \tag{4.45}$$

Squaring and summing over polarization and color indices, and integrating over k , we have

$$\frac{g_s^2}{N_c^2 - 1} \sum_{aa'bb'c} \int \frac{d^4 k}{(2\pi)^4} 4(U_a^- U_{a'}^{-\dagger})(L_b^+ L_{b'}^{+\dagger}) f^{abc} f^{a'b'c} \frac{k_\perp^2 (l_\perp - k_\perp)^2}{l_\perp^2}. \tag{4.46}$$

Now, to write a factorization formula for this result we have to untangle the color flow and at the same time make the appropriate kinematical approximations. Using (4.21), we now neglect k^- with respect to l^- in the U factors, and we set $k^+ = l^+$ in the L factors. The k^+ (k^-) integral then acts only on the U (L) factors.

For obtaining the differential single inclusive cross section we project the diagonal color components in U and L , and we find that the result can be written as

$$\begin{aligned}
\frac{d\sigma}{dy d^2 l_\perp} &= \frac{1}{2s} \frac{1}{2(2\pi)^3} \frac{4g_s^2 N_c (2\pi)^4}{N_c^2 - 1} \frac{1}{l_\perp^2} \int d^2 k_\perp \left[\int \frac{dk^+}{(2\pi)^4} \sum_a U_a^- U_a^{-\dagger} (l_\perp - k_\perp)^2 \right]_{k^-=0} \\
&\quad \times \left[\int \frac{dk^-}{(2\pi)^4} \sum_b L_b^+ L_b^{+\dagger} k_\perp^2 \right]_{k^+=l^+}.
\end{aligned} \tag{4.47}$$

We notice that up to this point the arguments have followed very closely those in section 3.1.3 that lead to equation (3.19). However, as we discussed after equation (3.19), a more careful treatment is needed since the integration over the momentum will include contributions which are not strictly in the region where the above kinematics holds. What we saw in equation (3.21) was that this could be treated by including subtractions in the hard factor. In this case, we instead need subtractions in the last factor of (4.46). In fact one must correctly treat the gluon production factor, the analog of the hard region, to all orders and make sure it is gauge independent. This, however, does not affect the definition of the gluon distribution.

Now, for the first bracket containing the upper blobs in (4.47) we have from (4.42) (we keep the summation over the color indices implicit)

$$\begin{aligned}
\frac{1}{p_B^-} \left[\int \frac{dk^+}{(2\pi)^4} U_a^- U_a^{-\dagger} (l_\perp - k_\perp)^2 \right]_{k^-=0} &= \frac{(l^-)^2}{p_B^-} \int \frac{dk^+}{(2\pi)^4} \int d^4 x e^{i(l-k)\cdot x} \langle p_B | A_a^i(x) A_a^i(0) | p_B \rangle \\
&= \int \frac{dx^+ d^2 x_\perp}{(2\pi)^3 p_B^-} e^{il^- x^+ - (l_\perp - k_\perp)\cdot x_\perp} \langle p_B | F_a^{-i}(x^+, 0^-, x_\perp) F_a^{-i}(0) | p_B \rangle
\end{aligned} \tag{4.48}$$

where we have chosen to include the factor $1/p_B^-$ into the definition. For the lower blobs, however, we cannot get the standard formula because of the asymmetric gauge choice $A^- = 0$. Using (4.41) we have (again keeping summation over color indices implicit)

$$\begin{aligned} & \frac{1}{p_A^+} \left[\int \frac{dk^-}{(2\pi)^4} L_b^+ L_b^{+\dagger} k_\perp^2 \right]_{k^+=l^+} \\ &= \sum_X \frac{1}{p_A^+} \int \frac{dk^-}{(2\pi)^4} \frac{k_\perp^2}{(k^-)^2} \int d^4x e^{ikx} \langle p_A | k^i A_b^i(x) | X, \text{out} \rangle \langle X, \text{out} | k^i A_b^i(0) | p_A \rangle \Big|_{k^+=l^+}. \end{aligned} \quad (4.49)$$

This expression is clearly different than (4.43) or (4.48), and does not correspond to any known distribution. One therefore does not obtain formula (4.8).

Let us now explain the other difficulty with the light-cone gauge that we mentioned just above equation (4.35). As we have seen, in $A^- = 0$ gauge we have a problem with the definition of the parton distribution for particle A which moves in the $+$ direction. Similarly if we chose $A^+ = 0$ gauge, then we will have a problem with the definition for particle B . Let $k_{A,B}$ denote momenta attached between the collinear regions A, B and any other region such as S or H . Where k_A attaches to A , the collinear lines of A will force k_A^- to generally be small as in figure 28. If we now work in the $A^- = 0$ gauge it means we additionally have the $1/k_A^-$ pole at the origin, and the combined poles from the propagator and the collinear lines of A will then generally pinch k_A^- at the origin. This, however, means that the higher order terms cannot be deformed out to $k_A^- \sim Q$ to power suppress them (terms for example such as \bar{G}^{i+} will be large). The gauge $A^- = 0$ therefore fails for the gluons attaching to A . A similar argument for B shows that the $A^+ = 0$ gauge similarly is not useful.

4.4 Non-light-like symmetric axial gauge

To get a formula that looks like (4.8) one must instead choose a gauge that treats the two hadrons symmetrically, this can for example be done by choosing the non light-like axial gauge $A^+ + A^- = 0$, *i.e.* the temporal gauge $A^0 = 0$. Using this gauge, one can again eliminate the extra gluon couplings to the collinear regions. We will here use this gauge to derive (4.8) and at the same time we will see what the definition of the TMD gluon distribution is. However, in section 4.5 we will explain the general case, and demonstrate the problem that is inherent in this axial gauge treatment as well.

In the gauge $A^+ + A^- = 0$, the numerator of the gluon propagator is given by

$$N^{\mu\nu}(k) = g^{\mu\nu} - \frac{n^\mu k^\nu + n^\nu k^\mu}{n \cdot k} + \frac{k^\mu k^\nu n^2}{(n \cdot k)^2} \quad (4.50)$$

where $n \cdot k = k^+ + k^-$ for any k . The contribution in figure 29 gives

$$-g_s \epsilon_\beta^*(l) U_a^\rho(p_B, l-k) N_{p\gamma}(l-k) V_{abc}^{\gamma\alpha\beta} N_{\sigma\alpha}(k) L_b^\sigma(p_A, k). \quad (4.51)$$

The last term proportional to n^2 in (4.50) then cancels in both propagators above when the Ward identity is applied on U and L . One is then left with the same expression as in

(4.35) which again reduces to (4.37) when applying the Ward identity. As before we have that

$$\vec{G}^{\sigma\alpha}(k) L_{b,\sigma}(p_A, k) \approx \vec{G}^{-\alpha}(k) L_b^+(p_A, k) \quad (4.52)$$

and

$$U_{a,\rho}(p_B, l - k) \vec{G}^{\rho\gamma}(l - k) \approx U_a^-(p_B, l - k) \vec{G}^{+\gamma}(l - k), \quad (4.53)$$

but in this case the leading G terms are different. We have

$$\left| \vec{G}^{++}(l - k) \right| = \left| \frac{l^+ - k^+}{l^+ - k^+ + l^- - k^-} \right| \sim \left| \frac{l^+ - k^+}{l^-} \right| \sim \frac{m}{\sqrt{s}} \ll 1 \quad (4.54)$$

$$\left| \vec{G}^{+-}(l - k) \right| = \left| 1 - \frac{l^- - k^-}{l^+ - k^+ + l^- - k^-} \right| \sim \left| \frac{k^-}{l^-} \right| \sim \frac{m}{\sqrt{s}} \ll 1 \quad (4.55)$$

$$\left| \vec{G}^{+i}(l - k) \right| = \left| \frac{l^i - k^i}{l^+ - k^+ + l^- - k^-} \right| \sim \left| \frac{l^i - k^i}{l^-} \right| \sim \frac{m}{m} = 1, \quad (4.56)$$

and

$$\left| \vec{G}^{--}(k) \right| = \left| \frac{k^-}{k^+ + k^-} \right| \sim \left| \frac{k^-}{k^+} \right| \sim \frac{m}{\sqrt{s}} \ll 1 \quad (4.57)$$

$$\left| \vec{G}^{-+}(k) \right| = \left| 1 - \frac{k^+}{k^+ + k^-} \right| \sim \left| \frac{k^-}{k^+} \right| \sim \frac{m}{\sqrt{s}} \ll 1 \quad (4.58)$$

$$\left| \vec{G}^{-i}(k) \right| = \left| \frac{k^i}{k^+ + k^-} \right| \sim \left| \frac{k^i}{k^+} \right| \sim \frac{m}{m} = 1. \quad (4.59)$$

The leading contributions are therefore the transverse components in both sides. Squaring the contribution from figure 29 and summing over gluon polarizations one is then left with (we neglect for simplicity the color factors since they are exactly the same as in the light-cone gauge calculation above)

$$g_s^2 (U^- U^{-\dagger})(L^+ L^{+\dagger}) \frac{1}{(l^+ - k^+ + l^- - k^-)^2} \frac{1}{(k^+ + k^-)^2} \times \sum_{\lambda} \left[-2(k^+ \epsilon_{\lambda}^- + k^- \epsilon_{\lambda}^+)(k_{\perp}^2 - l_{\perp} \cdot k_{\perp}) + \epsilon_{\lambda}^i k^i l_{\perp}^2 - \epsilon_{\lambda}^i l^i (-k_{\perp}^2 + 2l_{\perp} \cdot k_{\perp}) \right]^2. \quad (4.60)$$

We shall next choose the external polarization vector to satisfy $\epsilon^- = 0$, which means that $\epsilon^+ = \epsilon^i l^i / l^-$. Then the first term in the sum above gives

$$-2 \frac{k^-}{l^-} \epsilon^i l^i (k_{\perp}^2 - l_{\perp} \cdot k_{\perp}) \quad (4.61)$$

which is of the order of a transverse component multiplied by $k^- / l^- \sim m / \sqrt{s} \ll 1$ and can therefore be neglected compared to the other transverse terms. One then gets

$$g_s^2 (U^- U^{-\dagger})(L^+ L^{+\dagger}) \frac{1}{(l^+ - k^+ + l^- - k^-)^2} \frac{1}{(k^+ + k^-)^2} l_{\perp}^2 k_{\perp}^2 (l_{\perp} - k_{\perp})^2. \quad (4.62)$$

Inserting now all pre-factors and color indices, we get for the gluon production cross section

$$\frac{d\sigma}{dy d^2l_\perp} = \frac{1}{4} \frac{1}{2(2\pi)^3} \frac{(2\pi)^4 g_s^2 N_c}{N_c^2 - 1} \times \int d^4k \left[\frac{U_a^- U_a^{-\dagger} (l_\perp - k_\perp)^2}{p_A^- (2\pi)^4} \right] \left[\frac{L_b^+ L_b^{+\dagger} k_\perp^2}{p_B^+ (2\pi)^4} \right] \frac{l_\perp^2}{(l^+ - k^+ + l^- - k^-)^2 (k^+ + k^-)^2}. \quad (4.63)$$

To define the TMD gluon distribution we now notice that

$$\begin{aligned} U_a^- U_a^{-\dagger} (l_\perp - k_\perp)^2 &= (l^+ - k^+ + l^- - k^-)^2 \int d^4x e^{i(l-k)\cdot x} \langle p_A | A_a^i(x) A_a^i(0) | p_A \rangle \\ &= 2 \int d^4x e^{i(l-k)\cdot x} \langle p_B | F_a^{0i}(x) F_a^{0i}(0) | p_B \rangle, \end{aligned} \quad (4.64)$$

where $F^{0i} = (1/\sqrt{2})(F^{+i} + F^{-i})$. Similarly

$$L_b^+ L_b^{+\dagger} k_\perp^2 = 2 \int d^4x e^{ik\cdot x} \langle p_A | F_b^{0i}(x) F_b^{0i}(0) | p_A \rangle. \quad (4.65)$$

To obtain the canonical forms of the two gluon distributions, we notice that we can drop the F^{-i} contribution in (4.65), since it gives rise to the contributions $k^- L^i$, $k^i L^-$ and L^{i-} which are all power-suppressed. Therefore we might as well replace F^{0i} by $F^{+i}/\sqrt{2}$. Similarly for the expression in (4.64) we can replace F^{0i} by $F^{-i}/\sqrt{2}$. To get the factorization formula, one further needs to approximate $k^- = 0$ in the upper part, and $k^+ = l^+$ lower part. Furthermore we applied the approximations from the kinematics in (4.19)-(4.24) in the last factor in (4.63) which can then be written as (up to power-suppressed corrections)

$$\frac{l_\perp^2}{(l^+ - k^+ + l^- - k^-)^2 (k^+ + k^-)^2} \sim \frac{l_\perp^2}{(l^-)^2 (l^+)^2} = \frac{4}{l_\perp^2}. \quad (4.66)$$

Thus we find

$$\begin{aligned} \frac{d\sigma}{dy d^2l_\perp} &= \frac{2\pi^2 \alpha_s}{C_F l_\perp^2} \int d^2k_\perp \left[\int \frac{dk^+}{(2\pi)^4} \frac{1}{p_B^-} U_a^- U_a^{-\dagger} (l_\perp - k_\perp)^2 \right] \left[\int \frac{dk^-}{(2\pi)^4} \frac{1}{p_A^+} L_b^+ L_b^{+\dagger} k_\perp^2 \right] \\ &= \frac{2\pi^2 \alpha_s}{C_F l_\perp^2} \int d^2k_\perp f_B(x_B, l_\perp - k_\perp) f_A(x_A, k_\perp), \end{aligned} \quad (4.67)$$

with

$$f_A(x_A, k_\perp) = \int \frac{dx^- d^2x_\perp}{(2\pi)^3 p_A^+} e^{ix_A p_A^+ x^- - ik_\perp x_\perp} \langle p_A | F_a^{+i}(0^+, x^-, x_\perp) F_a^{+i}(0) | p_A \rangle, \quad (4.68)$$

and

$$f_B(x_B, l_\perp - k_\perp) = \int \frac{dx^+ d^2x_\perp}{(2\pi)^3 p_B^-} e^{ix_B p_B^- x^+ - i(l-k)_\perp x_\perp} \langle p_B | F_a^{-i}(x^+, 0^-, x_\perp) F_a^{-i}(0) | p_B \rangle, \quad (4.69)$$

where $x_A = l^+/p_A^+$ and $x_B = l^-/p_B^-$.

4.4.1 The coefficient of the formula

As for the coefficient in front of formula (4.67), we note that different values appear in the literature. Let us denote the coefficient in (4.67) by

$$C = \frac{2\pi^2 \alpha_s}{C_F} = \frac{4\pi^2 N_c \alpha_s}{N_c^2 - 1}. \quad (4.70)$$

In the papers [20,26,27,29,31,41] we instead find the formula (this is the value we used in writing (4.8))

$$C = \frac{2\alpha_s}{C_F} = \frac{4 N_c \alpha_s}{N_c^2 - 1}, \quad (4.71)$$

while in [96] we find,

$$C = \frac{N_c \alpha_s}{(2\pi)^6}, \quad (4.72)$$

and in [95]

$$C = 2\pi N_c \alpha_s. \quad (4.73)$$

Similarly we find in [28]

$$C = \frac{(2\pi)^8 C_F \alpha_s^3}{\pi N_c^2}, \quad (4.74)$$

and in [30]

$$C = \frac{2\pi^2 K C_F \alpha_s}{N_c^2} = \frac{\pi^2 K (N_c^2 - 1) \alpha_s}{N_c^3} \quad (4.75)$$

where K is a fit parameter which is quoted to be of the numerical value 1.5-2. We see that the coefficients in (4.71), (4.72), (4.73), (4.74) and (4.75) are all different from each other. It appears also that none agrees with the result above, equation (4.70). Our result (4.70) on the other hand agrees with the result in [107] where it was indeed observed that an extra factor π for each TMD distribution must be included to agree with (4.71) above.

The numerical differences between the pre factors used in different papers are clearly rather important. It should also further be noted that in the papers [16,30] the k_\perp integration is performed only up to l_\perp while such a bound does not appear in the other papers. Moreover in most of the phenomenological applications the coupling α_s is taken to run with some scale which also differs from paper to paper.

4.5 Higher order terms in axial gauge, and more complete view

From the contribution in figure 29 we have thus seen that we can in the non-light-like axial gauge, $A^+ + A^- = 0$, obtain the formula (4.8) where the TMD distributions are given by (4.68) and (4.69). We notice that exactly the same gauge is used in the CCH formalism [66] and in the GLR paper [96].

The question is of course what happens when we include higher order corrections to figure 29. We will now in this section first prove that the axial gauge does indeed eliminate to leading power the couplings to the collinear regions, and at the same time we will see what kinematics is necessary for this result to hold. We will show that the kinematics is actually opposed to the usual small- x kinematics. Thus for the higher order corrections to be generally negligible we will need contour deformations to ensure the desired kinematics. We shall then give an argument for why the needed contour deformations generally fail in the axial gauge.

Assume now that we have a collinear region C which carries momentum lines that are large in some direction w_C . For example this could be region C_A which has large momentum in the $+$ direction. Let \tilde{w}_C be the conjugate direction to w_C , such that $w_C \cdot \tilde{w}_C = 1$. The large component of C^μ is then given by $\tilde{w}_C \cdot C$. We now choose the axial gauge $n \cdot A = 0$ where n is not necessarily light-like. Let V be any vector. We then have

$$V \cdot C = V \cdot w_C \tilde{w}_C \cdot C + \text{p.s.c.} \quad (4.76)$$

where “p.s.c.” as before stands for “power suppressed corrections”. Now we let $V = n$, and using that we are in $n \cdot A = 0$ gauge, we obtain

$$0 = n \cdot C = n \cdot w_C \tilde{w}_C \cdot C + \text{p.s.c.} \quad (4.77)$$

Assuming now that $n \cdot w_C \neq 0$, we can separately scale the gauge vector

$$n \rightarrow \frac{n}{n \cdot w_C} \quad (4.78)$$

for each collinear region in the graph to get

$$0 = n \cdot C = \tilde{w}_C \cdot C + \text{p.s.c.} \quad (4.79)$$

Thus we conclude that the leading term vanishes in the axial gauge, and only power-suppressed contributions remain. Notice that if $n \cdot w_C = 0$ then we cannot necessarily conclude that the leading contribution is eliminated. It might also be that, depending on the exact kinematics, several directions of C^μ simultaneously become important. In that case the advantage of the axial gauge vanishes. Let us illustrate these points with some examples.

Consider now a gluon k coupling to region C_A , and denote $\tilde{C}_A^\mu = N^{\mu\nu}(k)C_{A,\nu}$. It is actually then \tilde{C}_A that corresponds to C above (since $n \cdot \tilde{C}_A = 0$ but $n \cdot C_A \neq 0$). Assume we are in the $A^- = 0$ gauge. Then

$$\tilde{C}_A^+ \sim N^{+-}C_A^+ = \left(1 - \frac{k^-}{k^+}\right)C_A^+ = 0, \quad (4.80)$$

$$\tilde{C}_A^i \sim N^{i-}C_A^+ = 0, \quad (4.81)$$

$$\tilde{C}_A^- \sim N^{--} = 0. \quad (4.82)$$

Therefore only power suppressed contributions from A will remain (we could have also immediately seen this from the fact that $n \cdot C_A = 0 + \text{p.s.c.}$). On the other hand if we

choose the gauge $A^+ = 0$ then

$$\tilde{C}_A^+ \sim N^{+-} C_A^+ = \left(1 - \frac{k^+}{k^+}\right) C_A^+ = 0, \quad (4.83)$$

$$\tilde{C}_A^i \sim N^{i-} C_A^+ = -\frac{k^i}{k^+} C_A^+, \quad (4.84)$$

$$\tilde{C}_A^- \sim N^{--} C_A^+ = -\frac{k^-}{k^+} C_A^+. \quad (4.85)$$

Here we see that \tilde{C}_A^i and \tilde{C}_A^- are suppressed only if k^+ is the dominant component of k . If not, then in the higher order terms all contributions can be important and the situation obviously gets complicated. The gauge $A^+ = 0$ is useful in DIS where the target hadron has large P^+ . In hadron-hadron collisions, however, as we have seen, the light-cone gauge cannot be used. There is moreover the problem with rapidity divergences which appear in TMD distributions via integrals like (3.27) (the light-cone distribution (4.42) for example leads to divergences and is therefore ill-defined). These divergences become visible starting from one loop calculations. Now assume we are instead in $A^+ + A^- = 0$ gauge. Then

$$\tilde{C}_A^+ \sim N^{+-} C_A^+ = \left(1 - \frac{k^+ + k^-}{k^+ + k^-} + \frac{k^+ k^- n^2}{(k^+ + k^-)^2}\right) C_A^+ = \frac{k^+ k^- n^2}{(k^+ + k^-)^2} C_A^+, \quad (4.86)$$

$$\tilde{C}_A^i \sim N^{i-} C_A^+ = \left(-\frac{k^i}{k^+ + k^-} + \frac{k^i k^- n^2}{(k^+ + k^-)^2}\right) C_A^+, \quad (4.87)$$

$$\tilde{C}_A^- \sim N^{--} C_A^+ = \left(-\frac{2k^-}{k^+ + k^-} + \frac{(k^-)^2 n^2}{(k^+ + k^-)^2}\right) C_A^+. \quad (4.88)$$

If for example k is collinear to C_A , then indeed the contributions are power suppressed.

Thus for the axial gauge to be useful, the momenta emerging from C_A (C_B) should be collinear to C_A (C_B). Actually none of the momentum components need to scale with \sqrt{s} , but the dominant component should be k^+ (or k^- for C_B). Remember indeed from our classification scheme in section 4.1 that momenta which have no components scaling with \sqrt{s} but whose components along C_A dominates are still classified as belonging to C_A . If, however, we are in a region where for example k_\perp dominates, then we see that we have a large contribution from the transverse components. In that case we cannot neglect the higher order corrections. This is why we must be able to always deform the contour into the region where k^+ (or k^- for C_B) is the large component.

The analysis above and in section 4.1 suggests a general picture like in figure 30. We consider the case where the observed hadron, p_C , has some component scaling with Q , the reason being that the scale Q is needed to suppress the higher order corrections as seen above. The regions in figure 30 are to be understood in the classification presented in section 4.1. The momentum Q is fixed and $Q/\sqrt{s} \rightarrow 0$ asymptotically. There are actually further lines going out from the hard region which give undetected collinear regions but we do not show them in figure 30 for simplicity. According to what we have just seen above, in axial gauge we generally expect the contributions in figure 30 to be reduced to that of figure 31. Here the extra collinear-to-hard gluons are missing, and the remaining gluons coupling to H are transversely polarized (indicated by black squares).

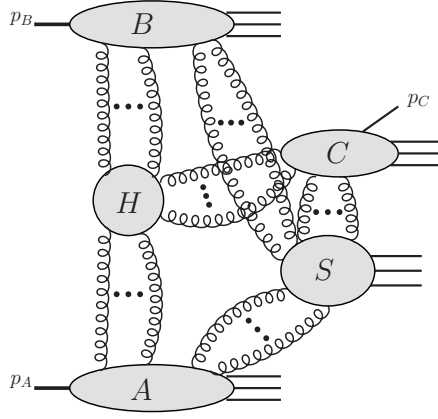


Figure 30: Leading regions for single inclusive hadron production via gluon initiated jet in hadron-hadron collisions. There is an additional collinear region associated with the produced hadron p_C . There will generally also be additional collinear regions associated with unobserved jets, these are not shown here for simplicity.

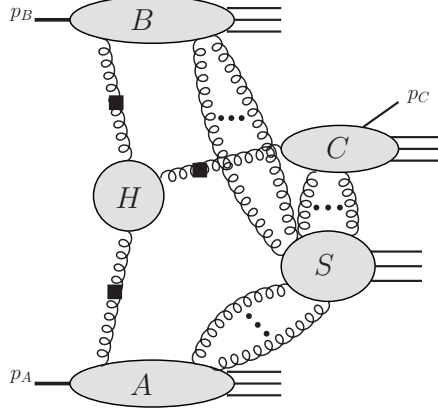


Figure 31: Single hadron production in axial gauge where the extra collinear-to-hard can be eliminated. The collinear regions then couple to the hard region via a single transversely polarized gluon, indicated by the black squares, each.

Note from figure 31 that the soft region still remains. Indeed the analysis above does not directly apply to the soft region since we needed a scale Q to suppress the higher order terms. To simplify the expression completely then, one must be able to show that the soft region can be eliminated or neglected.

In figure 32 we show examples of soft gluons exchanged between the different regions. In the first graph (top left) the gluon k attaches to the collinear-to- B gluon that goes into the hard scattering. The momentum k then runs in a loop from top to down, counterclockwise, via H into A and back again. The line $k_A - k$ then gives a pole (taking all k_\perp to be of

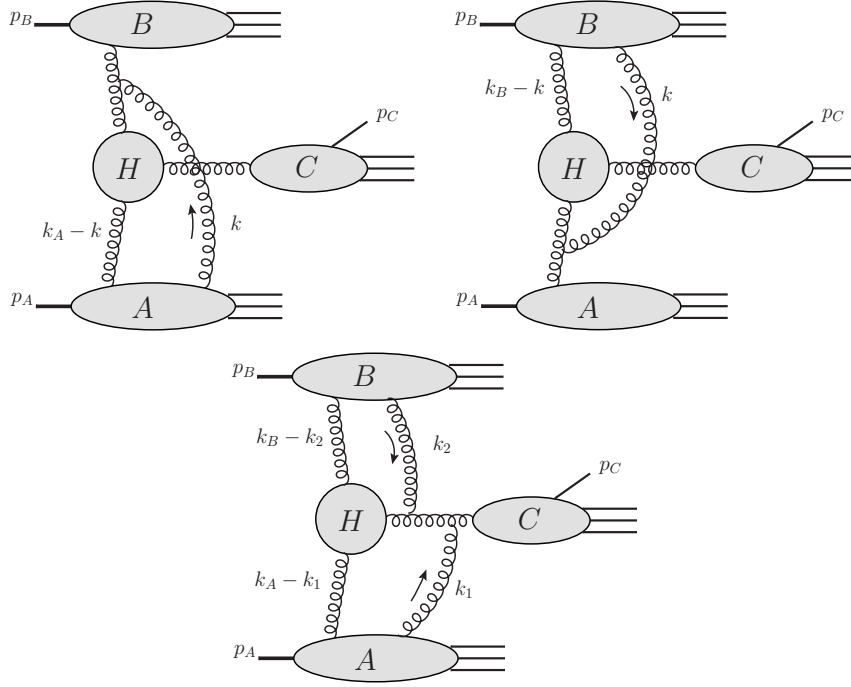


Figure 32: Examples of graphs in axial gauge where soft gluons are exchanged between the collinear regions. Each of these type of emissions require contour deformations in different directions to stay out of the Glauber region.

order m)

$$k^- \sim \frac{m^2}{k_A^+} - i\epsilon \sim \frac{m^2}{Q} - i\epsilon. \quad (4.89)$$

Inside the lower blob A , k will run along the large momentum p_A , and so there will be a typical pole of the type

$$k^- \sim \frac{m^2}{p_A^+} + i\epsilon \sim \frac{m^2}{\sqrt{s}} + i\epsilon. \quad (4.90)$$

We thus see that these poles pinch the integration contour of k^- . It might also be that k in the lower blob attaches to a line with plus component only of order Q instead of \sqrt{s} , but in any case we see that k^- is at least forced to be small as m^2/Q . One can still save the power counting arguments if k^+ can be deformed far out so that $k^+k^- \sim k_\perp^2$.

We must now, however, exactly specify how to treat the singularities of the axial gauge propagator (4.50). The canonical regularization of these singularities is given by the principal value prescription. The canonical regularization is useful because the corresponding generalized functions then obey elementary relations, such as ordinary differentiation, that are obeyed by the corresponding regular functions [72]. The use of principal value, however, also implies that one cannot deform the contours. The variable $k \cdot n$ must therefore remain on the real axis.

As we have seen above, for the contributions in figure 32 we must deform in the first graph (top left) k^+ but not k^- , in the second graph (top right) k^- but not k^+ while in the last graph (bottom) we must simultaneously deform k_1^+ and k_2^- while keeping k_1^- and k_2^+ fixed. We then, however, see that these requirements are in contradiction with the fact that we cannot deform on $k \cdot n$. For example, deforming in the first case k^+ , *i.e.* letting $k^+ \rightarrow k^+ + iC$ for some large $C \sim Q$, but keeping k^- fixed implies that

$$k \cdot n = k^+ + k^- \rightarrow (k^+ + iC) + k^- = k \cdot n + iC \quad (4.91)$$

which is not allowed. The required contour deformations therefore fail. We thus conclude that the treatment in axial gauge is not complete.

One may also consider the possibility of using the so-called “planar gauge” introduced in [105]. In this gauge, the gauge vector n is non-light-like, so that $n^2 \neq 0$, but the last term in the axial gauge propagator (4.50) is eliminated (by a clever choice of the gauge fixing term in the Lagrangian). Moreover, as shown in [105], Faddeev-Popov ghosts are still absent, just like in axial gauge. This gauge has thus all the advantages of the axial gauge, and in addition is free from the double pole in the propagator. It is therefore certainly much better behaved. However, the unphysical singularity $1/k \cdot n$ still remains and must be treated via the principal value. Therefore the above arguments still apply to this gauge. In [105] the authors argue that, since the propagator poles are unphysical and have to all cancel at the end of the day, one might as well treat $1/k \cdot n$ as a regular function, excluding this pole from loop integrals. The problem, however, is that one still needs to perform the contour deformations to prove factorization, and in doing this the term $1/k \cdot n$ cannot be neglected in the intermediate steps, even if the final result should be free from unphysical poles.

It is of course possible that one chooses a regularization which is not principal value. For example, we saw above that the choice in [33] for the light-cone gauge is given by (4.34). In any case, however, it is very hard to see how exactly a systematic procedure is developed that is capable of treating graphs of arbitrarily high order, as is required for the full proof of factorization. As far as we aware of, this has never been done. We leave the possibility open that a treatment in axial gauge might work out, but it is difficult to see how this would be achieved.

4.6 The gluon distribution function

We have systematically gone through single inclusive particle production at high energies, and we have concentrated especially on the small- x factorization formula (4.8). In this section we examine more closely the exact definition of the TMD gluon distribution. We will moreover at the end of the section make some final comments on the validity of factorization.

According to (4.11), the gluon distribution is a (modified) Fourier transform of the dipole scattering amplitude in the adjoint representation. The expression (4.11) is appropriate in a covariant gauge, and not in an axial gauge. In the canonical definition of the parton distributions, the direction of the Wilson lines in (4.12) are taken opposite to the

hadron, *i.e.* for a hadron moving with momentum p_A (p_B), the direction is taken as n_B (n_A), which is parallel to p_B (p_A). To leading power we can also take the directions to be $n_A + n_B$ for both hadrons, and the axial gauge $(n_A + n_B) \cdot A = 0$ then sets the Wilson lines to unity. At first sight, however, this does not seem to be strictly correct because if in (4.12) we set the Wilson lines to be unity then we find that (4.12) vanishes, $\mathcal{N} = 0$, which obviously cannot be true. Part of the answer is that a fully gauge invariant definition of (4.12) requires that we also insert transverse gauge links at infinity, and these are non-zero in any axial gauge. However, to match the axial gauge expressions, (4.68) and (4.69), one must also express the distribution (4.12) using the field tensors F^{+i} and F^{-i} . Let us now see how this can be done.

It is in fact a fundamental property of all gluon distributions that the field tensors $F^{\mu\nu}$ appear in the definitions. The underlying reason for this comes from the elementary parton model definition (2.1). As the QCD definitions are appropriate modifications and generalizations of the parton model result, it is then natural that the field tensors appear in the definitions of the integrated and TMD gluon distributions [1]. This is also the case in the construction scheme for the generalized TMD distributions given in [108,109]. It should therefore also be possible to write the dipole distribution (4.11) using the field tensors, if it indeed is a TMD gluon distribution as claimed.

Consider the lowest order contribution from (4.12) where we insert a set of outgoing states $|X, \text{out}\rangle$ between the Wilson lines and then expand each Wilson line to first order in g_s . We will *assume* that the averaging in (4.12) is given by an ordinary expectation value between momentum eigenstates of the hadron, but we are not actually sure whether this is consistent with the formalism from which (4.12) is supposed to arise. Nevertheless, without this assumption we cannot make any real comparison. We also neglect for the moment the regulator y in (4.11) and (4.12). The first order expansion of (4.12) in (4.11) for a hadron with momentum p_A gives

$$f_A^{(1)}(k_\perp) = \frac{N_c}{(2\pi)^4 \alpha_s} k_\perp^2 \int d^2 x_\perp \int d^2 y_\perp e^{-ik_\perp \cdot (x_\perp - y_\perp)} \sum_X \frac{g_s^2 N_c}{N_c^2 - 1} \int dx^- \int dy^- \frac{\langle p_A | A_a^+(x^-, x_\perp) | X, \text{out} \rangle \langle X, \text{out} | A_a^+(y^-, y_\perp) | p_A \rangle}{\langle p_A | p_A \rangle}. \quad (4.92)$$

The argument to convert $k^i A_a^+$ into F_a^{+i} can now be made as follows. In the power counting of the contributions from the region collinear to p_A , the largest contribution arises from the $+$ component as we have seen in sections 3.1.2 and 4.1. In the N gluon exchange term, the biggest contribution therefore arises from the terms where we pick up the contribution $A^{+\dots+}$ for all the N collinear-to- p_A gluons. For every contribution where we change one of the gluon polarizations from the longitudinal index $+$ to a transverse index i , we lose one power of \sqrt{s} . Thus one can let

$$k^i A_a^+ \rightarrow k^i A_a^+ - k^+ A_a^i \quad (4.93)$$

since the correction produces a power suppressed term. It is important to notice that this exchange is not permissible in the hard scattering factorization. From the power counting

in section 3.1.2 we actually see that $k^i A^+ \sim m Q$ and $k^+ A^i \sim Q m$ for a collinear-to- A gluon k . In the small- x case, however, $k^+ \ll \sqrt{s}$, so that $k^+ A^i \ll \sqrt{s} m \sim k^i A^+$.

For the lowest order term in (4.92) this is enough to convert each $k^i A_a^+$ into F_a^{+i} since the commutator in F^{+i} contributes at higher order. Removing the sum over the states X , one can then rewrite (4.92) as

$$\begin{aligned} f_A^{(1)}(k_\perp) &= \frac{N_c}{2\pi\alpha_s} \frac{g_s^2 N_c}{N_c^2 - 1} \int \frac{dx^- d^2 x_\perp}{(2\pi)^3 2p_A^+} e^{-ik_\perp \cdot x_\perp} \langle p_A | F_a^{+i}(0^+, x^-, x_\perp) F_a^{+i}(0) | p_A \rangle \\ &= \frac{N_c^2}{N_c^2 - 1} \int \frac{dx^- d^2 x_\perp}{(2\pi)^3 p_A^+} e^{-ik_\perp \cdot x_\perp} \langle p_A | F_a^{+i}(0^+, x^-, x_\perp) F_a^{+i}(0) | p_A \rangle. \end{aligned} \quad (4.94)$$

In the dipole model from which (4.12) arises, the large N_c limit is employed which means that the coefficient $N_c^2/(N_c^2 - 1)$ is set to unity. The result (4.94) then very strongly resembles (4.68).

We note, however, that in (4.94), there is no x dependence as in (4.68). This is a characteristics of the dipole formalism where the longitudinal component of the total momentum coupling to the collinear region is neglected. The rapidity dependence of the dipole distribution therefore purely arises from the rapidity cut-off. In (4.68), the rapidity cut-off is not yet included, and the x_A variable which is the longitudinal momentum fraction of the gluon k in figure 29 clearly does not play the role of a rapidity cut-off. This is also one of the reasons why the dipole distribution (4.11) or (2.10) cannot be directly related to the integrated distribution as in (4.10), since the meanings of the longitudinal variables in (4.10) are completely different on the right and the left hand sides. Despite this, however, the relation (4.10) is still widely advocated in the small- x literature.

When all the gluons coupling to the collinear region contribute with their longitudinal polarizations, however, there must be certain cancellations due to the Ward identities. In Feynman gauge the easiest way to see this is to use the K - G decomposition (4.30). Ward identities apply on the K terms, and these correspond to the longitudinally polarized gluons. For the region collinear to p_A , we choose the vector n in the K - G decomposition (4.30) to be in the opposite direction to p_A , *i.e.* $n = n_B$ (and the other way around for the B terms). Then as we saw in (4.31) and (4.32), the longitudinal components vanish for the G terms while for the K terms we get unity. The largest contribution therefore arises from the terms where we only pick up the K terms. Ward identities, however, imply that part of this largest contribution cancel, leaving behind a reminder term which is of the same order as the contributions where one gluon contributes as G^{i-} , while all the other terms contribute via the K^{+-} terms [1, 71]. It is then the combination of the G^{i-} term and the remainder term from the Ward identity cancellations that give rise to the field tensor term F^{+i} (including the commutator term) while the sum over all the K^{+-} terms give the Wilson lines. We explain this in the context of the small- x calculations in [42] where we derive the TMD gluon distribution that looks like (2.5). That is, a gluon distribution including the F^{+i} factors is naturally constructed.

Let us now extend the above analysis to all orders. In [108, 109] a construction scheme of TMD parton distributions was proposed. The proposed scheme is a method of converting

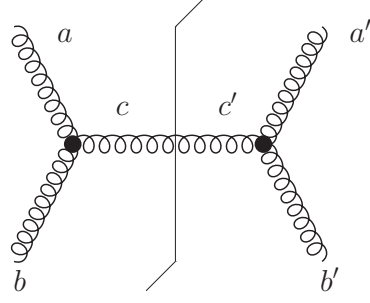


Figure 33: The elementary graph for the gluon production.

the collinear-to-hard gluons to Wilson lines, thus giving the “unsubtracted” TMD parton distributions. We now apply the scheme to the present process.

The scheme starts from studying the elementary “hard” graph for the process under consideration, that is figure 33. Of course here this graph does not involve any hard momenta, but that does not really affect the structure of the Wilson lines which parametrize the non-perturbative structure. According to [108, 109] then, the contribution from the process in figure 33 to the TMD gluon distribution of the lower particle (with momentum p_A) is

$$F_{b'}(x) F_b(0) i f^{abc} i f^{a'b'c'} (W_B^{(+)})_{cc'} (W_B^{(-)})_{aa'} \quad (4.95)$$

where

$$W_B^{(\pm)} = W_B(0; \pm\infty^-, 0_\perp) W_T(\pm\infty^-, 0_\perp; \pm\infty^-, x_\perp) W_B(\pm\infty^-, x_\perp; x^-, x_\perp), \quad (4.96)$$

and

$$W_B(x; y) = P \exp \left(-ig_s \int_x^y dz n_B \cdot A_a(z) T^a \right), \quad (4.97)$$

$$W_T(x, y) = P \exp \left(-ig_s \int_x^y dz_\perp \cdot A_{\perp, a}(z) T^a \right). \quad (4.98)$$

If we instead consider the TMD distribution of the upper hadron with momentum p_B then the longitudinal direction in (4.96) should be $+$ instead of $-$, and in (4.97) $n_B \rightarrow n_A$. Notice that in (4.95) the Wilson lines are in the adjoint representation as is clear from the color subscripts. We now use $T_{ac}^b = i f^{abc}$ for the adjoint representation to rewrite (4.95) as

$$\begin{aligned} F_{b'}(x) F_b(0) T_{ac}^b T_{a'c'}^{b'} (W_B^{(+)})_{cc'} (W_B^{(-)})_{aa'} \\ = F_{a'c'}(x) F_{ac}(0) (W_B^{(+)})_{cc'} (W_B^{(-)})_{aa'} \end{aligned} \quad (4.99)$$

where we have defined

$$F_{ac} \equiv F_b T_{ac}^b. \quad (4.100)$$

From equation (4.99) one then finds the following contribution to the correlator in the gluon distribution

$$\begin{aligned} \langle p_A | \left(F(x) W_B^{(+)\dagger} \right)_{a'c} \left(F(0) W_B^{(-)} \right)_{ca'} | p_A \rangle \\ = \text{Tr} \langle p_A | F(x) W_B^{(+)\dagger} F(0) W_B^{(-)} | p_A \rangle. \end{aligned} \quad (4.101)$$

The trace is taken with respect to the adjoint representation with the field tensor defined as in (4.100). The (unsubtracted) gluon distribution function is then given by

$$f_A(x_A, k_\perp) = \int \frac{dx^- d^2 x_\perp}{(2\pi)^3 p_A^+} e^{ix_A p_A^+ x^- - ik_\perp \cdot x_\perp} \text{Tr} \langle p_A | F^{+i}(0^+, x^-, x_\perp) W_B^{(+)\dagger} F^{+i}(0) W_B^{(-)} | p_A \rangle. \quad (4.102)$$

Actually, note that in the canonical definitions (2.1) and (4.43) we would instead of $1/p_A^+$ insert the factor $1/k_A^+ = 1/(x_A p_A^+)$. The reason we choose $1/p_A^+$ here is that we will connect the above distribution with that of the dipole result (4.11) and remember from above that the dipole result cannot be obtained if we have the factor $1/k_A^+$ (see also remarks just below).

Strictly speaking (4.102) involves only the bare fields. Remember from section 3.1.3 that the gluon distribution has to be renormalized as in equation (3.23). The soft region must also properly be subtracted to cancel the rapidity divergences in (4.102). A similar definition is easily obtained for the gluon distribution associated with p_B

$$f_B(x_B, k_\perp) = \int \frac{dx^+ d^2 x_\perp}{(2\pi)^3 p_B^-} e^{ix_B p_B^- x^+ - ik_\perp \cdot x_\perp} \text{Tr} \langle p_B | F^{-i}(x^+, 0^-, x_\perp) W_A^{(+)\dagger} F^{-i}(0) W_A^{(-)} | p_B \rangle. \quad (4.103)$$

Exchanging to leading order the Wilson line directions to $n_A + n_B$ in both cases and applying the axial gauge $(n_A + n_B) \cdot A = 0$ we then obtain (4.68) and (4.69) respectively. There is an additional factor N_c arising from the color traces in (4.102) and (4.103) (exactly as in (4.94)). Thus we can see (4.102) and (4.103) as possible generalizations of (4.68) and (4.69) to arbitrary gauge.

The connection to the dipole formula (4.11) and (4.12) can now be made as follows. We consider the transverse derivatives in (4.11) acting on the Wilson lines in (4.12). The effect of the derivative can be written as (for the hadron p_A)

$$\partial_x^i \tilde{W}(x_\perp) = -ig_s \int dx^- W_B(x; \infty^-, x_\perp) \partial_x^i A_a^+(x) T^a W_B(-\infty^-, x_\perp; x) \quad (4.104)$$

where as we recall \tilde{W} is given by taking (2.9) with the adjoint color matrices while $W_B(x; \infty^-, x_\perp)$ and $W_B(-\infty^-, x_\perp; x)$ are given by (4.97). We can again use (4.93) since the correction is power suppressed. One can also argue that the commutator of the field tensor is subleading since at given order in g_s it contains one factor A^i which replaces a factor A^+ from the Wilson line. In that case we could replace $-i\partial_x^i A_a^+(x) T^a \rightarrow F_a^{+i} T^a = F^{+i}$ in (4.104). This would imply that (4.11) contains the same structure as in (4.102), once we

also set $x = 0$ in (4.102) which as we remember from above is the standard approximation in the dipole formalism.

Thus as we have seen, in a sense the formula (4.11) together with (4.12) contains the contributions from the gluon field tensors as in (4.102). We motivated this by the power counting arguments, but a word of caution is in order here. We have mentioned above that the K terms in the K - G decomposition are subject to certain cancellations from the Ward identities. This implies actually that terms containing one factor of A^i at each side of the cut become leading. As explained above, these arise from the G^{i-} terms. Thus the transverse components in F^{+i} , including the commutator, may not be automatically dropped. The expression in (4.102) is therefore more correct than (4.11), assuming of course that factorization holds. If not, then neither expression needs to be correct. Let us therefore now finish our analysis with a discussion on the validity of factorization.

What we have thus seen is that (4.11) and (4.12) can be related to the distribution, (4.102) or (4.103), constructed using the scheme of [108, 109]. However, the scheme in [108, 109] by itself does not prove whether factorization holds or not. When a TMD parton distribution associated with a given collinear region is being constructed, one considers the attachments of the collinear-to-hard gluons to each line of the hard graph, and replace each set of connections by a Wilson line that correctly carries the color of the hard line. Since TMD factorization is used for two particle production in the almost back-to-back region, as in the examples of e^+e^- annihilation and Drell-Yan production in section 3.1.5, the relevant hard graphs are usually $2 \rightarrow 2$ partonic graphs, and one can then use these basic graphs to construct the possible gauge links for a given collinear region. An extensive list of possible gauge links is given in [109].

For proving factorization, however, one must consider all gluon attachments from the collinear regions to the hard graph *simultaneously*, as well as all possible soft attachments between the collinear regions. For example, in (4.95), following [108, 109], the attachments from the collinear regions C_A and C_B in figures 23, 25 or 30, are considered separately, and each is summed into the Wilson lines in (4.95). Considering all possible attachments, however, as for example in the graphs in figure 32, it may very well be that the resulting structure is more complicated than in (4.95) or that it is not even possible to identify any gauge link contributions to the TMD distributions. At the same time, one must be able show that deformations out of the Glauber region are possible, or that the poles producing the Glauber pinch cancel. Cancellation of the Glauber region has been demonstrated explicitly in the case of Drell-Yan (Ch 14, [1]), but difficulties may easily arise for the more complicated processes studied in [108, 109].

In reference [77], the breakdown of ordinary TMD factorization (*i.e.* the TMD factorization that is relevant for the processes in section 3.1.5) was explicitly demonstrated in di-hadron production in hadron-hadron collisions at the level of 2 gluon exchange between the hard part and the collinear part. We illustrate in figure 34 two examples of the type of graphs considered in [77]. To distinguish the hard scattering we draw the hard gluons by zig-zag lines, while the collinear-to-hard gluons are illustrated by curly lines. In the elementary model considered in [77], the gluons are massive Abelian gluons, and the active lines that enter the hard scattering are scalar “di-quarks” while the spectator lines

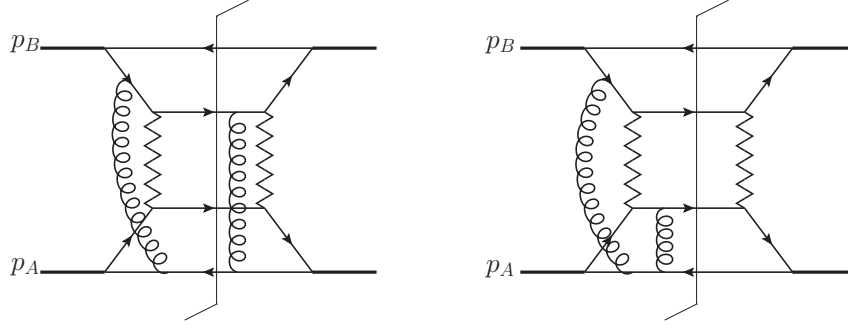


Figure 34: Production of two hadrons in an elementary model considered in [77]. We indicate the hard scattering by the exchange of the zig-zag lines. The additional gluon contributions correspond to breakdown of ordinary factorization.

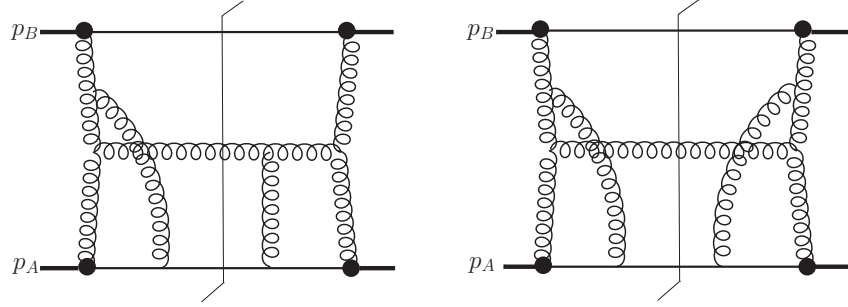


Figure 35: Examples of the type of graphs that are taken into account in the construction scheme of equation (4.95). The solid lines indicate the spectator parts of each hadron.

are fermions. The breakdown of ordinary factorization is then understood as being due to the attachments of the collinear gluons from the lower hadron lines to the upper active “quark” line which is of course color connected to the upper hadron. The collinear-to- p_A gluons in figure 34 which couple to the upper active lines of the hard part are precisely the gluons that in the scheme of [108,109] give rise to the gauge links of the generalized TMD distributions. The construction in (4.95) therefore contains these contributions. We illustrate these in the single gluon production case in figure 35.

As discussed above, however, for a complete proof of factorization one must also consider the simultaneous gluon couplings between the upper hadron and the hard part. This was considered in reference [78] which calculated in a slightly different model than [77] the type of graphs shown in figure 36 (the zig-zag lines for example correspond to a massive color singlet scalar boson). These graphs have an entangled color structure which makes it impossible to factorize the color flows even in the scheme of [108,109]. The examples shown in figure 36 then break factorization for the Double Spin Asymmetry (DSA), while in the specific model considered the contributions from figure 36 to the unpolarized cross section cancel. Breakdown of factorization for the unpolarized cross section instead appears for graphs where three additional gluons are exchanged, with at least one gluon coupling to

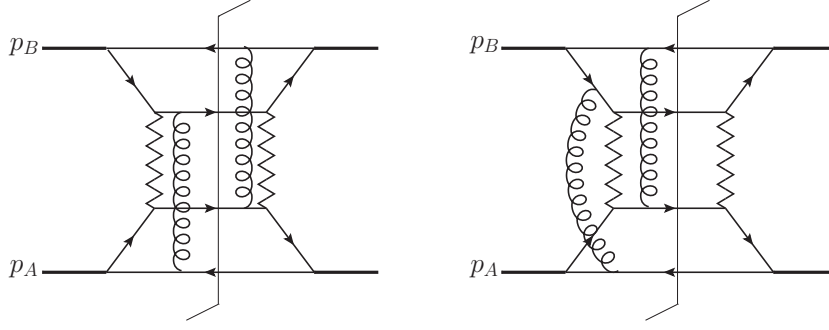


Figure 36: Examples of the class of graphs considered in [78] that lead to the breakdown of TMD factorization for DSA. We indicate the hard scattering by the exchange of the zig-zag lines.

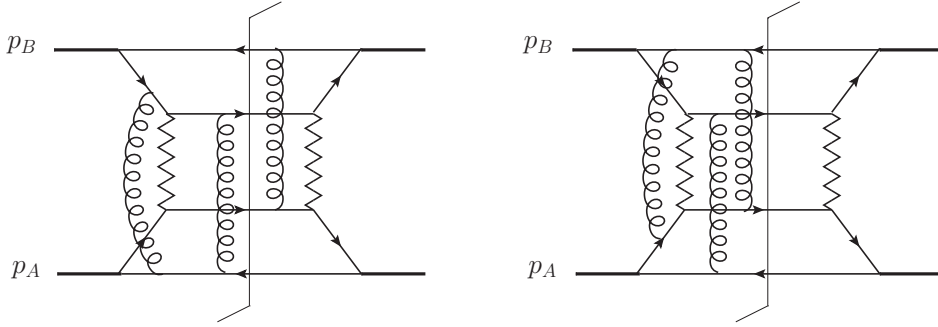


Figure 37: Examples of graphs where TMD factorization is broken for the unpolarized cross section. We indicate the hard scattering by the exchange of the zig-zag lines.

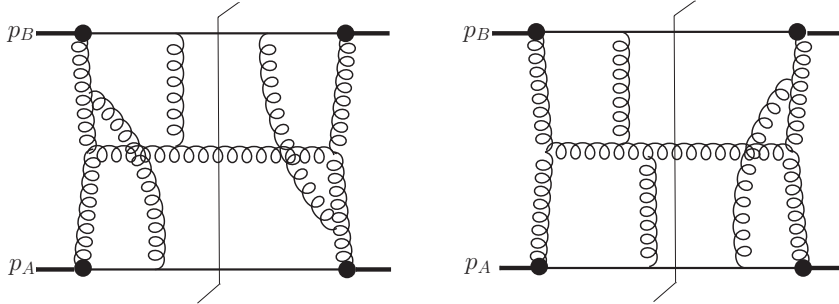


Figure 38: Examples of the type of graphs that may go beyond the construction scheme of equation (4.95) in QCD. The solid lines indicate the spectator parts of each hadron.

each hadron. We illustrate this in figure 37.

What this shows to us in the case of gluon production at small- x is that to answer the question of factorization one needs to consider graphs like in figure 38. These graphs have non-trivial color flows that do not seemingly factorize into color singlet factor associated with each collinear region. In that case one must demonstrate explicitly that such contribu-

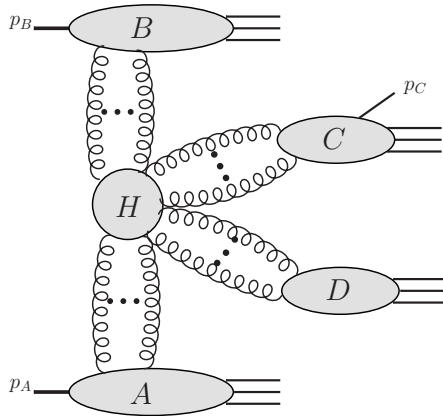


Figure 39: Single hadron production where the second jet emerging from the hadron is integrated over. Arbitrarily many gluons can be exchanged between each collinear region and the hard region, as indicated by the dots. We do not show the soft region.

tions cancel. Given, however that they do not even cancel in the simple models considered in [77, 78] it seems rather difficult to see how they would in full QCD. Indeed we note that the results from [78] have further been systematized in [110] where simultaneous couplings to different parts are considered, generalizing the scheme in [108, 109]. The difficulties with the color entangled contributions are there clearly demonstrated.

We mentioned earlier that the gluon production in figures 27, 29, 33, 35 and 38 corresponds to the case of soft particle production, illustrated in figure 23. To instead consider hard gluon (or rather hadron) production with large transverse momentum, so that a scale Q is present which can be used to suppress transverse polarizations, we need to take into account that the hard part contains additional jets. It can be shown that the case where more than two jets emerge from the hard region is suppressed in the almost back-to-back region [1]. We then consider the case where two gluon jets emerge from the hard region, and where only one of them contains the detected hadron. We illustrate this case in figure 39.

The case in figure 39 equals to taking di-hadron production and then integrating over one of the hadron momenta. The $2 \rightarrow 2$ hard scattering is now more intricate, and the scheme of [108, 109] becomes rather complicated as can be seen from table 8 in reference [109]. More importantly, however, the results in [77, 78, 110] become highly relevant and show us that generally factorization is broken in di-hadron production. Cancellation of the factorization breaking terms occur for the integrated distribution, but not if we merely integrate over the momentum of one of detected final state particles. In fact this can be seen in [110] where simplifications occur only when one integrates over *all* momenta except for a single hadron. Even in that case, however, the simplification only occurs for contributions that are termed "tree-level". It may be of course that the color structures simplify in the strict large N_c limit where $N_c \rightarrow \infty$. The factorization breaking graphs studied in [78], see figure 36, are for example non-leading in N_c . Their effect on the production cross section

may still, however, be important if there is no kinematical suppression.

Finally we note that in more general processes like in figure 39 there is also the soft factor which will now be more complicated than in standard TMD factorization. Assuming that factorization holds, according to [109] the unsubtracted TMD gluon distribution is a highly complicated function containing many different Wilson lines. Each light-like Wilson line produces rapidity divergences that must be regulated. In addition to the rapidity divergences there appear divergences related to the self energy corrections of the Wilson lines. All these divergences are regulated by subtracting the soft factor from the collinear region, which leads to definitions like in equation (3.36). In the case of the gauge link structures that appear for figure 39 using the scheme of [109], however, we dare not even ask how exactly all these issues would be dealt with. It appears to be an immensely difficult task to obtain final definitions of the highly complicated TMD distributions which are free from all divergences. Yet this would be extremely helpful for precise phenomenological applications.

5. Summary

Our main aim has been to provide a coherent analysis of TMD factorization and the TMD gluon distribution, especially as used in the small- x region, and to examine many important points that usually are not well explained or are overlooked in the literature.

In section 3 we have given a unified analysis of the concept of factorization in different formalisms, the hard scattering formalism (section 3.1), the BFKL formalism (section 3.2) and the CGC formalism (section 3.3). We also analyzed in section 3.4 what we called hybrid approaches which combine collinear factorization with the use of TMD distributions.

The main point in section 3.1 has been to explain what exactly is meant by factorization in the hard scattering case, and what approximations and methods are built into the analysis. We have then compared these to the small- x treatments which use somewhat different methods. We emphasized in section 3.3.4 the difference between factorization which is constructed to be valid to leading power and the leading logarithmic approximation (LLA) that is based on the one-loop calculation. As we have explained the former is of much greater accuracy and generality which is important to understand when comparing the different treatments.

In section 3.4 we explained the idea behind the so-called factorization of mass singularities that is built into the hybrid formalisms. Let us note here that it has been demonstrated in [1] that for the simplest partonic reactions as relevant for DIS, the method gives the same results as the hard scattering factorization for the massless limit of the hard scattering coefficient. It is, however, not clear to us whether this still holds in the cases studied in the hybrid formalisms, where one includes also TMD distributions, and studies proton-nucleus collisions. We also note that the CCH and CCFM formalisms essentially base their underlying formulas on the same approach. The use of the method in these formalisms is discussed in [42]. We have explained here why this procedure is physically misleading, and caution should be taken before trying to move on to more complicated reactions.

In section 4 we have given an extensive analysis of single particle production in the small- x region. We started by showing in section 4.1 that one can perform a power counting analysis very much as in section 3.1.2 to identify the leading structure. This is crucial to understand when the higher order corrections can be neglected and how the asserted formulas can be justified. The main factorization formula (4.8) has been extensively used in phenomenological applications of small- x QCD, at both RHIC and the LHC. It is therefore crucial to understand the physics behind it and the justifications given for its validity. We noted that many treatments in the literature are based on the axial gauge, and we therefore examined the application of the axial gauge in justifying the factorization formula (4.8). We showed in section 4.3 why the light-cone gauge is inappropriate for the formulation while in section 4.4 we showed how one can obtain the standard factorization formula in a symmetric axial gauge.

Then in section 4.5 we demonstrated the technical difficulties with the use of the axial gauge and suggested that a more complete treatment be based instead on covariant gauge. In section 4.6 we then discussed the gluon distribution that is associated with (4.8) and how it could generally be constructed from Feynman graphs, and we examined the graphs that are problematic for the full proof of factorization.

There have lately been many applications of TMD factorization in the small- x region, in pp , pA and AA collisions. To fully prove factorization, however, one must show that the graphs of the type we showed in section 4.6 cancel. In the case of pA collisions we emphasize that the gluon couplings from the proton side cannot be neglected. In particular it does not follow that one can automatically treat the proton using integrated parton distributions and fragmentation functions. If the observed particle is at low p_{\perp} then the transverse momentum of the collinear region of the proton and the soft region cannot be neglected outside of these regions, and as a consequence TMD distributions must be used everywhere. A more complete factorization formula must then be constructed, taking into account the difficulties outlined in sections 4.5 and 4.6.

Finally, a point which did not discuss much here concerns the scattering coefficient in the gluon production formula, equation (4.8). Note that this factor diverges as $l_{\perp} \rightarrow 0$. This is in fact a sign that the standard treatment cannot be complete. One should provide for the scattering factor a full definition that is valid to all orders, is gauge independent, and which contains necessary subtractions to remove all divergences. An example for the scattering factor in heavy $q\bar{q}$ production is given in [89].

Acknowledgements

I would like to thank John Collins, Anna Stasto and Bo-Wen Xiao for useful discussions during an extended period of time. This work is supported by U.S. D.O.E. grant number DE-FG02-90-ER-40577

References

- [1] J. C. Collins, *Foundations of Perturbative QCD*. Cambridge University Press, Cambridge, UK, 2011.

- [2] J. Collins and H. Jung, *Need for fully unintegrated parton densities*, [hep-ph/0508280](#).
- [3] J. C. Collins and D. E. Soper, *Parton Distribution and Decay Functions*, *Nucl. Phys.* **B194** (1982) 445.
- [4] J. C. Collins and D. E. Soper, *Back-To-Back Jets in QCD*, *Nucl. Phys.* **B193** (1981) 381.
- [5] J. C. Collins, D. E. Soper, and G. Sterman, *Transverse momentum distribution in Drell-Yan pair and W and Z boson production*, *Nucl. Phys.* **B250** (1985) 199–224.
- [6] R. Meng, F. I. Olness, and D. E. Soper, *Semi-inclusive deeply inelastic scattering at small q_T* , *Phys. Rev.* **D54** (1996) 1919–1935, [[hep-ph/9511311](#)].
- [7] J. C. Collins, *What exactly is a parton density?*, *Acta Phys. Polon.* **B34** (2003) 3103, [[hep-ph/0304122](#)].
- [8] G. F. Sterman, *Mass Divergences in Annihilation Processes. 1. Origin and Nature of Divergences in Cut Vacuum Polarization Diagrams*, *Phys.Rev.* **D17** (1978) 2773.
- [9] S. B. Libby and G. F. Sterman, *Mass Divergences In Two Particle Inelastic Scattering*, *Phys.Rev.* **D18** (1978) 4737.
- [10] J. Jalilian-Marian, A. Kovner, A. Leonidov, and H. Weigert, *The BFKL equation from the Wilson renormalization group*, *Nucl. Phys.* **B504** (1997) 415–431, [[hep-ph/9701284](#)].
- [11] J. Jalilian-Marian, A. Kovner, A. Leonidov, and H. Weigert, *The Wilson renormalization group for low x physics: Towards the high density regime*, *Phys. Rev.* **D59** (1999) 014014, [[hep-ph/9706377](#)].
- [12] J. Jalilian-Marian, A. Kovner, and H. Weigert, *The Wilson renormalization group for low x physics: Gluon evolution at finite parton density*, *Phys. Rev.* **D59** (1999) 014015, [[hep-ph/9709432](#)].
- [13] E. Iancu, A. Leonidov, and L. D. McLerran, *Nonlinear gluon evolution in the color glass condensate. I*, *Nucl. Phys.* **A692** (2001) 583–645, [[hep-ph/0011241](#)].
- [14] E. Iancu, A. Leonidov, and L. D. McLerran, *The renormalization group equation for the color glass condensate*, *Phys. Lett.* **B510** (2001) 133–144, [[hep-ph/0102009](#)].
- [15] E. Ferreiro, E. Iancu, A. Leonidov, and L. McLerran, *Nonlinear gluon evolution in the color glass condensate. II*, *Nucl. Phys.* **A703** (2002) 489–538, [[hep-ph/0109115](#)].
- [16] D. Kharzeev, Y. V. Kovchegov, and K. Tuchin, *Cronin effect and high $p(T)$ suppression in pA collisions*, *Phys.Rev.* **D68** (2003) 094013, [[hep-ph/0307037](#)].
- [17] F. Gelis and R. Venugopalan, *Large mass q anti- q production from the color glass condensate*, *Phys.Rev.* **D69** (2004) 014019, [[hep-ph/0310090](#)].
- [18] J. P. Blaizot, F. Gelis, and R. Venugopalan, *High-energy pA collisions in the color glass condensate approach. 1. Gluon production and the Cronin effect*, *Nucl.Phys.* **A743** (2004) 13–56, [[hep-ph/0402256](#)].
- [19] C. Marquet, *A QCD dipole formalism for forward-gluon production*, *Nucl.Phys.* **B705** (2005) 319–338, [[hep-ph/0409023](#)].
- [20] D. Kharzeev, E. Levin, and M. Nardi, *Color glass condensate at the LHC: Hadron multiplicities in pp , pA and AA collisions*, *Nucl.Phys.* **A747** (2005) 609–629, [[hep-ph/0408050](#)].

- [21] H. Fujii, F. Gelis, and R. Venugopalan, *Quark pair production in high energy pA collisions: General features*, *Nucl.Phys.* **A780** (2006) 146–174, [[hep-ph/0603099](#)].
- [22] F. Gelis and R. Venugopalan, *Particle production in field theories coupled to strong external sources*, *Nucl.Phys.* **A776** (2006) 135–171, [[hep-ph/0601209](#)].
- [23] F. Gelis and R. Venugopalan, *Three lectures on multi-particle production in the glasma*, *Acta Phys.Polon.* **B37** (2006) 3253–3314, [[hep-ph/0611157](#)].
- [24] F. Gelis, T. Lappi, and R. Venugopalan, *High energy factorization in nucleus-nucleus collisions*, *Phys.Rev.* **D78** (2008) 054019, [[arXiv:0804.2630](#)].
- [25] F. Gelis, T. Lappi, and R. Venugopalan, *High energy factorization in nucleus-nucleus collisions. 3. Long range rapidity correlations*, *Phys.Rev.* **D79** (2009) 094017, [[arXiv:0810.4829](#)].
- [26] E. Levin and A. H. Rezaeian, *Gluon saturation and inclusive hadron production at LHC*, *Phys. Rev.* **D82** (2010) 014022, [[arXiv:1005.0631](#)].
- [27] E. Levin and A. H. Rezaeian, *Hadron multiplicity in pp and AA collisions at LHC from the Color Glass Condensate*, *Phys. Rev.* **D82** (2010) 054003, [[arXiv:1007.2430](#)].
- [28] J. L. Albacete and C. Marquet, *Single Inclusive Hadron Production at RHIC and the LHC from the Color Glass Condensate*, *Phys.Lett.* **B687** (2010) 174–179, [[arXiv:1001.1378](#)].
- [29] E. Levin and A. H. Rezaeian, *Gluon saturation and energy dependence of hadron multiplicity in pp and AA collisions at the LHC*, [arXiv:1102.2385](#).
- [30] J. L. Albacete and A. Dumitru, *A model for gluon production in heavy-ion collisions at the LHC with rcBK unintegrated gluon densities*, [arXiv:1011.5161](#).
- [31] E. Levin and A. H. Rezaeian, *Hadron production at the LHC: Any indication of new phenomena*, [arXiv:1011.3591](#).
- [32] P. Tribedy and R. Venugopalan, *QCD saturation at the LHC: comparisons of models to p+p and A+A data and predictions for p+Pb collisions*, [arXiv:1112.2445](#).
- [33] Y. V. Kovchegov and A. H. Mueller, *Gluon production in current nucleus and nucleon nucleus collisions in a quasi-classical approximation*, *Nucl. Phys.* **B529** (1998) 451–479, [[hep-ph/9802440](#)].
- [34] L. D. McLerran and R. Venugopalan, *Computing quark and gluon distribution functions for very large nuclei*, *Phys. Rev.* **D49** (1994) 2233–2241, [[hep-ph/9309289](#)].
- [35] L. D. McLerran and R. Venugopalan, *Gluon distribution functions for very large nuclei at small transverse momentum*, *Phys. Rev.* **D49** (1994) 3352–3355, [[hep-ph/9311205](#)].
- [36] Y. V. Kovchegov, *Non-Abelian Weizsaecker-Williams field and a two- dimensional effective color charge density for a very large nucleus*, *Phys. Rev.* **D54** (1996) 5463–5469, [[hep-ph/9605446](#)].
- [37] Y. V. Kovchegov, *Quantum structure of the nonAbelian Weizsacker-Williams field for a very large nucleus*, *Phys.Rev.* **D55** (1997) 5445–5455, [[hep-ph/9701229](#)].
- [38] L. D. McLerran and R. Venugopalan, *Fock space distributions, structure functions, higher twists and small x*, *Phys.Rev.* **D59** (1999) 094002, [[hep-ph/9809427](#)].
- [39] E. Iancu, A. Leonidov, and L. McLerran, *The colour glass condensate: An introduction*, [hep-ph/0202270](#).

- [40] T. Lappi, *Energy density of the glasma*, *Phys.Lett.* **B643** (2006) 11–16, [[hep-ph/0606207](#)].
- [41] Y. V. Kovchegov and K. Tuchin, *Inclusive gluon production in DIS at high parton density*, *Phys. Rev.* **D65** (2002) 074026, [[hep-ph/0111362](#)].
- [42] E. Avsar and J. C. Collins, *Analysis of the treatments of TMD gluon distribution and factorization*, *In preparation*.
- [43] E. Avsar *In preparation*.
- [44] R. P. Feynman, *Photon-Hadron Interactions*. Benjamin, Reading, MA, 1972.
- [45] N. N. Nikolaev and B. Zakharov, *Color transparency and scaling properties of nuclear shadowing in deep inelastic scattering*, *Z.Phys.* **C49** (1991) 607–618.
- [46] N. Nikolaev and B. G. Zakharov, *Pomeron structure function and diffraction dissociation of virtual photons in perturbative QCD*, *Z.Phys.* **C53** (1992) 331–346.
- [47] A. H. Mueller, *Soft gluons in the infinite momentum wave function and the BFKL pomeron*, *Nucl. Phys.* **B415** (1994) 373–385.
- [48] A. H. Mueller, *Unitarity and the BFKL pomeron*, *Nucl. Phys.* **B437** (1995) 107–126, [[hep-ph/9408245](#)].
- [49] A. H. Mueller, *Parton saturation: An overview*, [hep-ph/0111244](#).
- [50] I. Balitsky, *Operator expansion for high-energy scattering*, *Nucl. Phys.* **B463** (1996) 99–160, [[hep-ph/9509348](#)].
- [51] I. Balitsky, *High-energy QCD and Wilson lines*, [hep-ph/0101042](#).
- [52] A. Kovner and U. A. Wiedemann, *Eikonal evolution and gluon radiation*, *Phys.Rev.* **D64** (2001) 114002, [[hep-ph/0106240](#)].
- [53] W. Buchmuller, M. McDermott, and A. Hebecker, *Gluon radiation in diffractive electroproduction*, *Nucl.Phys.* **B487** (1997) 283–310, [[hep-ph/9607290](#)].
- [54] W. Buchmuller, T. Gehrmann, and A. Hebecker, *Inclusive and diffractive structure functions at small x* , *Nucl.Phys.* **B537** (1999) 477–500, [[hep-ph/9808454](#)].
- [55] F. Gelis and J. Jalilian-Marian, *Photon production in high energy proton nucleus collisions*, *Phys. Rev.* **D66** (2002) 014021, [[hep-ph/0205037](#)].
- [56] F. Gelis and J. Jalilian-Marian, *From DIS to proton nucleus collisions in the color glass condensate model*, *Phys. Rev.* **D67** (2003) 074019, [[hep-ph/0211363](#)].
- [57] F. Gelis and J. Jalilian-Marian, *Drell-Yan production and Lam-Tung relation in the color glass condensate formalism*, *Phys.Rev.* **D76** (2007) 074015, [[hep-ph/0609066](#)].
- [58] F. Dominguez, C. Marquet, B.-W. Xiao, and F. Yuan, *Universality of Unintegrated Gluon Distributions at small x* , [arXiv:1101.0715](#).
- [59] V. S. Fadin, E. A. Kuraev, and L. N. Lipatov, *On the Pomeranchuk Singularity in Asymptotically Free Theories*, *Phys. Lett.* **B60** (1975) 50–52.
- [60] E. A. Kuraev, L. N. Lipatov, and V. S. Fadin, *The Pomeranchuk Singularity in Nonabelian Gauge Theories*, *Sov. Phys. JETP* **45** (1977) 199–204.
- [61] I. I. Balitsky and L. N. Lipatov, *The Pomeranchuk Singularity in Quantum Chromodynamics*, *Sov. J. Nucl. Phys.* **28** (1978) 822–829.

- [62] J. Weis, *Factorization of multi-regge amplitudes*, *Phys.Rev.* **D4** (1971) 1777–1787.
- [63] J. Bartels, *A Reggeon Calculus for the Production Amplitude. 1.*, *Phys.Rev.* **D11** (1975) 2977.
- [64] J. Bartels, *A Reggeon Calculus for the Production Amplitude. 2.*, *Phys.Rev.* **D11** (1975) 2989.
- [65] S. Catani, M. Ciafaloni, and F. Hautmann, *Gluon Contributions To Small x Heavy Flavor Production*, *Phys. Lett.* **B242** (1990) 97.
- [66] S. Catani, M. Ciafaloni, and F. Hautmann, *High-energy factorization and small x heavy flavor production*, *Nucl. Phys.* **B366** (1991) 135–188.
- [67] S. Catani and F. Hautmann, *High-energy factorization and small x deep inelastic scattering beyond leading order*, *Nucl.Phys.* **B427** (1994) 475–524, [[hep-ph/9405388](#)].
- [68] M. Ciafaloni, *Coherence Effects in Initial Jets at Small q^{*2} / s* , *Nucl.Phys.* **B296** (1988) 49.
- [69] S. Catani, F. Fiorani, and G. Marchesini, *QCD Coherence in Initial State Radiation*, *Phys.Lett.* **B234** (1990) 339.
- [70] S. Catani, F. Fiorani, and G. Marchesini, *Small x Behavior of Initial State Radiation in Perturbative QCD*, *Nucl.Phys.* **B336** (1990) 18.
- [71] J. Collins and T. Rogers, *The Gluon Distribution Function and Factorization in Feynman Gauge*, *Phys.Rev.* **D78** (2008) 054012, [[arXiv:0805.1752](#)].
- [72] I. M. Gel'fand and G. E. Shilov, *Generalized Functions Vol. 1*. Academic Press, New York, NY, 1964.
- [73] D. Campbell, *2 to n production processes and the multi-regge model*, *Phys.Rev.* **188** (1969) 2471–2485.
- [74] V. Fadin, R. Fiore, M. Kozlov, and A. Reznichenko, *Proof of the multi-Regge form of QCD amplitudes with gluon exchanges in the NLA*, *Phys.Lett.* **B639** (2006) 74–81, [[hep-ph/0602006](#)].
- [75] V. S. Fadin and L. Lipatov, *Radiative corrections to QCD scattering amplitudes in a multi - Regge kinematics*, *Nucl.Phys.* **B406** (1993) 259–292.
- [76] J. C. Collins and D. E. Soper, *Back-To-Back Jets: Fourier Transform from B to K -Transverse*, *Nucl.Phys.* **B197** (1982) 446.
- [77] J. Collins, *2-soft-gluon exchange and factorization breaking*, [arXiv:0708.4410](#).
- [78] T. C. Rogers and P. J. Mulders, *No Generalized TMD-Factorization in Hadro-Production of High Transverse Momentum Hadrons*, *Phys.Rev.* **D81** (2010) 094006, [[arXiv:1001.2977](#)].
- [79] T. Lappi and L. McLerran, *Some features of the glasma*, *Nucl.Phys.* **A772** (2006) 200–212, [[hep-ph/0602189](#)].
- [80] G. T. Bodwin, S. J. Brodsky, and G. Lepage, *Initial State Interactions and the Drell-Yan Process*, *Phys.Rev.Lett.* **47** (1981) 1799. Revised version.
- [81] G. T. Bodwin, S. J. Brodsky, and G. Lepage, *Effects Of Initial State QCD Interactions in the Drell-Yan Process*, *Phys.Rev.* **D39** (1989) 3287.

- [82] F. Gelis and J. Jalilian-Marian, *Dilepton production from the color glass condensate*, *Phys.Rev.* **D66** (2002) 094014, [[hep-ph/0208141](#)].
- [83] A. Dumitru, A. Hayashigaki, and J. Jalilian-Marian, *The Color glass condensate and hadron production in the forward region*, *Nucl.Phys.* **A765** (2006) 464–482, [[hep-ph/0506308](#)].
- [84] A. Dumitru, A. Hayashigaki, and J. Jalilian-Marian, *Geometric scaling violations in the central rapidity region of $d + Au$ collisions at RHIC*, *Nucl.Phys.* **A770** (2006) 57–70, [[hep-ph/0512129](#)].
- [85] R. Ellis, J. Stirling, and B. Webber, *QCD and Collider Physics*. Cambridge University Press, Cambridge, UK, 2003.
- [86] G. A. Chirilli, B.-W. Xiao, and F. Yuan, *One-loop Factorization for Inclusive Hadron Production in pA Collisions in the Saturation Formalism*, [arXiv:1112.1061](#).
- [87] R. Ellis, H. Georgi, M. Machacek, H. Politzer, and G. G. Ross, *Perturbation Theory and the Parton Model in QCD*, *Nucl.Phys.* **B152** (1979) 285.
- [88] G. Curci, W. Furmanski, and R. Petronzio, *Evolution of Parton Densities Beyond Leading Order: The Nonsinglet Case*, *Nucl.Phys.* **B175** (1980) 27.
- [89] J. C. Collins and R. Ellis, *Heavy quark production in very high-energy hadron collisions*, *Nucl.Phys.* **B360** (1991) 3–30.
- [90] F. Hautmann and H. Jung, *Angular correlations in multi-jet final states from k -perpendicular - dependent parton showers*, *JHEP* **0810** (2008) 113, [[arXiv:0805.1049](#)].
- [91] M. Deak, F. Hautmann, H. Jung, and K. Kutak, *Forward Jet Production at the Large Hadron Collider*, *JHEP* **0909** (2009) 121, [[arXiv:0908.0538](#)].
- [92] M. Deak, F. Hautmann, H. Jung, and K. Kutak, *Transverse Energy Flow with Forward and Central Jets at the LHC*, [arXiv:1112.6386](#).
- [93] B. Ermolaev, M. Greco, and S. Troyan, *QCD factorization for forward hadron scattering at high energies*, [arXiv:1112.1854](#).
- [94] L. V. Gribov, E. M. Levin, and M. G. Ryskin, *High $P(T)$ hadrons in the pionization region in QCD*, *Phys. Lett.* **B100** (1981) 173–176.
- [95] L. V. Gribov, E. M. Levin, and M. G. Ryskin, *Large - $E(T)$ processes as a main source of hadrons at very high-energies*, *Phys. Lett.* **B121** (1983) 65–71.
- [96] L. V. Gribov, E. M. Levin, and M. G. Ryskin, *Semihard Processes in QCD*, *Phys. Rept.* **100** (1983) 1–150.
- [97] **ATLAS Collaboration** Collaboration, G. Aad *et. al.*, *Charged-particle multiplicities in pp interactions measured with the ATLAS detector at the LHC*, *New J.Phys.* **13** (2011) 053033, [[arXiv:1012.5104](#)]. Long author list - awaiting processing.
- [98] **CMS Collaboration** Collaboration, V. Khachatryan *et. al.*, *Charged particle multiplicities in pp interactions at $\sqrt{s} = 0.9, 2.36$, and 7 TeV*, *JHEP* **1101** (2011) 079, [[arXiv:1011.5531](#)].
- [99] **ALICE Collaboration**, K. Aamodt *et. al.*, *Charged-particle multiplicity measurement in proton-proton collisions at $\sqrt{s} = 0.9$ and 2.36 TeV with ALICE at LHC*, *Eur. Phys. J.* **C68** (2010) 89–108, [[arXiv:1004.3034](#)].

- [100] **ALICE** Collaboration, K. Aamodt *et. al.*, *Charged-particle multiplicity measurement in proton-proton collisions at $\sqrt{s} = 7$ TeV with ALICE at LHC*, *Eur. Phys. J.* **C68** (2010) 345–354, [[arXiv:1004.3514](#)].
- [101] A. Grinyuk, H. Jung, G. Lykasov, A. Lipatov, and N. Zotov, *Unintegrated gluon distribution and soft pp collisions at LHC*, [arXiv:1203.0939](#).
- [102] **CMS Collaboration** Collaboration, S. Chatrchyan *et. al.*, *Measurement of the inclusive production cross sections for forward jets and for dijet events with one forward and one central jet in pp collisions at $\sqrt{s} = 7$ TeV*, [arXiv:1202.0704](#).
- [103] M. Deak, F. Hautmann, H. Jung, and K. Kutak, *Forward-Central Jet Correlations at the Large Hadron Collider*, [arXiv:1012.6037](#).
- [104] M. Deak, F. Hautmann, H. Jung, and K. Kutak, *Forward Jets and Energy Flow in Hadronic Collisions*, [arXiv:1112.6354](#).
- [105] Y. L. Dokshitzer, D. Diakonov, and S. Troian, *Hard Processes in Quantum Chromodynamics*, *Phys.Rept.* **58** (1980) 269–395.
- [106] J. Grammer, G. and D. Yennie, *Improved treatment for the infrared divergence problem in quantum electrodynamics*, *Phys.Rev.* **D8** (1973) 4332–4344.
- [107] A. Schafer and J. Zhou, *Higgs boson production in high energy proton-nucleus collisions*, [arXiv:1203.1534](#).
- [108] C. Bomhof, P. Mulders, and F. Pijlman, *Gauge link structure in quark-quark correlators in hard processes*, *Phys.Lett.* **B596** (2004) 277–286, [[hep-ph/0406099](#)].
- [109] C. Bomhof, P. Mulders, and F. Pijlman, *The Construction of gauge-links in arbitrary hard processes*, *Eur.Phys.J.* **C47** (2006) 147–162, [[hep-ph/0601171](#)].
- [110] M. Buffing and P. Mulders, *Gauge links for transverse momentum dependent correlators at tree-level*, *JHEP* **1107** (2011) 065, [[arXiv:1105.4804](#)].